FUNDAMENTAL AND APPLIED ASPECTS OF SOL-GEL BASED AFFINITY ASSAYS

FUNDAMENTAL AND APPLIED ASPECTS OF SOL-GEL BASED AFFINITY ASSAYS FOR MEMBRANE RECEPTORS USING MASS SPECTROMETRY DETECTION

By

JAI SHARMA, B.Sc

A Thesis Submitted to the School of Graduate Studies

in Partial Fulfillment of the Requirements

for the Degree

Master of Science

McMaster University

MASTER OF SCIENCE (2007) McMaster University

(Biochemistry) Hamilton, Ontario

TITLE: Fundamental and Applied Aspects of Sol-gel based Affinity Assays for Membrane Receptors using Mass Spectrometry Detection.

AUTHOR: Jai Sharma, B.Sc. (University of Toronto)

SUPERVISOR: Dr. John Brennan

NUMBER OF PAGES: xiii, 139

ABSTRACT

This thesis focuses on fundamental and applied aspects of sol-gel based affinity assays for screening membrane receptor targets. Fundamental studies investigate the role of non-specific interactions between polycationic polymers and sol-gel derived monoliths prepared from sodium silicate precursors. Previous studies from our group using time-resolved fluorescence anisotropy (TRFA) have shown that both the sidechain motion (ϕ_1) and backbone motion (ϕ_2) of polycationic polymers, such as poly-D-lysine, can be measured by fitting anisotropy decays of fluorescein labeled polymers to a two component hindered rotor model. These studies demonstrated that polycationic polymers remain fairly mobile in sol-gel derived materials made from sodium silicate precursors, despite the strong electrostatic interactions between the cationic polymers and the anionic silica materials. The first objective of my work was to assess the nature of the electrostatic interactions between several polycationic polymers and a silica material made from sodium silicate using a novel two-point labeling technique with a pyranine dye to determine if previous studies were indeed correct. Our results show that the two-point labeling technique with pyranine provides a more rigid interaction between the polymer and the dye compared to the previous labeling method using fluorescein, allowing for more accurate monitoring of dynamic motions of cationic polymers in sol-gel derived materials. The dynamics of poly-D-lysine entrapped in sol-gel derived materials was indeed seen to be highly restricted, contrary to results obtained in previous studies.

While the first project provided a framework for understanding the effect of electrostatic interactions on the dynamics of biomolecules, it also provide valuable insight into the effect of non-specific interactions between cationic species and sol-gel derived materials in general. These considerations are important when using sol-gel based affinity columns for small molecule screening. The second study outlines a competitive affinity-based screening method using mass spectrometry (MS) detection that can help reduce the effect of non-specific interactions between test compounds and the column matrix in small molecule screening applications. This technique relies on the use of a high-affinity indicator compound pre-equilibrated on column to identify weak affinity ligands in mixtures through transient spikes in the indicator signal that result from the competition between the indicator and test compounds. The results of this study demonstrate the ability to identify weak affinity ligands for the *nicotinic* acetylcholine receptor (*n*AChR) using low to sub-picomole amount of active receptor on column. The technique results in a reproducible signal output that can potentially be used to obtain quantitative data on the binding affinities of target-ligand interactions. The assay is amenable to automation and can be performed at high speeds, thereby demonstrating the potential of this technique as a high-throughput screening tool for screening membrane receptors.

ACKNOWLEDGEMENTS

I would like to thank my supervisor Dr. John D. Brennan for his continued guidance and support throughout the duration of my studies. I would also like to thank Dr. Dina Tleugabulova, Dr. Travis Besanger and Dr. Nick Rupcich for their help with my various projects and for the great insight and ideas they provided throughout my project.

Thank you to my current and former labmates for their support and friendship during my studies. Thanks to my committee members, Dr. Eric Brown, Dr. Paul Berti and Dr. Graham McGibbon for their support, continued input in the project and for reading and revising my work. Thanks also to the support staff in the biochemistry office for assisting me throughout my studies.

Finally, thanks to the close friends who have so closely supported me. Special thanks to my parents, my brother, my sister and my brother in-law for their support, encouragement and advice throughout my journey.

TABLE OF CONTENTS

LIST OF TABLES

LIST OF FIGURES

LIST OF ABBREVIATIONS

ALIS	Automated Ligand Identification System
AM1	Semi-empirical Austin Method
AR	Acoustic Resonance
Arg	Arginine
AS	Affinity selection
AS-MS	Affinity Selection Mass Spectrometry
AUC	Area under the curve
Avg	Average
B_t	Amount of active receptor
cAMP	Cyclic adenosine monophosphate
CDC	Competitive Displacement Chromatography
D2R	Dopamine D2 Receptor
Da	Dalton (g/mol)
DC	Direct current
DGS	Diglycerylsilane
DHFR	Dihydrofolate reductase
DNA	Deoxyribonucleic acid
DSC	Differential Scanning Calorimetry
Eph B2	Erythropoietin-producing hepatocellular B2 receptor
EPR	Electron paramagnetic resonance
ESI	Electrospray Ionization
FAC	Frontal Affinity Chromatography
FAC-MS	Frontal Affinity Chromatography Mass Spectrometry
Fl	Fluorescein
FRET	Fluorescence resonance energy transfer
GLUT1	Glucose transporter 1 receptor
GnT-V	N-acetylcholine glucosaminyl transferase
GPCRs	G-coupled protein receptors
GTP	Guanosine triphosphate
HEPES	4-(2-hydroxyethyl)-1-piperazineethanesulfonic acid
HGP	Human Genome Project
hOCT1	Human organic cation 1 receptor
HPLC	High performance liquid chromatography
HSA	Human serum albumin
HTS	High-throughput screening
IAM	Immobilized Artificial Membranes
IC_{50}	Half maximal inhibitory concentration
k'	Chromatographic capacity factor or retention factor
[L]	Ligand concentration
LC	Liquid Chromatography
LGICs	Ligand-Gated Ion Channels

Lys	Lysine
M^+	positively charged molecular ion
M^-	negatively charged molecular ion
MALDI	Matrix Assisted Laser Desorption Ionization
Min	Minutes
MM+	molecular mechanics
MRM	Multi Reaction Monitoring
MS	Mass Spectrometry
MS-MS	Mass spectrometry-Mass spectrometry
MW	Molecular Weight
m/z	mass to charge ratio
*n*AChR	*nicotinic* Acetylcholine Receptor
NH_4Oac	Ammonium acetate
NMDA	N-methyl d-aspartate receptor
NMR	Nuclear Magnetic Resonance
PAM	Polyallylamine
PEI	Polyethylene imine
PgP	P-glycoprotein
Phe	Phenylalanine
PL	poly-D-Lysine
PO	Poly-L-Ornithine
PR	Poly-L-Arginine
PUF-MS	Pulsed Ultrafiltration Mass Spectrometry
Pyr	Pyranine
rf	radiofrequency
RFLP	Restriction Fragment-length Polymorphism
RNA	Ribonucleic Acid
RNAse A	Ribonucleic acid nuclease A
SEC	Size exclusion chromatography
TCSPC	Time-correlated Single Photon Counting
TOF	Time-of-flight
TRFA	Time-Resolved Fluorescence Anisotropy
TRIS	Tris(hydroxymethyl)aminomethane hydrochloride
Trp	Tryptophan
Tyr	Tyrosine
UF	Ultrafiltration
V_e	Elution volume
V_o	Void volume

Chapter 1

Introduction

1.1 Chemical Genetics in Understanding Gene Function

1.1.1 Introduction to Chemical Genetics:

While the completion of the human genome project (HGP) in 2003 helped identify numerous human genes likely associated with disease, the function of these genes in particular disease states is poorly understood.[1] Fueled by the potential to produce highly specific drug therapies, many have sought easy and efficient methods for elucidating the cellular events controlled by disease-related genes to provide further insight into the causes of non-native cellular responses. In particular, cellular events modulated by membrane proteins have become particularly interesting of late, as recent studies have implicated these target proteins in many diseases, including cancer, Parkinson's and Alzheimer's disease.[1,2,3] Traditionally, classical genetics methods have been used to study gene function by conditionally or permanently altering gene function through the introduction of random mutations to genomic DNA or through other common genetics techniques, including using knockout/knock-in organisms or performing RNA interference experiments.[4] However, specific challenges have emerged that have prompted many to seek complementary approaches, such as chemical genetics, to understand the role of these gene products in certain processes, particularly those expressed on the cell surface.

Whereas the classical genetics approach seeks to understand gene function through genetic mutations, the chemical genetics approach uses small molecule

compounds to mimic genetic mutations by indirectly altering gene expression through the inhibition of a gene's cognate protein.[5] Based on concepts developed as early as the eighteenth century, chemical genetics relies on identifying pure biologically active compounds that bind to specific molecular targets within an organism.[6] The goal of chemical genetics is to use these compounds to perturb biological systems to gain information that illuminates the function of particular genes in biological processes.

As in classical genetics, chemical genetics uses two analogous approaches to probe biological function, namely forward and reverse chemical genetics.[6,7,8] In the forward approach, gene function is elucidated by linking specific phenotypes (e.g. morphology, growth, behaviour) to a genetic cause without knowledge of a specific gene-target.[7,8] That is, a desired phenotype is identified and subsequently correlated to a specific gene by identifying the genetic mutation responsible for the observed phenotype through genetic mapping (e.g. sequencing, restriction fragment length polymorphism (RFLP) mapping etc).[9] In the same way, the forward chemical genetics approach (phenotype-based) connects phenotypes induced by small molecules to particular genes by identifying the target protein being acted upon. Typically, small molecule libraries are screened for compounds that induce non-native phenotypes and the probe is then used to identify the target protein through affinity capture techniques, allowing one to infer a gene's function.

In contrast to forward approaches, the reverse approach requires prior knowledge of a gene target and searches for the corresponding phenotype that results from altering its expression.[6] In classical genetics, molecular biology approaches are often used to

introduce specific mutations in a known gene and differences between mutant and wild-type phenotypes are used to infer gene function.[7,8] Using similar logic, the reverse chemical genetics approach (target-based) uses small molecules to alter the activity of a known protein target and the phenotypes are studied to determine the resultant effect on the biological system. That is, small molecule libraries are screened for compounds that have affinity for a known protein target *in vitro* and the subset of compounds identified is used to perturb a functioning biological system *in vivo* to study the resultant phenotypes.

1.1.2 Advantages of Chemical Genetics

While classical genetics approaches have traditionally been invaluable for studying gene function, chemical genetics approaches offer several unique advantages. In classical genetics, the process of making genetic mutations can be a difficult and time consuming task, particularly when studying complex organisms (e.g. mammals) with large diploid genomes, slow reproduction rates and large physical size.[6,7] In addition, many genetic mutations are not conditional and may prove to be lethal to the organism under study, hence providing little information on the biological processes regulated by specific genes given that no unique phenotype is observable.[7] Classical genetics approaches are also not suitable for studying genes expressed in the later stages of the life cycle, particularly when organisms with long life spans are being studied, and cannot be easily applied to study proteins with multiple functions, since gene-deletion results in the loss of all functions of the removed gene.[6,7]

By contrast, the chemical genetics approach provides a more flexible means to study cellular processes in both cellular and animal systems, as small molecules can be rapidly introduced into biological systems under physiological conditions.[7] In addition, the time required for a change in phenotype is limited only by diffusion, hence, chemical genetics screens are much less time-consuming than those performed using the classical genetics approach. Although chemical genetics approaches attain less specificity in controlling gene function, given that small molecules can often have 'off-target' effects, small molecules can be administered in sub-lethal doses and interactions with the target are often short-lived and reversible, thereby limiting the possibility of permanently damaging the system being studied.[7] This latter benefit also provides an opportunity for the therapeutic development of the small molecule probe once the biological process being regulated is fully understood.[8] The potential for studying multiple 'knockouts' using chemical genetic screens also exists, since a number of small molecules can be introduced to the system simultaneously.[7] Finally, the opportunity to dissect the function of proteins with multiple roles remains feasible, as small molecules can be tuned to target one specific protein isoform.

1.2 Phenotype-Based vs. Target-Based Screening

While noticeably different in approach, both forward (phenotype-based) and reverse (target-based) chemical genetics offer unique insight into the functional roles of genes in biological processes (Scheme 1.1).

*Scheme 1.1: Forward (Phenotype-based) vs. Reverse (Target-based) Chemical Genetics**

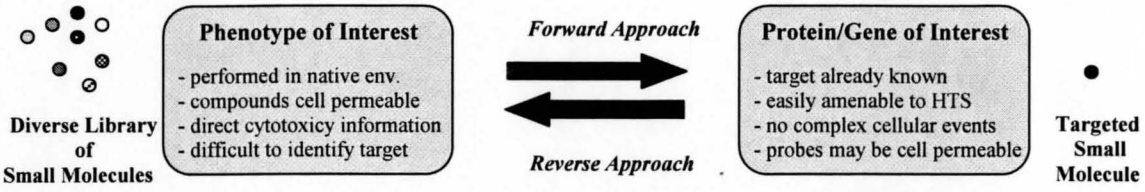

*Adapted from reference 7.

1.2.1 Forward Chemical Genetics-The Phenotype-based Approach

In the forward chemical genetics approach, phenotype-based screens are developed around a quantifiable phenotype output and bioactive small molecules are screened for their ability to induce that phenotype using high-throughput screening (HTS) methods.[6,7,8] The desired phenotype can range from cell shape to sub-cellular localization of specific biomarkers; however, phenotypes that present in two-states (e.g. phosphorylated vs. unphosphorylated target) are often more favorable, given that they can be easily distinguished from wild-type phenotypes. Although the complexity of cellular processes can complicate the development of HTS formats, a successful phenotype-based screen can potentially identify small molecules capable of regulating networks of molecular interactions,[6] the best-known example being the identification of FK506 in modulating calcineurin in the T-cell mediated signaling pathway.[10] In addition, phenotype-based screens also yield small molecules that are cell-permeable and provide immediate information on the cytotoxicity of a probe, as the majority of phenotype-based screens are conducted in cellular environments, thereby preserving the complexity of the

biological system.[6,7,8] This eliminates the need for time-consuming optimization of newly identified chemical probes, a major drawback that complicates target-based approaches.[7]

While it can be argued that phenotype-based screens provide a superior approach to understanding a target's activity in its native environment, the process of identifying the target biomolecule once a chemical probe has been identified presents a significant challenge due to biological complexity.[7,11] Traditionally, target identification has involved using an immobilized form of the bioactive small molecule to 'affinity-capture' the target from cellular extracts.[11] However, these methods are ineffective in identifying targets when low affinity small molecules are discovered, as the low specificity and selectivity often results in many non-specific proteins being isolated from cellular extracts. Although advantageous for understanding proteins with redundant function, the process of deconvoluting non-specific proteins from the actual target can be cumbersome and time-consuming. Additionally, affinity-capture methods often require that the target protein be in high abundance to distinguish the target from background and may necessitate chemical modifications to the small molecule probe to produce a suitable capture platform, potentially compromising the integrity of the ligand-target interaction.[11] While several alternative approaches to identify targets exist (e.g. three-hybrid systems),[5,11,12] the value of these approaches has yet to be fully explored and their use with a diverse range of target classes may be limited.

1.2.2 Reverse Chemical Genetics: The Target-based Approach

In contrast to the forward approach, reverse chemical genetic screens provide a simpler alternative to study gene function, given that these approaches build upon previous studies that have identified and validated important biomolecular targets using techniques, such as over-expression systems, RNA interference experiments and informatics approaches.[6,7,8] These validated targets are used to develop small molecule screens *in vitro* to discover bioactive small molecules that act on the isolated target. Target-based screens can be developed around functional or affinity-based outputs to screen small molecule probes using assay formats amenable to HTS, however, the need to optimize newly identified probes for cell permeability and the lack of potency of these probes are often cited as major drawbacks.[7] Nonetheless, target-based screens are generally easily adaptable to HTS formats and the potential to rapidly and efficiently identify new compounds using HTS adds to the appeal of reverse chemical genetics screens.

Although target-based techniques provide little useful information on the complexity of cellular pathways, the reverse chemical genetics approach provides an orthogonal approach for understanding gene function when cellular complexity complicates phenotype-based screens.[12] In particular, target-based approaches have proven effective in elucidating the function of many membrane protein targets,[13,14] a target class that have presented major challenges to phenotype-based screens due to their diverse roles in multifaceted cell signaling pathways.[11] A disproportionate number of therapeutic targets identified for currently approved drugs are membrane proteins,[2,3]

hence, recent efforts have been directed towards understanding the role of these targets in disease states. With information stemming from the human genome project indicating that ~750 genes show ~45% sequence identity to known G-protein coupled receptors (GPRCs),[15] an important class of membrane receptors involved in signal transduction, methods for identifying the function and ligands for the remaining orphan GPCRs and other orphan membrane receptors remain a priority.

1.3 Target-based Approaches Applied to Membrane Proteins

1.3.1 Target-based Functional Assays for Membrane Proteins

Several functional target-based assays have been developed to study membrane receptors with unknown function (i.e., orphan receptors), a great deal of these relying on the use of second messenger reporters to monitor receptor activity through activation of common signaling cascades (Table 1.1). While using classical reporter gene systems activated by cAMP response elements (e.g. luciferase-based reporter systems) has been the standard method for monitoring activation of signalling cascades,[13,16] the need to construct an appropriate reporter system can be difficult and usually requires knowledge of the signaling pathways being regulated. Because these methods also lack the necessary throughput required for large scale screening campaigns, assays utilizing fluorescence detection systems (e.g. florescence polarization and fluorescence energy transfer) to quantify the release of fluorescent or radioactive analogs of second messengers (e.g., cAMP or [^{35}S]GTPγS) upon receptor activation have become more favorable,[17,18,19] as these methods are less laborious and can be coupled to standard HTS instrumentation

(i.e., microtiter plate screening formats). The synthesis of specialized ion sensitive fluorescent dyes that quantitate intracellular Ca^{+2} levels upon ligand induced stimulation of membrane receptors (e.g. Alexafluor and Cy5, fluo-4, fura-2) have provided yet another method for detecting receptor activity in response to test compounds and further increased throughput.

Table 1.1 Common Functional HTS Techniques used to Screen Membrane Receptors

Method	**Procedure/Detection**	**Major Advantages**	**Major disadvantages**	**Throughput**
Second Messenger Reporter Systems	-2^{nd} messengers systems (e.g. luciferase or fluorescent analogs of 2^{nd} messengers) report changes in signalling events in response to test compounds	-provides details on specific cellular events being modulated by chemical probes	-prior knowledge of signalling pathway required to construct appropriate reporter assay -can be complicated by targets with redundant function. -only applicable to targets involved in specific signalling events.	Low
Fluorometric Imaging Plate Reader (FLIPR™)	-calcium or voltage-sensitive dyes report on intracellular events through changes in fluorescence. -compounds are screened for activity based on their ability to induce changes in fluorescence.	-amenable to standard HTS instrumentation. -very high throughput	-cellular response may be to fast to detect transient changes in fluorescence -generally used with live cells, hence length of screening campaign can compromise cell function when large libraries are screened	High
FRET-based reporter systems to monitor conformational changes.	-monitors conformational changes in membrane receptors using FRET-based detection. -receptor is expressed with fluorescent proteins tagged at C-terminus (e.g. CFP donor) and N-terminus (YFP acceptor). -intramolecular FRET monitored upon ligand stimulation.	-very specific information at single protein level. -not complicated by off-target effects.	-need to engineer appropriate FRET donors/acceptor system into target receptor. -may be complicated by interfering fluorescence phenomena.	Low
Automated Patch-clamping	-microelectrodes attached to single receptor on cell surface monitor fluctuations in membrane potential. -changes in membrane potential	-information provided at single protein level. -very specific information provided	-requires high skill and precision to perform experiments -generally low throughout and labour	Medium

	are monitored in response to different test ligands.	for ligand gated ion channels.	intensive, although automated systems are now available.	

While effective, techniques that rely on second messenger reporters require a detailed understanding of the signaling pathways controlled by the target membrane receptor to construct an appropriate reporter assay and are not generally applicable to membrane protein targets that are not involved in signaling cascades. Functional techniques that probe activity of other membrane receptors have recently been developed and employ a range of assay formats. For example, assays that measure fluorescence resonance energy transfer (FRET) between two fluorophores situated in close proximity on the protein have been used to monitor structural changes of membrane proteins in response to ligand stimuation.[17] In addition, several methods that monitor ion flux through specific targets have also been developed allowing activity measurements at the single protein level, patch clamping being one such technique that measures changes in membrane potential through tiny microelectrodes attached to the cell surface.[13] Radioactive ion flux assays that monitor influx and efflux of radiotracers in response to ligand stimulation have also been successfully adapted for functional screening.[19] The high-precision and skill required for many of these techniques, however, has been viewed as an obstacle to adapting these techniques to HTS strategies, thereby favouring the development of simpler, more robust affinity-based alternatives.

1.3.2 Target-based Affinity Assays for Membrane Proteins

Target-based screens that identify novel small molecule interactions through affinity provide a more generic approach to screen receptor targets and are being used to screen membrane receptors with diverse functions (Table 1.2). While fluorescence or absorbance-based detection systems have generally predominated (e.g., proximity or fluorescence polarization assays), interfering factors resulting from the auto-fluorescence of small molecules or the quenching of reporter fluorophores by test compounds have limited the potential of using these detection methods to screen multiplexed compound mixtures,[18,20] a trend that is becoming increasingly popular to increase screening throughput. The introduction of labels to either the target or the compound libraries can also compromise the target-ligand interactions by altering the molecular conformation of the target or by blocking ligand binding through steric hindrance and has encouraged many to develop label-free assays that identify novel compounds through affinity.[20]

Table 1.2 Common Affinity HTS Techniques used to Screen Membrane Receptors

Method	Procedure/Detection	Major Advantages	Major disadvantages	Throughput
Label-dependent Assays AlphaScreen™ (Proximity Assays)	-receptors and test ligands are coupled to photosensitive donor/acceptor beads. -binding events bring acceptor and donor beads into close proximity leading to chemiluminescence of acceptor bead.	-very sensitive to binding events. -amenable to HTS instrumentation -low cost	-requires covalent coupling of receptors to beads, thereby compromising activity -ligands also need to be coupled to bead, limiting the ability to screen complex mixtures	High
Radioligand-binding Assays	- purified receptors are incubated with radiolabelled ligands. -amount of specific ligand bound quantified using scintillation counting.	-provides accurate binding data for ligands.	-use of radioligands causes safety concerns -poor sensitivity	Low

Method	Procedure/Detection	Major Advantages	Major disadvantages	Throughput
Fluorescence Polarizations Assays	-receptor is incubated with fluorescently labelled ligands and polarization of the fluorescent ligand is monitored to detect binding events -increase in polarization indicated a compound has bound to the receptor	-generally used as a cell-based screening technique, avoid problems with receptor activity. -relatively facile -amenable to current HTS instrumentation.	-need fluorescently labelled ligands -problems with interfering fluorescent phenomena prevent screening of complex mixtures.	Medium to High
Label-Free Methods:				
Surface Plasmon Resonance Biosensors (Optical Detection)	-receptors are immobilized to surface of gold-plated sensor illuminated with a beam of light. -ligand binding is detected based on changes in the refractive index that results from the presence of the ligand at the surface.	-highly sensitive -can detect amount of bound analytes and provides kinetic parameters.	-Not amenable to complex mixtures -can be complicated by high backgrounds -may be complicated by different components in buffers.	Low
Acoustic Biosensor Assays	-targets are coupled to a piezoelectric (oscillating) quartz crystal. -binding events are detected based on changes in the frequency of oscillating quartz crystal that result when ligands bind to the receptor.	-not sensitive to changes in solvents -low rate of false positives.	-Low through-put -Technically challenging due to various components involved in the instrument setup.	Low
Calorimetry Assays (Isothermal titration calorimetry)	-measures heat released or absorbed upon a titration of ligand into a solution contain the receptor target.	- best method to determine thermodynamic parameter of a molecular interaction.	-limited throughput, although automation and miniaturization is being introduced.	Medium to High
Mass Spectrometry Affinity Assays	-target is used to affinity select compounds from a complex mixture. Bound compounds are identified by MW using MS detection. -compounds in a mixture can be screened for affinity using frontal chromatography. MS detection is used to monitor the frontal retention of compounds.	-can be used for complex mixtures -potential to elucidate structural features of unknown compounds	-high rate of false positives due to non-specific interactions. -relatively low throughput, although recent developments have achieve respectable levels	Medium

In general, label-free methods are recognized as an easier alternative to label-dependent methods, as they provide accurate, information-rich data that is not skewed by

the interfering factors outlined above.[20,21] Although initial label-free methods employed highly specialized optical biosensors to detect ligand-target interactions (e.g., surface plasmon resonance),[22] these techniques are slowly being replaced by platforms based on other detection systems, such as acoustical resonance (AR), differential scanning calorimetry (DSC) and mass spectrometry (MS), as the former systems attain limited throughput, lack the flexibility required to screen certain receptor targets and are complicated by high background due to extremely high sensitivity.[20] Recent developments to the latter platforms, however, have enabled users to easily probe the function of a variety of membrane protein targets and have provided information on kinetic and thermodynamic parameters related to compound binding. The use of mass spectrometry in affinity-based screens has attracted particular interest recently,[23,24] as the potential to identify structural features of unknown compounds in complex mixtures using MS detection has provided yet another dimension that adds to the allure of label-free detection systems.

1.4 Affinity-Based Methods using MS

The introduction of MS detection in affinity screening formats has provided superior sensitivity and a greater potential for characterizing compounds in complex mixtures, as compound fragmentation can be used to elucidate potential structures of unknown compounds. Although a number of affinity assays have been developed that utilize MS detection,[23,25,26] the majority of these techniques can be classified into two

categories, namely off-line (discontinuous-flow) and on-line (continuous-flow) techniques.

1.4.1 Off-line Affinity Based Techniques with MS Detection

The pioneering work of Kaur and coworkers[27,28] introduced the concept of affinity selection-mass spectrometry (AS-MS) experiments, whereby a target is used to first 'affinity-select' small molecule probes from mixtures off-line and MS detection is used to separately identify the selected compounds. Early models of this approach, such as that used by Kelly et al. (29) to identify novel ligands for SH2 domains,[29] involved the incubation of the target biomolecule with a mixture of compounds in solution followed by the removal of unbound compounds using size exclusion chromatography (SEC). The isolated protein/ligand complexes were then denatured to release bound compounds and injection of bound compounds into an MS detector identified compounds from their molecular weight (MW). The early success of this approach has since led to more sophisticated approaches that increase throughput through the use of microtiter plates for incubation steps[30] and ultrafiltration[31] methods for separating unbound compounds from protein/ligand complexes and have successfully been used to identify small molecule probes of key cellular proteins, including the cell cycle checkpoint protein, Chk1.[32]

While the AS-MS approach has been incorporated into current drug discovery platforms, including the microwell-based SpeedScreen™ format at Novartis Pharma AG,[30] these techniques are limited by several factors. Specifically, because the incubation, separation and detection steps are performed discontinuously, the length of

these experiments can compromise the ability identify bound compounds, as complexes with fast-off rates are often poorly recovered and dilution can leave very little bound compound for detection. In addition, isolation steps are often carried out under non-equilibrium conditions, leading to significant dissociation of protein-ligand complexes and a high rate of false negatives.[33] An additional desalting step is also usually required following isolation of the protein-ligand complexes to ensure buffer salts do not interfere with MS detection, further diluting samples. Most importantly, separation steps based on SEC or ultrafiltration are not favourable for membrane protein targets, as the flow in SEC resins or MW cut-off filters may be obstructed by the receptor, given that these targets are often purified as large liposomes or membrane fragments. While direct detection of protein/ligand complexes can eliminate separation steps in AS-MS experiments,[34,3536] interpretation of data generated from membrane protein complexes is difficult due to the presence of a lipid bilayer.

1.4.2 On-line Affinity Based Techniques with MS Detection

The development of several on-line approaches that directly couple various steps in affinity selection experiments using liquid chromatography (LC) systems have helped alleviate many of the problems associated with off-line techniques. In the simplest approach, compounds are incubated with the target off-line and subsequently applied to an SEC column that is directly coupled to an LC-MS detection system, thereby reducing the time required for an experiment and minimizing the risk of protein-ligand dissociation.[33] Pulsed-ultrafiltration (PUF) systems use a similar approach that directly

couples an ultrafiltration cell containing the target to an LC-MS detection system.[37,38,39] Compounds are first introduced into the ultrafiltration cell as a short pulse in the LC mobile phase. The resultant protein/ligand complexes are retained in the reaction cell, while unbound compounds are carried through a MW-cutoff filter in the ultrafiltration cell with the mobile phase. A denaturant is subsequently applied to dissociate protein/ligand complexes and bound compounds are able to directly flow into an MS detector for analysis. A third technique, known as the automated-ligand identification system (ALIS), integrates a rapid on-line SEC separation step into a fully automated on-line system that rapidly identifies missing compounds from a mass encoded compound library following an affinity selection step.[40,41] While this latter approach has recently been successful in identifying ligands for membrane proteins, the general application of AS-MS methods to screening receptor targets is complicated due to problems inherent in the separation step, as discussed above.

Recent developments in column chromatography techniques have provided alternative approaches to the traditional AS-MS methods and combine incubation, separation and detection steps using LC-MS systems for rapid detection of compounds having affinity for the target. In particular, the use of frontal affinity chromatography (FAC) with MS-based detection (FAC-MS) has emerged as a powerful technique to characterize small molecule interactions with biomolecules, as FAC-MS can be performed on-line and provides kinetic parameters of test compounds under equilibrium conditions.[42,43,44] With the ability to screen membrane receptor targets using high volume

compound libraries becoming apparent[45] and the potential for automation recently being realized,[46] FAC-MS is being viewed as viable on-line affinity-screening method.

1.4.3 Frontal Affinity Chromatography-MS for Membrane Protein Screening

Developed by Kasai et al. (47) as a generic tool for studying biomolecular interactions,[47,48] the coupling of FAC to MS detection by Schriemer et al. (42) has led to significant improvements in affinity-based screening using MS detection.[42] In the FAC-MS approach, a set of compounds is continually infused into an affinity column containing the immobilized target, allowing an equilibrium to be established between the test compounds and the target protein. Once equilibrium is established between a given compound and the target receptor, compounds emerge from the column in order of their relative affinity for the target, high affinity ligands eluting first followed by lower affinity ligands as predicted by the following equation derived from the law of mass action: [43]

$$V = V_0 + \frac{B_t}{K_D + [L]} \tag{1.1}$$

where V is the elution volume of a test compound, V_o is the elution volume of a column void marker, B_t is the amount of active receptor contained on column, K_d is the dissociation binding constant of a compound for a given target and [L] is the ligand concentration being infused. Using a detection mode that allows for the monitoring of multiple compounds at once, known as multi reaction monitoring (MRM) mode, the user

can observe the equilibrium state of compounds on the column in real-time. Unlike conventional chromatography, compounds that have reached equilibrium emerge from the affinity column appearing as sigmoidal fronts, initially showing no signal intensity and eventually plateauing at the original concentration of ligand being infused (Fig. 1.1).

Figure 1.1. Typical Set-up and Output of FAC-MS Affinity Experiments.

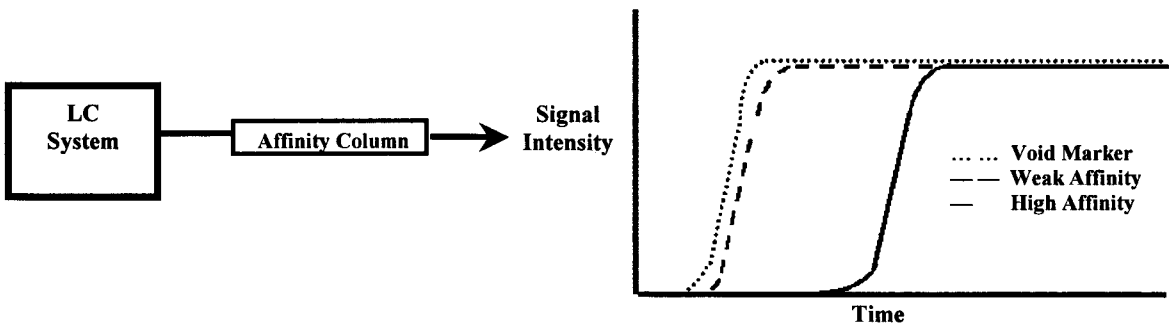

Being an equilibrium-based technique, the problems associated with the separation of protein/ligand complexes encountered in affinity selection techniques are generally avoided in the FAC-MS approach. In addition, because columns containing an immobilized form of the target are employed, no separation steps are necessary to remove unbound compounds and the denaturation of protein-ligand complexes is avoided, allowing for the re-use of proteins for multiple screening trials. Recent advances in the fabrication of affinity columns containing active membrane receptors have also accelerated the use of FAC-MS for screening membrane protein targets,[49,50,51] a significant accomplishment given the limitation of other techniques outlined above.

Original affinity columns containing active membrane receptors employed bead-packed matrices, whereby beads containing an immobilized form of the receptor target comprise the stationary phase of the affinity column.[49,50] The most widely used platform utilizes derivatized silica beads, known as immobilized artificial membrane (IAM) beads,[49,52] containing a monolayer of phospholipid analogs that provide a hydrophobic surface to embed membrane fragments containing the target receptor. These columns have proven effective for characterizing ligands for the human organic cation 1 (hOCT1) receptors using FAC with radiometric detection,[53] and more recently for understanding the binding affinities of several inhibitors of the $\alpha_3\beta_4$ isoform of the *nicotinic* acetylcholine receptor using FAC-MS.[54] Other methods for preparing affinity columns containing membrane receptors have included electrostatic or covalent coupling of liposomes to controlled pore glass beads, or the reconstitution of purified membrane receptors into gel bead, as demonstrated by Lundahl et al. (50) using the GLUT1 receptor.[50]

Recent advances in sol-gel technology have provided yet another alternative for protein immobilization, as monolithic columns containing sub-picomolar levels of active membrane receptors can be produced using biocompatible silica matrices.[51] Specifically, entrapment of active forms of the *nicotinic* acetylcholine receptor (*n*AChR) from *Torpedo Californica* and the Dopamine D2 Receptor using a biocompatible sol-gel processing method has been recently demonstrated[55,56] and the potential for performing small molecules screens using FAC-MS has been shown with capillary-scale affinity columns containing *n*AChR.[51] While the simple two step process used in fabricating these

columns[57,58] (Scheme 1.2) eliminates the need for complicated steps used in the preparation of bead-based columns and alleviates problems with active site accessibility due to improper orientation,[59] several challenges remain when using these affinity columns for small molecule screening.

Scheme1.2: Biocompatible Sol-gel Processing Method

1) $Si(OR)_4 + H_2O + H^+$	$Si(OR)_{4-n}(OH)_n$ + n ROH	***Hydrolysis***
2) 2 $Si(OR)_{4-n}(OH)_n$	$(OH)_{n-1}(OR)_{4-n}Si\text{-}O\text{-}Si(OR)_{4-n}(OH)_n + H_2O$	***Condensation***
3) n -Si-O-Si-	$[\text{-Si-O-Si-O-Si-O-Si-O-}]_n + H_2O$	***Polycondensation***
4) n $[\text{-Si-O-Si-O-Si-O-Si-O}]_n$ + buffer + protein	Entrapped Protein	***Gelation***
5) Condensation and Polycondensation continue for days, shrinking gel		***Aging***
where R=biocompatible functional group (e.g. glycerol)		

1.4.4 Challenges to the FAC-MS Approach when Screening Membrane Proteins

The variables governing compound separation in FAC-MS experiments (equation 1.1) shows that the resolution of compound separation (i.e., $V\text{-}V_o$) improves with increasing amounts of active receptor, B_t. In practice, however, the ability to attain efficient separation for a range of compounds with varying affinities remains a significant challenge,[43,60] partly due to the desire to build assays using less target but mainly due to the low abundance of many membrane receptors. That is, because these targets are often purified as membrane fragments or liposomes containing more than one cell surface protein, the purified membranes are generally poorly enriched in the desired target. Over expression systems may be used to produce large quantities of a given receptor but are

not suitable in all cases, as these systems can often result in the production of inactive or insoluble aggregates of the desired target and can be toxic to the host organism.[61] Even when successful, improper orientation of the target receptor in the host membranes may leave the receptor inaccessible for affinity-based studies and an appropriate purification protocol is required to preserve function, a difficult task due to problems with detergent incompatibilities. Furthermore, immobilization of the receptor target in a suitable affinity column matrix must also preserve the conformational mobility required for the receptor to bind to a particular ligand.[62,63] These considerations have restricted the ability to produce membrane protein affinity columns with high loading densities for many targets and as such, the FAC-MS approach has been more successful at identifying and characterizing high affinity ligands (nM range) for receptor targets, while lower affinity ligands (μM range) are more commonly undetected due to poor retention.[60]

Non-specific interactions have also been known to obscure data interpretation in FAC-MS affinity screening applications, as unwanted interactions of test compounds with either the column matrix or lipid membranes can cause a non-specific 'hit' to falsely appear as a high affinity ligand.[64] In cases where sub-picomolar amounts of receptor are employed, the number of non-specific binding sites can approach the same order of magnitude as the number of specific binding sites present on column, leading to a high rate of false positives. Specific precautions are warranted when employing silica-based stationary phases using the sol-gel processing method, seeing as the net negative charge on the exposed silica surface can lead to significant retention of cationic small molecules.[65] Affinity columns prepared using IAM bead matrices have also shown

significant non-specific retention of hydrophobic compounds due to unwanted interactions with the phospholipid analogs grafted on the surface of these beads, the classic example being the non-specific retention of hydrophobic substrates for the drug efflux pump, P-glycoprotein (PgP).[64] Although several strategies have been devised to neutralize these types of non-specific interactions, such as employing modified silica surfaces in sol-gel columns to create a zwitterionic surface[66] or employing other immobilization strategies to reduce the degree of hydrophobicity in IAM-based columns,[64] the general applicability of these strategies is unknown and may indeed render certain receptors inactive.

Yet another type of non-specific interaction that complicates FAC-MS affinity screens is the interactions of test compounds with other proteins present in the purified membrane fragments. Although control columns containing heat denatured membrane fragments have been effective for ascertaining non-specific interactions between test compounds and the lipid membrane,[51] these columns are ineffective for ascertaining non-specific interactions with off-target proteins since all proteins in a given sample are denatured. While control columns that employ target-specific antibodies to 'cap' the active site of the target receptor can conceivably eliminate off-target interactions, the inclusion of an antibody on the column may introduce unwanted interactions between the capping antibody and the test compounds, further complicating analysis. The ideal control experiment involves testing affinity columns prepared using membrane fragments purified from +/- cell lines, however, this luxury is often not afforded when previously uncharacterized orphan receptors are being screened. As such, FAC-MS experiments

usually employ a range of different control columns to ascertain the degree of non-specific interactions, oftentimes requiring complicated setups to run multiple columns in parallel to increase productivity.[67,68]

Perhaps the greatest perceived flaw of the FAC-MS approach is the relatively limited throughput achieved in mixture screening applications.[45,46] While the potential to screen complex mixtures exists, the ability to screen large mixtures has been complicated by several factors, including buffer incompatibilities and the inability to individually monitor several hundred or thousands of compounds each having a unique molecular weight.[45] More specifically, because MS detection monitors compounds in an ionized state, compound mixtures need to be prepared in a buffer that favors ionization, a requirement that is often not met given that many mixtures exist in incompatible organic solvents. In addition, because the FAC-MS approach monitors frontal retention of individual compounds, the ability to resolve the mass of each compound in a given library is compulsory, a requirement that has also proven to be beyond the capability of current MS detectors when large compound libraries are screened.

Given the above considerations, FAC-MS has been commonly coupled to complementary approaches to screen large libraries containing thousands of compounds, the most successful example employing forward phase chromatography systems in tandem with FAC-based separations to screen a compound library of 1000 compounds for bioactive compounds targeting the *N*-acetyl-glucosaminyltransferase V (GnT-V) enzyme.[45] Briefly, this approach applied a directed compound library to a GnT-V affinity column and used frontal chromatography to separate the mixture into nine fractions of

increasing affinity, early fractions having lower affinity, later fractions having higher affinity for the target, as dictated by equation 1.1. Fractions were subsequently resolved into individual compounds using hydrophilic-interaction chromatography and injected into an MS detector to identify the bioactive components in each fraction. While this two-step approach in identifying ligands for GnT-V was indeed successful, the added labor required for this multidimensional approach adds significant time to the screening campaign. Recent attempts to automate the FAC-MS approach may well increase the throughput of these multidimensional approaches, potentially enabling the screening of up to 10,000 compounds per day.[46]

1.5 Thesis Goals:

This thesis attempts to build upon recent successes in the development of the FAC-MS approach, and addresses specific challenges outlined in the previous section from both fundamental and applied perspectives.

1.5.1 Fundamental Aspects of Sol-gel Based Bioaffinity Columns

The first objective was to understand the nature of electrostatic interactions between fluorescently labeled polycationic species and the exposed anionic surface of silica materials. The initial goal was to gain a thorough understanding on how electrostatic interactions between silica materials and biomolecules influence the dynamics of polypeptides, with the ultimate objective being to understand the forces that influence the activity of encapsulated biomolecules in sol-gel derived bioaffinity

columns. Time-resolved fluorescence anisotropy (TRFA) has been a useful tool for evaluating these types of interactions, as it allows one to assess the rotational motions of fluorescently labeled species in sol-gel derived materials.[69,70,71] However, previous studies in our group have yet to provide an explicit understanding of the role that electrostatic interactions have on the behaviour of polycationic species in sol-gel derived materials.[72]

More specifically, previous studies employed the anionic dye flourescein to ionically label a single sidechain of cationic polypeptides;[72] however, rapid motions of the polymer sidechains as well as local motion of the probe about its bond axis can contort the anisotropy data giving the false impression that polycationic species are highly mobile in silica materials, an unexpected result given the anionic nature of silica materials and the cationic nature of the polymers. The first study, therefore, aims to clarify this misconception by utilizing an alternative anionic dye, pyranine, that rigidly binds to the polycationic species through a two-point interaction, therefore more accurately reporting on the true dynamics of the entrapped polycationic species.

The information from this initial study is envisioned to provide a starting point for the development of fluorescence-based techniques that are able to ascertain the conformational mobility of both soluble proteins and membrane receptors in sol-gel derived affinity columns, an important consideration when developing column based screening technologies, as the amount of active receptor clearly influences the resolution and efficiency of FAC-MS screens.[62,63] More generally, a thorough understanding of the role that electrostatic interactions play in non-specific retention of test compounds in

FAC-MS experiments can also be gained. Given that many GPCR receptors are stimulated by cationic polypeptide ligands,[73] this study should provide insight into non-specific interactions that may be encountered when using sol-gel derived affinity columns to screen for ligands that interact with orphan GPCRs.

1.5.2 Applied Aspects of Small Molecule Screening using Sol-gel derived Affinity Columns

The second objective of this thesis was to develop an alternative competitive assay based on the principle of FAC-MS that addresses many of the short-comings of FAC-MS outlined above. In this approach, a known high affinity indicator ligand is first equilibrated on an affinity column containing the immobilized membrane receptor target and test compounds are subsequently injected onto the equilibrated column. The resulting competition between the indicator and the test compounds leads to a transient over-concentration of the indicator while the test compound is present on column. By directly monitoring only the indicator ligand with MS detection, bioactive compounds in test mixtures can be identified through their ability to compete for the same active site occupied by the indicator ligand.

While clearly not all the deficiencies can be addressed, this second study aims to improve three specific areas outline above. First, it is envisioned that the competitive assay format will improve the ability to identify weak-affinity ligands (μM range) with low abundance receptors (sub-picomolar) without having to resort to over-expression systems to obtain larger quantities of active receptor. Second, the competitive approach

to this assay is designed to reduce the rate of false-positives that are associated with non-specific interactions outlined, given that potential ligands are identified strictly by their ability to compete for the specific site occupied by the indicator ligand. This latter point also avoids the need to monitor the molecular weights of each compound in large compound libraries. By utilizing an autosampler to introduce compounds in an automated fashion, it is envisioned that the competitive assay format can achieve higher throughputs compared to the approaches outlined above that use the conventional FAC-MS screening method.

1.6 Thesis Overview:

Chapter 2 provides a basic introduction to the key theoretical concepts involved in the techniques employed in this thesis. Specifically, the relevant theory of TRFA as applied to the study of electrostatic interactions with silica-derived materials and the basics of mass spectrometry as applied to small molecule screening is provided. These are intended to provide the reader sufficient background to understand both the experimental protocols and the models used to interpret data when employing these techniques.

Chapter 3 focuses on a novel two-point binding labeling technique that can be used to accurately assess electrostatic interactions between polycationic species and sol-gel derived monoliths. Specifically, molecular modeling was used to show that the anionic dye, pyranine, favors a two-point interaction with amine groups at positions *i* and *i*+2 along the backbone of several polycationic species, including poly-D-lysine, poly-L-ornithine, poly-L-arginine and polyallylamine. TRFA was used to monitor backbone

motion of the polymers labeled with both flourescein and pyranine and comparison to nuclear magnetic resonance (NMR) dynamics studies revealed closer correlation with TRFA data generated using pyranine labeled polymers compared to that generated with fluorescein. The correlation between TRFA data and NMR data was seen to improve as side chain length decreased, owing to the increased rigidity of the dye-polypeptide interaction. The improved two-point labeling technique was then used to reveal the strong electrostatic interactions between polycationic species and the anionic silica surface in sol-gel derived monoliths prepared using sodium silicate precursors.

In Chapter 4, a competitive assay format is developed using affinity columns containing the *nicotinic* acetylcholine receptor (*n*AChR) as a model protein. The strong affinity ligand epibatidine is used as an indicator compound to pre-equilibrate the affinity column. Nicotine is used as a weak affinity test compound to demonstrate that weak affinity ligands can be identified based on their ability to produce transient spikes in the indicator signal that result from the competition between test ligands and the indicator. Experiments show that the response is specific to actual ligands for the chosen target and that binding events can potentially be correlated to kinetic parameters of the test ligand. Optimization of assay speed demonstrated the potential of this technique for use as a HTS technology to identify and characterized novel ligand-target interactions.

Finally, chapter 5 provides an overall summary of the thesis work with particular focus on the use LC-MS methods in affinity screening. A broad discussion on the implications of this thesis work in the field of chemical genetics follows and future perspectives for the application of this technology are also provided.

1.7 References:

1. Ohlstein, E. H.; Ruffolo, R. R.; Elliott, J. D. *Annu. Rev. Pharmacol. Toxicol.* **2000**, *40*, 177-91.

2. Imming, P.; Sinning, C.; Meyer, A. *Nat. Rev. Drug Discovery* **2006**, *5*, 821-835.

3. Overington, J.P.; Al-Lazikani, B.; Hopkins, A.L. *Nat. Rev. Drug Discovery* **2006**, *5*, 993-996.

4. Broeckel, U.; Maresso, K.; Kugathasan, S. *Pediatr. Clin. North Am.* **2006**, *53*, 807-816.

5. Smukste, I.; Stockwell, B. *Annu. Rev.Genomics Hum. Genet.* **2005**, *6*, 261-86.

6. Stockwell, B. *Nat. Rev. Genet.* **2005**, *1*, 116-125.

7. Walsh, D. P.; Chang, Y. T. *Chem. Rev.* **2006**, *106,* 2476-2530.

8. Kawasumi, M.; Ngheim, P. *J. Invest. Dermatol.* **2007,** *127*, 1577-1584.

9. Jonsson, J. J.;Weissman, S. M. *Proc. Natl. Acad. Sci. USA*. **1995,** *92,* 83-85.

10. Harding, M.W.; Galat, A.; Uehling, D.E.; Schreiber, S.L. *Nature* **1989**, *341*, 758-760.

11. Burdine, L.; Kodadek, T. *Chem. Biol.* **2004**, *11*, 593-597.

12. Stockwell, B. *Trends Biotechnol.* **2000**, *18*, 449-455.

13. Cooper, M. A. *J. Mol. Recognit.* **2004**, *17*, 286-315.

14. Zheng, W.; Spencer, R.H.; Kiss, L. *Assay Drug Dev. Technol.* **2004**, *2*, 543-552.

15. Lin, S.H.; Civelli, O. *Ann. Med.* **2004**, *36*, 204-214.

16. Engel, R. M. *Comb. Chem. High Throughput Screen.* **2005**, *8*, 311-318.

17. Leifert, W. R.; Aloia, A. L.; Bucco, O.; Glatz, R. V.; McMurchie, E. J. *J. Biomol. Screen.* **2005**. *10*, 765-779.

18. Gribbon, P; Sewing, A. *DDT.* **2003**, *8,* 1035-1043.

19. Gonzalez, J. E.; Oades, K.; Leychkis, Y.; Harootunian, A.; Negulescu, P.A.. *DDT.* **1999**, *4,* 431-439.

20. Cooper, M. A. *DDT.* **2006**, *11*, 1068-1074.

21. Proll, G.; Steinle, L.; Proll, F.; Kumpf, M.; Moehrle, B.; Mehlmann, M.; Gauglitz, G. *J. Chromatogr. A* **2007**, [Epub ahead of print].

22. Cunningham, B.T.; Li, P.; Schulz, S.; Lin, B.; Baird, C.; Gerstenmaier, J.; Genick, C.; Wang, F.; Fine, E.; Laing, L. *J. Biomol. Screen.* **2004**. *9*, 481-490.

23. Kelly, M. A.; McClennan, T. J.; Rosner, P. J. *Anal. Chem.* **2002**, *74*, 1-9.

24. Deng, G.; Sanyal, G. *J. Pharm. Biomed. Anal.* **2006**, *40*, 528-538.

25. Johnson, B. M.; Nikolic, D.; van Breemen, R. B. *Mass Spectrom. Rev.* **2002**, *21*, 76-86.

26. Comess, K.M.; Schurdak, M.E. *Curr. Opin Drug Discov. Devel.* **2004**, *7*, 411-416.

27. Kaur, S.; Huebner, V.; Tang, D.; McGuire, L., Drummond, R.; Csetjey, J.; Stratton-Thomas, J.; Rosenberg, S.; Figliozzi, G.; Banville, S.; Zuckermann, R.; Dollinger, G. *in 43rd Conference on Mass Spectrometry and Allied Topics,* p30. Altanta, GA.

28. Kaur, S.; McGuire, L; Tang, D.; Dollinger, G.; Huebner, V. *J. Protein Chem.* **1997,** *16*, 505-511.

29. Kelly, M. A.; Liang, H.; Sytwu, I. I.; Vlattas, I.; Lyons, N.L.; Bowen, B. R.; Wennogle, L. P. *Biochemistry* **1996**, *35*, 11747-11755.

30. Zehender, H.; Le Goff, F.; Lehmann, N.; Filipuzzi, I.; Mayr, L. M. *J. Biomol. Screen.* **2004**. *9*, 498-505.

31. Wabnitz, P. A.; Loo, J. A. *Rapid Comm. Mass Spectrom.* **2002**, *16*, 85-91.

32. Comess, K. M.; Trumbull, J. D.; Park, C.; Chen, Z.; Judge, R. A.; Voorback, M. J.; Coen, M.; Gao, L.; Tang, H.; Korvak, P.; Cheng, X.; Schurdak, M. E.; Zhang, H.; Sowin, T.; Burns, D. J. *J. Biomol. Screen.* **2006**. *11*, 755-764.

33. Blom, K. F.; Larsen, B. S.; McEwen, C. N. *J. Comb. Chem.* **1999**. *1*, 82-90.

34. Sun, J.; Kitova, E. N.; Klassen, J. S. *Anal. Chem.* **2007**, *79,* 416-425.

35. Burkitt, W. I.; Derrick, P. J.; Lafitte, D.; Bronstein, I. *Biochem. Soc. Trans.* **2003**, *31 (Pt 5)*, 981-985.

36. Hofstadler, S. A.; Sannes-Lowery, K. A.; *Nat. Rev. Drug Discovery* **2006**, *5*, 585-595.

37. Gu, C.; Nikolic, D.; Lai, J.; Xu, X.; van Breemen, R. B. *Comb. Chem. High Throughput Screen.* **1999**, *2*, 353-359.

38. Nikolic, D.; van Breemen, R. B. *Comb. Chem. High Throughput Screen.* **1998**, *1*, 47-55.

39. Zhoa, Y. Z.; van Breemen, R. B.; Nikolic, D.; Huang, C. R.; Woodbury, C. P.; Schilling, A.; Venton, D. L.; *J. Med. Chem.* **1997,** *40*, 4006-4012.

40. Annis, D. A.; Nazef, N.; Chuang, C. C.; Scott, M. P.; Nash, H. M. *J. Am. Chem. Soc.* **2004,** *126*, 15495-15503..

41. Whitehurst, C. E.; Nazef, N.; Annis, D. A.; Hou, Y.; Murphy, D. M.; Spacciapoli, P.; Yao, Z.; Ziebell, M.R.; Cheng, C. C.; Shipps Jr, G. W.; Felsch, J.S.; Lau, D.; Nash, H. M. *J. Biomol. Screen.* **2006,** *11*, 194-207.

42. Schriemer, D.C.; Bundle, D. R.; Li, L.; Hindsgaul,O. *Angew. Chem. Int. Eng. Ed.* **1998**, 155-170.

43. Schriemer, D.C. *Anal. Chem.* **2004**. 441A-448A

44. Slon-Usakiewicz, J. J.; Ng, W.; Dai, J.R.; Pasternak, A.; Redden, P. R. *DDT.* **2005**, *10,* 409-416.

45. Ng, E. S. M.; Feng, Y.; Kameyama, A.; Palcic, M. M.; Hindsgaul, O.; Shcriemer D.C.; *Anal. Chem.* **2005**, *77*, 6125-6133.

46. Ng, W.; Dai, J.R.; Slon-Usakiewicz, J. J.; Redden, P. R. Pasternak, A.; Reid, N.; *J. Biomol. Screen.* **2007**. *12*, 167-174.

47. Kasai, K; Ishii, S. *J. Biochem.* **1975**, *14*, 261-264

48. Kasai, K; Oda, Y.; Nishikata, M.; Ishii, S. *J. Chromatogr.* **1986**, *376*, 33-47.

49. Zhang, Y.; Xiao, X.; Kellar, K.; Wainer, I. W. *Anal. Biochem.* **1998**, *264*, 22-25.

50. Gottschalk, I; Lagerquist, C.; Zuo, S. S.; Lundqvist, A.; Lundahl, P.; *J. Chromatogr. B* **2002**, *768*, 31-40.

51. Besanger, T. R.; Hodgson, R. J.; Guillon, D.; Brennan, J. D. *Anal. Chim. Acta.* **2006**, *561*, 107-118.

52. Moaddel, R.; Lu, L; Baynham, M.; Wainer, I. W. *J. Chromatogr. B. Analyt. Technol. Biomed. Life Sci.* **2002**, *768*, 41-53.

53. Bighi, F.; Yamaguchi, R.; Patel, S.; Ho, P.; Wainer, I. W.; Moaddel, R. *Clin Phamacol. Ther.* **2005**, *79*, P76-P76.

54. Baynham, M. T.; Patel, S.; Moaddel, R.; Wainer, I. W. *J. Chromatogr. B* **2002**, *772*, 155-161.

55. Besanger, T. R.; Easwaramoorthy, B.; Brennan, J. D. *Anal. Chem.* **2004**, *76*, 6470-6475.

56. Besanger, T. R.; Brennan, J. D. *J. Sol-Gel Sci. Technol.* **2006**, *40*, 209-225.

57. Brook, M.A.; Chen, Y.; Guo, K.; Zhang, Z.; Brennan, J. D. *J. Mat. Chem.* **2004**, *14*, 1469-1479.

58. Hodgson, R. J.; Chen, Y.; Zhang, Z.; Tleugabulova, D.; Long, H.; Zhao, X.; Organ, M.; Brook, M. A.; Brennan, J. D.; *Anal. Chem.* **2004**, *76*, 2780-2790.

59. Jin, W.; Brennan, J. D. *Anal. Chim. Acta.* **2002**, *461*, 1-36.

60. Chan, N. W. C.; Lewis, D. F.; Rosner, P. J.; Kelly, M. A.; Schriemer, D. C. *Anal. Biochem.* **2003**, *319*, 1-12.

61. Dobrovetsky, E.; Menendez, J.; Edwards, A. M.; Koth, C. M. *Methods* **2007**, *41*, 381-387.

62. Moaddel, R.; Jozwiak, K.; Whittington, K.; Wainer, I. W. *Anal. Chem.* **2005**, *77*, 895-901.

63. Moaddel, R.; Wainer, I. W. *J. Pharm. Biomed. Anal.* **2007**, *43*, 399-406.

64. Moaddel, R.; Bullock, P. L.; Wainer, I. W. *J. Chromatogr. B. Analyt. Technol. Biomed. Life Sci.* **2004**, *799*, 255-263.

65. Scheil, J. E.; Mallik, R.; Soman, S.; Joseph, K. R.; Hage, D. S. *J. Sep. Sci.*, **2006**, *29*, 719-737.

66. Hodgson, R.J.; Chen, Y.; Zhang, Z.; Tleugabulova, D.; Long, H.; Zhao, X.; Organ, M; Brook, M. A.; Brennan, J. D. *Anal. Chem.*, **2004,** *76*, 2780-90.

67. Moaddel, R.; Wainer, I. W. *Anal. Chim. Acta.* **2006**, *564*, 97-105.

68. Nakamura-Tsuruta, S.; Uchiyama, N.; Hirabayashi, J. *Methods Enzymol.* **2006**, *415*, 311-325.

69. Sui, J.; Tleugabulova, D.; Brennan, J. D. *Langmuir* **2005**, *21*, 4996-5001.

70. Tleugabulova, D.; Sui, J.; Ayers, P. and Brennan, J. D. *J. Phys. Chem. B* **2005**, *109*, 7850-7858.

71. Tleugabulova, D.; Zhang, Z.; Chen, Y.; Brook, M. A. and Brennan, J. D. *Langmuir*, **2004**, *20*, 848-854.

72. Tleugabulova, D., Czardybon, W. and Brennan, J.D. *J. Phys. Chem. B.* **2004,** *108,* 10692.

73. Jacoby, E.; Bouhelal, R.; Gerspacher, M.; Seuwen, K. *Chem. Med. Chem.* **2006**, *1*, 760-782.

Chapter 2

Theory

2.1 Basic Concepts in Fluorescence

2.1.1 The Fluorescence Process

The absorption of a photon of ultraviolet or visible radiation by a molecule leads to the promotion of an electron to the first (or higher) excited singlet state. Following excitation, the molecule can undergo a number of excited state processes, including vibrational relaxation, intersystem crossing to a triplet state, and variations in excited state energy owing to changes in the local solvent microenvironment. After a few nanoseconds, the excited electron can return to the ground state, either by a non-radiative process termed internal conversion, or by the emission of a photon. The latter process, involving movement from the singlet excited state to the ground state, is termed fluorescence. Emission from the triplet state, on the other hand, is termed phosphorescence, and typically has a much longer excited state lifetime and a longer emission wavelength than fluorescence.[1,2]

Given that the excited state exists for several nanoseconds, the nature of the fluorescence emission is highly dependent on processes that occur on this timescale. This can include solvent reorientation, collisions with other molecules, transfer of energy to nearby "acceptor" molecules, and overall rotational motion of the excited fluorescent molecule. In this thesis, it is the effects of molecular rotation on fluorescence that are of importance, and thus this process will be described in further detail. The nature of the fluorescent probes that can be used in such studies is also briefly described to provide insight into the types of systems that can be used to examine molecular dynamics and, ultimately, biomolecule:surface interactions.

2.1.2 Intrinsic and Extrinsic Fluorescence

Molecules capable of undergoing electronic transitions that ultimately result in fluorescence are known as fluorescent probes, fluorophores or simply dyes. In general, fluorophores are divided into two broad classes, termed intrinsic and extrinsic.

Intrinsic fluorophores are any probe that is inherently part of the system under study. In proteins, intrinsic fluorophores include three naturally occurring aromatic amino acids: phenylalanine (Phe), tyrosine (Tyr) and tryptophan (Trp). These three residues are responsible for the characteristic absorption of proteins and polypeptides in the wavelength region between 260 and 300 nm. The structures and absorption spectra of the aromatic amino acids are presented in Figures 2.1 and 2.2, respectively.

Figure 2.1: Structures of Aromatic Amino Acids

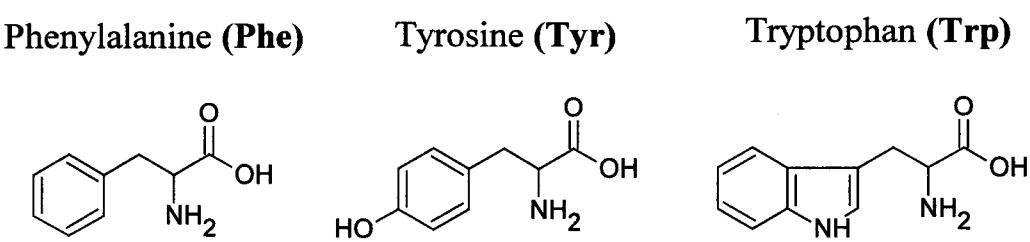

Figure 2.2: Absorption Spectra of Amino Acids (extinction coefficient at pH 6) [3]

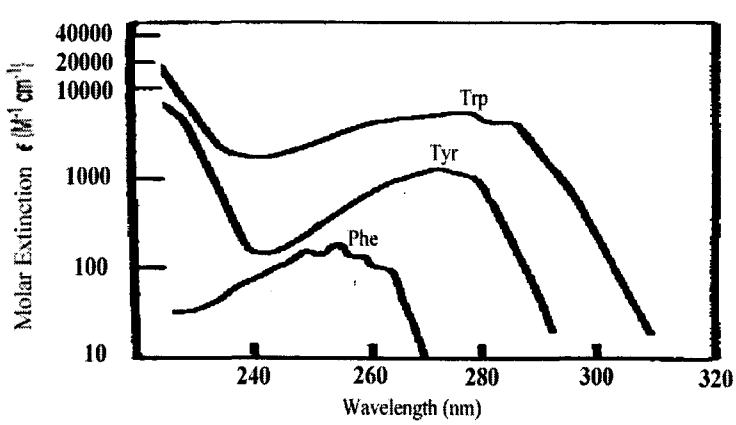

Trp and Tyr have stronger absorption than Phe, making them better suited to spectroscopic studies. More importantly, Trp has a red extended absorption spectrum and the highest extinction coefficient relative to either Phe or Tyr, and thus one can selectively excite Trp in the presence of other amino acids at $\lambda_{ex} > 295$nm, allowing one to observe the fluorescence originating solely from the Trp residues within the protein. The Trp emission spectrum is moderately sensitive to the external environment, shifting from an emission maximum of ~310 nm in hydrophobic environments to 350 nm in polar solvents. The Trp residue will also display anisotropic emission when excited with polarized light (see below), making it amenable to studies of molecular rotation.

Extrinsic fluorophores are typically synthetic dyes or modified biochemicals that are added to a specimen such as proteins to produce fluorescence with specific spectral properties. The characteristics of fluorescence (excitation and emission spectrum, quantum yield, lifetime, limiting anisotropy, solvent sensitivity, excited state behaviour), can be selected by choosing the appropriate dye, which then allows one to monitor specific excited state processes involving interactions of the excited molecule with its close environment. The choice of a fluorescent probe is crucial for obtaining an unambiguous interpretation of a particular property of the microenvironment in which the probe is located.

2.1.3 Fluorescence Anisotropy[1,2]

Light is an electromagnetic wave consisting of an electric field **E** and a magnetic field **B** perpendicular both to each other and to the direction of propagation, and

oscillating in phase. For natural light, these fields have no preferential orientation, but for linearly polarized light, the electric field oscillates along a given direction.

In the quantum mechanical approach, a transition moment is introduced for characterizing the transition between the initial and final state of a molecule. The transition moment represents the transient dipole resulting from the displacement of charges during the transition; therefore, it is not strictly a dipole moment. In most cases, the transition moment can be drawn as a vector in the coordinate system defined by the location of the nuclei of the atoms; therefore, the molecules whose absorption transition moments are parallel to the electric vector of a linearly polarized incident light are preferentially excited. This probability is maximized when the two vectors are parallel to each other and zero when they are perpendicular.

When a population of fluorophores is illuminated by linearly polarized incident light, those molecules whose transition moments are oriented in a direction close to that of the electric vector of the incident beam are preferentially excited. This is called photoselection. Because the distribution of excited fluorophores has a preferred orientation parallel to the electric vector of the excitation beam, the resulting distribution of excited fluorophores is anisotropic. Thus, in the absence of molecular motion during the excited state lifetime, the emitted fluorescence will also be anisotropic. However, any change in direction of the transition moment during the lifetime of the excited state will cause this anisotropy to decrease, i.e., it will induce a partial (or total) depolarization of fluorescence.

Depolarization of fluorescence can result from a number of phenomena such as internal conversion to a lower energy state with a different dipole direction, energy transfer to another molecule with a different orientation, or rotational diffusion of the

fluorophores. In the absence of internal conversion and energy transfer, the fluorescence anisotropy can provide useful information on molecular mobility, size, shape and the flexibility of molecules, and on the microviscosity of the surrounding medium.

2.2 Fluorescence Anisotropy Measurements and Data Analysis

2.2.1 Steady - state Fluorescence Anisotropy[1,2]

The basic experimental setup for measuring fluorescence anisotropy is shown in Figure 2.3.

Figure 2.3: Experimental Setup of Fluorescence Anisotropy

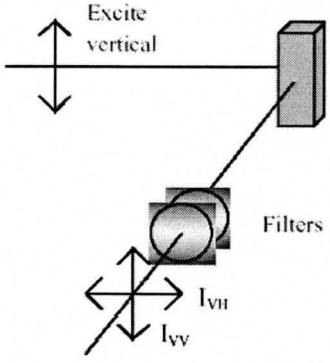

Steady-state fluorescence anisotropy involves measurement of the intensity of parallel and perpendicularly polarized emission from a sample after continuous excitation parallel polarized light. The steady-state anisotropy r is given by:

$$r = \frac{I_{VV} - I_{VH}}{I_{VV} + 2I_{VH}} \qquad (2.1)$$

where I_{VV} is the intensity of parallel polarized emission and I_{VH} is the intensity of perpendicularly polarized emission after excitation with a parallel polarized excitation beam. The relationship between the average rotational correlation time of the fluorescent species (ϕ) and the steady-state anisotropy is given by:

$$r = \frac{r_0}{1 + \phi / \tau} \tag{2.2}$$

where r_0 is the limiting anisotropy in the absence of rotational motion and τ is the mean lifetime of the probe. Based on equation (2.2) it is clear that the ratio of the fluorescence lifetime to the rotational correlation time determines the average anisotropy. The anisotropy value is sensitive to changes in the ratio of ϕ/τ over the range from ~1/15 to 15. Thus, probes with short lifetimes will be best suited to report on rapid rotational motions, while those with long lifetimes will be better suited for reporting slower rotational motions. Given this relationship, it is important to know both r_0 and τ, and to ensure that these do not change as a result of a given perturbation to the fluorescent system, if one wishes to quantitatively evaluate changes in ϕ from steady-state anisotropy measurements.

The steady-state anisotropy value is averaged over all rotational motions of the fluorescent species, and is not able to monitor the underlying rotational components that go into producing the average value. On the other hand, steady-state fluorescence anisotropy measurements can be done considerably faster than time-resolved fluorescence anisotropy, which allows for more measurements of a given sample per unit time, which is useful to following kinetic processes, or for analysis of more samples per unit time, increasing throughput.

2.2.2 *Time-Resolved Fluorescence Anisotropy* [1,2]

To evaluate the underlying rotational components that go into the steady-state anisotropy value, it is necessary to measure the temporal evolution of I_{VV} and I_{VH}. This can be done in a number of ways, however for the purposes of this work only the time-domain measurement method will be described. In this case, the sample is excited with a series of extremely short pulses of vertically polarized light and the intensity of the resulting emission is monitored as a function of time after the excitation pulse in both the vertical and horizontal polarization planes to yield $I_{VV}(t)$ and $I_{VH}(t)$. These curves will display both the inherent decay of fluorescence intensity, which will occur with the characteristic lifetime of the fluorophore (τ), and the additional alterations in fluorescence intensity owing to rotation of the fluorescent species. Typical $I_{VV}(t)$ and $I_{VH}(t)$ curves are shown in Figure 2.4.

Figure 2.4: Experimentally obtained $I_{VH}(t)$ and $I_{VV}(t)$ curves in time-resolved fluorescence anisotropy

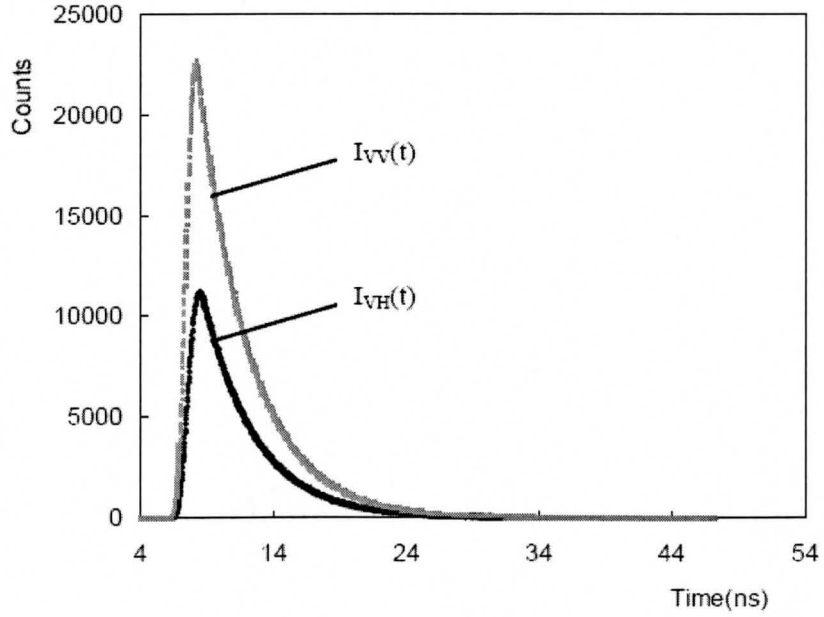

The I_{VV}(t) decay curve shows an more rapid initial decay profile owing to the rotation of vertically polarized fluorophores out of the vertical plane, while the $I_{VH}(t)$ curve shows an initial rising portion owing to rotation of such molecules into the horizontal plane.

By summing the decay traces (noting that the decay can occur into two mutually independent orthogonal directions), one obtains the sum $S(t)= I_{VV}(t)+2I_{VH}(t)$, which cancels the rotational contributions and thus results in a normal intensity decay, and can therefore be used to extract the excited state lifetime of the probe. The difference $D(t)=I_{VV}(t)-I_{VH}(t)$ gives the decay owing to rotational components only, but this curve is still scaled to the intensity in any given channel, which decreases with time, as shown in Figure 2.5.

Figure 2.5: S(t) and D(t) curves obtained from $I_{VH}(t)$ and $I_{VV}(t)$ curves in time-resolved fluorescence anisotropy

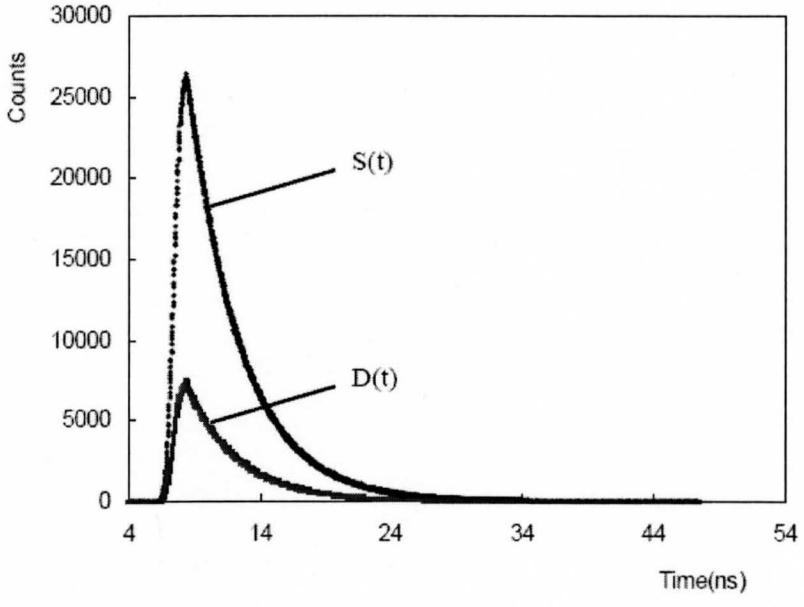

By dividing the difference function by the sum function, the intensity variations are normalized across all channels, canceling the contributions from the intensity decay and leaving only the time resolved fluorescence anisotropy r(t) decay data:

$$r(t) = \frac{D(t)}{S(t)} = \frac{I_{VV}(t) - I_{VH}(t)}{I_{VV}(t) + 2I_{VH}(t)} \tag{2.3}$$

A typical fluorescence anisotropy decay curve calculated by software based on experimentally obtained decays $I_{VV}(t)$ and $I_{VH}(t)$ is shown below:

Figure 2.6: A typical fluorescence anisotropy decay curve

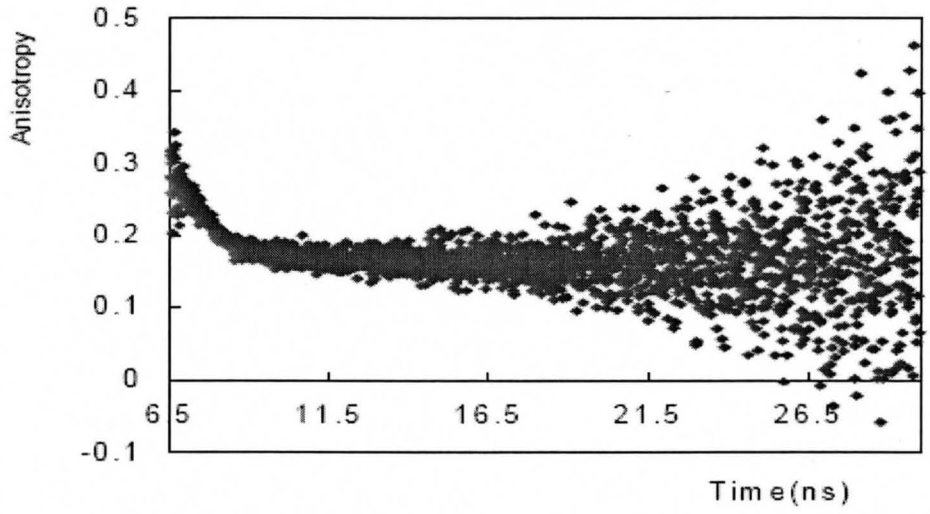

2.2.3 TRFA Data Analysis

The measured $r(t)$ decay contains information about the probe motion through its relationship to the Fourier transform of the orientational time correlation function $P_2(t)$ of a rotating emission dipole[4]

$$r(t) = P_2(t) = \frac{3}{2} < \cos^2 \alpha(t) > -\frac{1}{2} \qquad (2.4)$$

where α is the displacement angle between the absorption and emission dipole moments of the probe. Depending on the probe structure, shape and its environment, several mathematical models have been developed to describe $P_2(t)$.[4] The fit of a particular model to the experimental r(t) decay is usually achieved via an algorithm[5] that minimizes the difference between the experimental and simulated data and finds the global minimum in the fitting function. The acceptance criteria for goodness of the fit include a satisfactory reduced chi-squared value (χ_R^2) and a random distribution of weighted residuals. Since more than one mathematical solution can potentially exist that will fit the experimental r(t) data equally well, a statistically good fit may generate meaningless decay parameters.[6] Hence, the fulfillment of the statistical requirements by itself cannot be regarded as a definitive proof of the rotational diffusion model. Rather, the validity of the model is judged by its physical significance in describing the system under study.

2.2.3.1 Free Dynamics In Non-Interacting Environments

The rotation of a fluorescent probe in water is usually taken as a reference point. The probe molecule is approached as a small rigid body (sphere, ellipsoid or rod) and its motion in water is modeled as isotropic Brownian rotation in an unhindered environment. In the case of a probe in buffer containing other species such as small peptides, the motion of the probe molecule is also unhindered provided there are no interactions between probe molecule and the second species in the solution. The

simplest model for this free motion is that of the rigid sphere[7], which describes as a single-exponential function

$$r(t) = r_0 \exp(-t/\phi) \tag{2.5}$$

where r_0 is the limiting anisotropy at time zero and ϕ is the rotational correlation time. The r_0 value indicates the initial anisotropy after internal conversion and vibrational relaxation, prior to probe rotation, and should nearly correspond to the steady-state anisotropy of the fluorescent probe in a glassy frozen solvent. The theoretical value of r_0 depends upon the nature of the excitation process: maximum values are r_0 = 0.4 using one-photon excitation.[8]

The rotational correlation time (ϕ) indicates how fast the initially polarized emission is randomized due to Brownian diffusion. Provided that the viscosity of the surrounding solution is known, the nanosecond anisotropy decay component can be related to the hydrodynamic radius (R) of the primary particles by applying the Debye-Stokes-Einstein equation,[9]

$$\phi = \frac{\eta V}{kT} = \frac{4\eta\pi R^3}{3kT} \tag{2.6}$$

where η is the microviscosity of the sol solution, k is the Boltzmann constant and T is the temperature.

2.2.3.2 Restricted Dynamics of Probe-Polycationic Polymer Complexes[10]

The anisotropy decay of ionically labeled polyamine polymers can be fit to a two-component hindered rotor model according to the following equation (2.7):

$$r(t) = \beta_1 \exp(-t/\phi_1) + \beta_2 \exp(-t/\phi_2) + r_\infty = r_0 f_1 \exp(-t/\phi_1) + r_0 f_2 \exp(-t/\phi_2) + g r_0 \tag{2.7}$$

where β_1 and β_2 are the pre-exponential terms ($0 \leq \beta \leq r_0$, $\beta_1 + \beta_2 = r_0$) representing the extent to which the probe emission is depolarized by each correlation time; $r_0 = (\beta_1 + \beta_2)$ is the experimental initial anisotropy at $t = 0$ also called the limiting anisotropy; r_∞ is the residual anisotropy due to hindered motion of species with $\phi > 15\tau$; ϕ_1 reflects rapid rotational motions associated with the sidechain of the polymer, ϕ_2 reflects slower segmental motions of the polymer backbone, $f_1 = \beta_1 \phi_1/(\beta_1 \phi_1+\beta_2 \phi_2)$ is the fractional fluorescence associated with ϕ_1, and $f_2 = \beta_2 \phi_2/(\beta_1 \phi_1+\beta_2 \phi_2)$, is the fractional fluorescence corresponding to ϕ_2, and $g = r_\infty/r_0$ is the fraction of fluorescence due to the hindered rotation of the macromolecule as a whole.

2.3 Fluorescence References

1. Bernard Valeur. Molecular Fluorescence: An Introduction: Principles and Applications. Canada: John Wiley & Sons, 2002
2. Joseph R. Lakowicz. Principles of Fluorescence Spectroscopy. New York: Kluwer Academic/Plenum, c1999.
3. D. B. Wetlaufer. Adv. Protein Chem. **1962,** 17, 303–390.
4. J. M. Beechem, J. R. Knutson and L. Brand, Global analysis of multiple dye fluorescence anisotropy experiments on proteins, Biochem. Soc. Trans. **1986**, 14, 832-835.
5. B. Imhof, Decay Analysis Software Support Manual, (IBH Consultants Ltd, Glasgow, **1989**).
6. D. Tleugabulova, J. Sui, P. W. Ayers and J. D. Brennan, J. Phys. Chem. B. **2005**, 109,7850-7858.
7. F. Perrin, Ann. Phys. Paris. 1929, 12, 169-175

8. J. R. Lakowicz, Principles of Fluorescence spectroscopy (Klüwer Academic Plenum Publishers, New York, **1999**).

9. Debye, P. Polar Molecule; Chemical Catalog Co.: New York, 1929

10. Tleugabulova, D.; Czardybon, W.; Brennan, J. D. J. Phys. Chem. B **2004**, 108, 10692-10699.

2.4 Basic Concepts of Mass Spectrometry

Mass spectrometry is an analytical technique that separates compounds based on the mass (*m*) to charge (*z*) ratio (*m/z*) of ions in the gas phase[1] and can be used for a number of purposes, two principle uses being the identification of compounds and determining structural properties of compounds through fragmentation.[2,3] Recent applications in the biological sciences have enabled users to identify and characterize biomolecules, determine kinetic and thermodynamic properties of biological interactions and have also allowed for the screening novel target-ligand interactions.[3]

While many types of mass spectrometers are available, the set-up of each is similar, consisting of four basic components, namely a sample inlet, an ionization source, a mass analyser and a detection system (Fig. 2.7).[2] The sample is introduced into a sample inlet using a variety of techniques (e.g. liquid chromatography, gas chromatography, direct injection etc.) that can be interfaced directly to an ionization source which generates either positively (M^+) or negatively (M^-) charged ions from the molecules (M) in a sample. The resultant ions in the gas phase are then separated from each in a mass analyser that uses an electric or magnetic field to impart a force on the gaseous ions. A compounds behaviour in the applied field is influenced by both the mass and the charge of the gaseous ion, as governed by Newton's second law (equation 2.4.1) and the Lorentz's force law (equation 2.4.2):[1]

$$\mathbf{F} = m\mathbf{a} \qquad (2.4.1)$$

$$\mathbf{F} = q(\mathbf{E} + \mathbf{v} \times \mathbf{B}) \qquad (2.4.2)$$

where F is the force applied to an ion, m is the mass of an ion, **a** is the acceleration of the ion, q is the ionic charge and **E** is the electric field being applied and **v x B** is the cross product of the ion velocity and the applied magnetic field. Simply put, Newton's law states that the applied force causes an acceleration of the ion that is mass dependent. Lorentz's law states that the applied force also depends on the charge of the ion. Hence, the unique *m/z* ratios of compounds can be used to resolve and separate individual compounds in a sample. Once separated, a detector is used to measure the quantity of ions with a particular *m/z* ratio.

*Figure 2.7: Basic Components of a Mass Spectrometer**

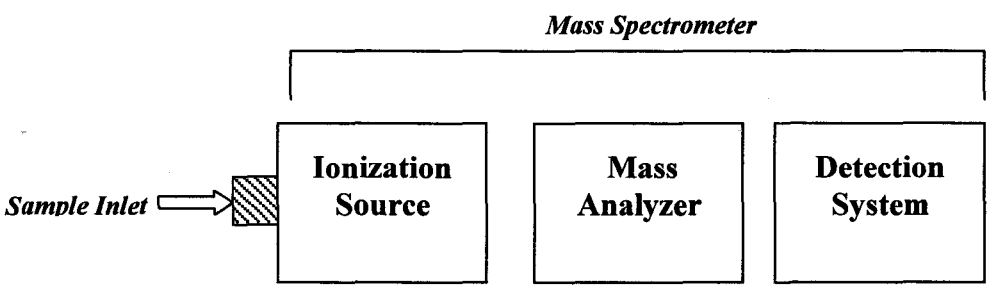

*Figure adapted from reference (2)

2.5 Ionization Sources — Electrospray Ionization (ESI)

Although numerous strategies can be used to generate gaseous ions from a sample (e.g. chemical ionization, electron ionization, electrospray ionization, matrix assisted laser desorption ionization etc.)[2] the appropriate type of ionization source usually depends on the nature of the sample being analysed. In the biological sciences, electrospray ionization (ESI) is commonly used, as it is technique that can be done at atmospheric pressure and is

a so-called 'soft' ionization method capable of preserving the integrity of biological samples.[4]

2.5.1 Priniciples of Electrospray Ionization[5]

Electrospray ionization generates multiply charged ions (positive or negative) from a sample in the liquid state by pumping the sample through a narrow bore stainless steel capillary directly interface to the ionization source of the mass spectrometer. A high voltage (3-5 kV) electric field is applied to the capillary, heating the sample and creating an aerosol of highly charged particles within the capillary (Fig. 2.8). Nitrogen gas is simultaneously pumped through the capillary helping the solvent evaporate while still in the capillary. As the fine charged droplets emerge from the tip of the heated capillary, they accelerate towards a counter electrode on the front face of the ionization source due to the large potential difference between the heated capillary and the counter electrode.

Figure 2.8: Electrospray Ionization Principles[*]

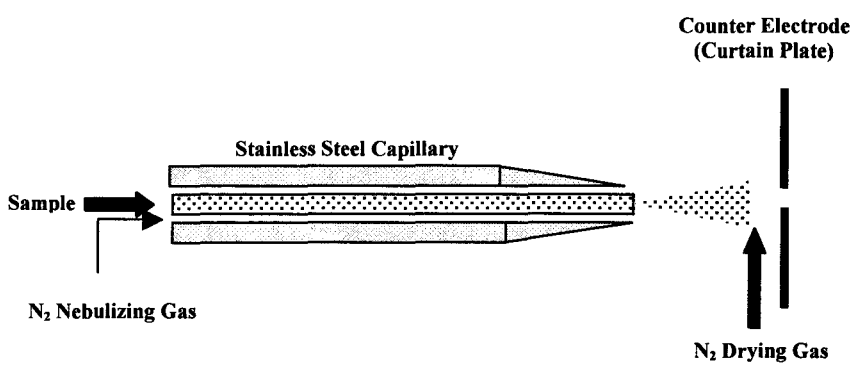

* Figure adapted from reference 4.

While accelerating towards the counter electrode, solvent evaporation reduces the size of the charged droplets concentrating the molecules into a small sphere (Fig 2.9). This process is aided by the constant flow of heated nitrogen gas on the face of the counter electrode, called the curtain or drying gas. When the size of the charged droplets are sufficiently small, sample ions free from solvent emerge from the droplets and pass through a small orifice to the mass analyzer portion of the mass spectrometer. Positive ions are generated by applying a positive electric charge to the stainless steel capillary, while negative ions are generated by applying a negative electric charge. Formation of positive ions results from sample molecules (M) forming adducts with free protons (H^+) present in the sample solvent, the number of protons gained being proportional to the number of charged groups present on the molecule. Similarly, negative ions are generated by the loss of protons in the ionization process.

*Figure 2.9: Ion Formation in ESI Ion Sources**

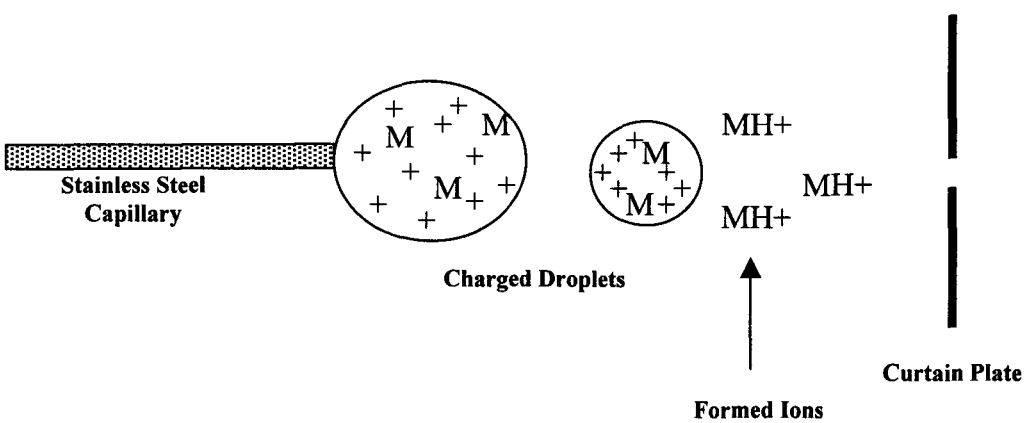

* Figure adapted from reference 4.

2.6 Mass Analysers — Triple Quadrupole Mass Spectrometry

Many mass analysers can be used in conjunction with ESI ionization sources in mass spectrometry experiments, including single quadrupule mass analyzers, time-of-flight (TOF) mass spectrometers, ion trap mass spectrometers and triple quadrupole MS-MS systems.[2] The priniciples of each analyser is markedly different, hence only the principles of the triple quadrupole MS-MS mass analyser used in this thesis are discussed (Fig 2.10).[1]

2.6.1 Priniciples of Quadrupole Mass Analyzers[1]

Once ionized in the ESI ionization sources, charged ions (parent ions) enter the mass analyser through a small hole in the curtain plate. The parent ions enter the first chamber of the mass analyser, called Q0, which focuses multiple parent ions generated from the sample into the second region, called Q1, using an applied radio frequency (rf) field. In the Q1 chamber, ions are trapped in space by applying a strong radio frequency field as well as a strong DC current, the former field trapping parent ions radially in space and the latter field trapping parent ions axially. At a certain ratio of the applied DC current and rf field (DC:rf ratio), a particular ion can be selected and is allowed to pass through Q1 into other regions of the mass analyser or directly through to the detector. As the behaviour of ions in the applied fields is dependent on the m/z ratio, ions each have a unique DC:rf ratio that will allow them to pass through the Q1 region. A mass spectrum of all parent ions, called a Q1 scan, can be generated by scanning an entire range of DC:rf ratios. While this method provides a highly sensitive spectrum of all parent ions in the Q1

region, Q1 spectrums do not achieve great selectivity as the possibility of two compounds having the same or similar *m/z* ratios does exist.

Once through the Q1 region, ions can either travel through the remaining regions of the mass analyser untouched and pass directly to the detector (as is the case in Q1 scans) or ions can be subjected to further analysis in the Q2 and Q3 regions of the mass analyser, as in MS-MS or tandem MS experiments. In tandem MS experiments, specific parent ions in Q1 are selected and allowed to pass through to the Q2 chamber. The presence of an inert gas (e.g. N_2) in Q2 is used to break up parent compounds into smaller compounds (daughter ions) in a process known as collision-induced fragmentation, the intense kinetic energy transfer between the inert gas and the selected parent ions results in the fracture of the least stable molecular bonds in the parent ions. The newly produced daughter ions are imbued with a positive charge as well, as these ions also form adducts with protons in the sample buffer. Daughter ions are then allowed to pass into the Q3 region, where a spectrum of daughter ions (called a Q3 scan) can be generated in a manner analogous to the Q1 scan. Because the parent ions are fragmented in highly a specific manner in tandem MS experiments, the selectivity these experiments is greater than that seen in Q1 scans since the likelihood of two compounds having similar fragmentation patterns is very low. However, the signal intensity in tandem MS experiments is significantly lower than in simple MS experiments due incomplete fragmentation of parent ions. In a mode called multiple reaction monitoring (MRM) mode, multiple daughter ions can be selected from Q2 and the signals from each can be individually monitored as a function of time.

*Figure 2.10: Basic Setup of Triple Quadrupole Mass Spectrometer**

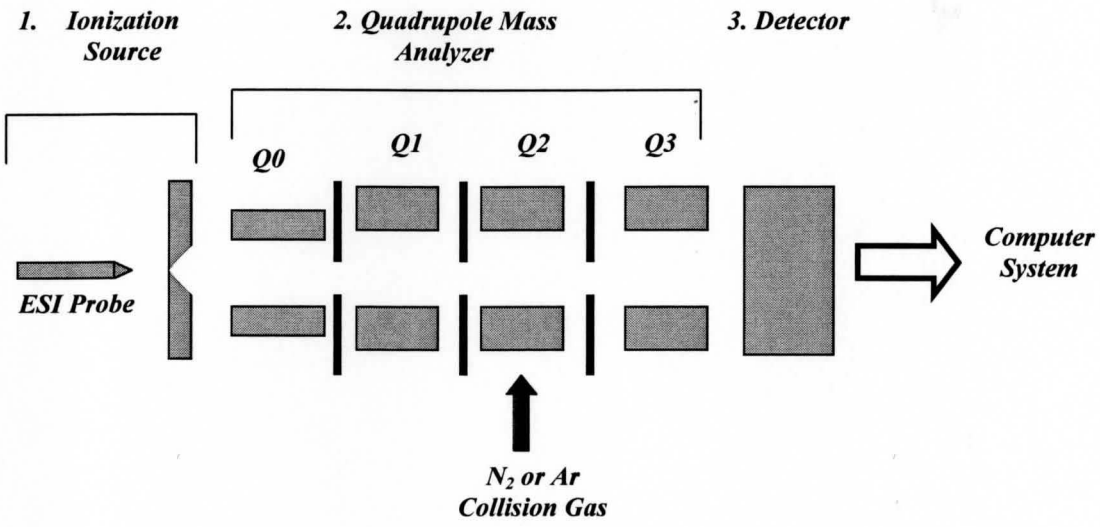

* Figure adapted from reference 2.

2.6.2 Detection System

The basic detection system contains of a electron multiplier tube coupled to computer systems. Ions picked up by the detector are converted into electrical signal, which are then amplified and translated by computer software into interpretable data as a mass to charge ratio.

2.7 References:

1. J. T. Watson, *Introduction to Mass Spectrometry* (Raven Press, New York, 1985)

2. Korffmacher, W. A. *DDT*, **2005**, *10*, 1357-1367.

3. Xu, Xiaoying; Lan, J.; Korfmacher, W. A. *Anal. Chem.* **2005**, *77*, 389A-394A.

4. M. L. Gross, A. K. Ganguly, B. Pramanik, *Applied Electrospray Mass Spectrometry* (Marcel Dekker Inc., New York, 2002)

5. J. Fenn *J. Phys. Chem.*, **1984**, *88*, 4451-4459.

Chapter 3

Two-Site Ionic Labeling with Pyranine: Implications for Structural Dynamics Studies of Polymers and Polypeptides by Time-Resolved Fluorescence Anisotropy

The following chapter was published in the journal *J. Am. Chem. Soc.* under the citation:

Sharma, J.; Tleugabulova, D.; Czardybon, W.; Brennan, J.D.* Two-Site Ionic Labeling with Pyranine: Implications for Structural Dynamics Studies of Polymers and Polypeptides by Time-Resolved Fluorescence Anisotropy. *JACS.* **2006**, *128*, 5496-5505.

The idea and experimental design for the technique presented was conceived by Dr. Tleugabulova and Dr. Brennan. Dr. Tleugabulova generated single-point binding TRFA data and preliminary double point binding data. Dr. Czardybon generated molecular modelling data. I was responsible for collecting and analyzing the steady state and TRFA double point binding data presented here under the supervision of Dr. Tleugabulova. I also collected and analyzed absorbance data presented in this manuscript. All figures related to double-point binding data were generated by myself with input from Dr. Tleugabulova and Dr. Brennan. Dr. Tleugabulova was responsible for writing the first draft of the manuscript, while I was responsible for writing the final draft with editorial input from Dr. Tleugabulova and Dr. Brennan.

Abstract

Time-resolved fluorescence anisotropy (TRFA) is used to study dynamic motions of biomolecules in a variety of environments. However, depolarization due to rapid sidechain motions often complicates the interpretation of anisotropy decay data and interferes with the observation of segmental motions, and hence the true dynamics of fluorescently-labeled biomolecules. Here, we demonstrate a new method for multi-point ionic labeling of polymers and biomolecules that have appropriately spaced amino groups using the fluorescent probe 8-hydroxyl-1,3,6-trisulfonated pyrene (pyranine). Molecular modeling of pyranine and various homogeneous polyamines showed that the charged residues at positions *i* and (*i*+2) are between ~4.0-8.0Å apart, a range that matches the distances between adjacent sulfonate groups in pyranine and allows for a two-point ionic interaction between pyranine and the charged polymers. TRFA analysis shows that such labeling provides a more rigid attachment of the fluorophore to the macromolecule than the covalent or single-point ionic labeling of amino groups. As a result, the time-resolved anisotropy decays with a longer rotational correlation time ϕ_2, which is coupled to the backbone motion of the labeled polymer segment. This is demonstrated by the improved correspondence of rotational dynamics data from fluorescence and nuclear magnetic resonance spectroscopy, particularly for polyamines with shorter and/or more rigid sidechains. Optimal coupling of pyranine to biomolecule dynamics is shown to be obtained for appropriately spaced Arg groups, and in such cases the ionic binding is stable up to 150 mM ionic strength. The improved non-covalent fluorescent labeling technique was used to monitor the behaviour of poly(allylamine) (PAM) and poly-D-

Lysine (PL) in sodium silicate derived sol-gel materials and revealed significant restriction of backbone motion upon entrapment for both polymers, an observation that was not readily apparent in a previous study with entrapped fluorescein-labeled PAM and PL. The implications of these findings for fluorescent studies of polymer and biomolecule dynamics are discussed.

3.1 Introduction

The use of fluorescence methods to monitor the dynamics of biomolecules often requires that the biomolecule of interest be labeled with an extrinsic fluorescent dye. While the vast majority of fluorescence labeling is achieved by covalent attachment of fluorophores to a macromolecule, this method of labeling may compromise protein activity and function due to the harsh conditions required to carry out the labeling reaction.[1] As an alternative, non-covalent labeling through ionic, hydrophobic, hydrogen bonding or donor-acceptor interactions is attracting interest, as these methods better preserve protein function and activity, require less time, can be done at physiological pH and do not require purification steps when the stoichiometry of the complex is known.[1,2] The viability of such non-covalent labeling, however, is dependent on the biomolecule having surface accessible residues or side chains that can bind dyes with high efficiency and selectivity.

Lysine, glutamic acid and arginine have the highest frequency of occurrence among the common amino acids found on protein surfaces[3] and hence these amino acids provide the best opportunity for non-covalent labeling of proteins. Specifically, lysine and arginine have cationic sidechains that are appropriate for selective labeling using anionic fluorophores. These residues form strong ionic complexes with sulfonate dyes,[4,5] which are ideal for fluorescence measurements[6] since these ionic complexes exhibit high emission intensity due to ionization of the probe.[7] However, the sidechain length of these residues creates a significant drawback when studying backbone motions of a protein using either covalent or ionic fluorescent labels. A long linker can cause the probe to

experience motions that are independent of the protein backbone due to high flexibility at the site of attachment[8] and can decouple the probe motion from the peptide backbone motion.[9] Indeed, reduction in linker length has led to improved measurements of the segmental motions near the residue to which the probe is attached in both covalently[10] and ionically labeled systems;[9] however, these findings may not be generally applicable to the study of protein segmental or backbone motions where attachment of the probe via a short linker is not an option.

An alternative approach to reduce independent probe motions is to use bifunctional labels that tether the probe to the biomolecule at two sites, thereby reducing probe flexibility.[11,12] The success of this approach has previously been demonstrated in EPR studies[13] and fluorescence studies[14,15] and has the advantage of allowing the measurement of slow (microsecond) rotational motions of biomolecules using covalent bifunctional probes, as outlined in detail by Corrie *et al.*[11] While there are some reports of the use of bifunctional probes to measure protein dynamics,[12,16] this technique has not been used widely for protein dynamics studies using time-resolved fluorescence anisotropy (TRFA), likely owing to the fact that many of these dyes are Cys-reactive and require the presence of two closely spaced, surface accessible cysteine residues.

Recently, extensive research using MALDI mass spectrometry[4,7,17,18] and isothermal titration calorimetry[5] has led to a better understanding of the non-covalent interaction between basic amino acids and sulfonic acid ligands and has provided evidence to suggest that a two-point interaction can be achieved using a non-covalent fluorescent labeling approach. Specifically, mass spectrometry studies of protein complexes with a

trisulfonated pyrene probe have shown that fewer dye:protein adducts were formed than expected given the number of surface accessible arginine residues, a result that suggested a complex of two arginine residues per single sulfonated pyrene molecule.[18] Other evidence has shown electrostatic binding of 8-hydroxyl-1,3,6-trisulfonated pyrene (pyranine) to proteins through all three sulfonate groups.[7,19,20]

While the multi-site electrostatic interaction between trisulfonic acid derivatized fluorophores and basic residues has proven to be of limited use for mapping protein surfaces by mass spectrometry,[18] we demonstrate that it can be advantageous in TRFA measurements, as it significantly reduces rapid probe motions arising from the flexible linker between the probe and protein[9,10] (i.e. an amino acid sidechain) or flexibility of the probe at its point of attachment.[8] In the present work, we use TRFA to probe segmental motions of homogeneous polyamines using single-point and double-point ionic labeling with fluorescein and pyranine, respectively, and show that the reduction of independent probe motions resulting from a double-point ionic interaction leads to a closer correspondence between segmental motions measured using TRFA and NMR spectroscopy, particularly in cases where appropriately spaced Arg residues are present.

To demonstrate the utility of this labeling method the segmental mobility of polyamines entrapped in sodium silicate derived hydrogels was assessed using both fluorescein and pyranine-labeled polymers. Vast interest in the field of protein encapsulation using the sol-gel process merits such studies, as a clear understanding of the effects of sol-gel entrapment on protein dynamics can provide important information on how such encapsulation influences protein function and activity. The charged

polymers, poly(allylamine) and poly-D-Lysine, represent suitable model systems for both flexible and rigid biomolecules entrapped in sol-gel derived materials and were selected since each is expected to undergo significant electrostatic interactions with silica, which should restrict motion. Our results suggest that pyranine-labeled polymers more accurately reflect the dynamics of cationic polymers, demonstrating the potential for using non-covalent labeling of polypeptides with pyranine to study polypeptide backbone dynamics in a wide range of environments, and highlighting the effects that independent probe motions have on the accurate interpretation of fluorescence anisotropy decay data.

3.2 Experimental

3.2.1 Chemicals:

Fluorescein was supplied by Sigma (St. Louis, MO). 8-hydroxyl-1,3,6-trisulfonated pyrene (pyranine) was purchased from Molecular Probes (Eugene, Oregon). Sodium silicate solution (~ 14% NaOH, ~ 27% SiO_2), Dowex 50WX8-100 ion-exchange resin, poly(allylamine) (20% aqueous solution, MW 17 000, pK_a of 10.5[21]), linear poly(ethyleneimine) (M_n 13 000), poly-D-lysine hydrobromide (MW 17 000), poly-L-ornithine hydrochloride (MW 23 500) and poly-L-arginine hydrochloride (MW 26 000) were purchased from Sigma-Aldrich (Milwaukee, WI). All water was distilled and deionized using a Milli-Q Synthesis A10 water purification system. All reagents were used without further purification.

3.2.2 Sample Preparation:

Stock solutions containing ~ 500 μM of fluorescein in dimethylformamide or ~250 μM pyranine in water[6] were used to prepare samples containing 1.4 μM fluorescein or 2 μM pyranine and 0.05 wt % of a given polyamine in 5 mM Tris-HCl, pH 8.3. An aliquot of the stock probe solution was added to a concentrated aliquot of aqueous polyamine solution to initially form the probe-polyamine complex. The resulting solution was then diluted with water followed by buffer to reach the final concentrations noted above. Samples were analyzed in polymethacrylate fluorimeter cuvettes (transmittance curve C) obtained from Sigma.

A sodium silicate stock solution was prepared according to the procedure described by Bhatia *et al.*[22] Sol-gel derived hydrogels (~2 wt % SiO_2) were prepared by mixing (1:4, v/v) the sodium silicate stock solution and the probe-polyamine stock solution to reach final concentrations of 5 mM Tris-HCl, ~pH 7, 0.05 wt % of the polyamine and either 1.4 μM fluorescein or 2 μM pyranine, as previously described.[9] To avoid flocculation, the pH of the preformed probe-polyamine complex was adjusted to pH ~4 with an aliquot of concentrated HCl prior to mixing with the sodium silicate stock solution. The mixtures were quickly poured into disposable polymethacrylate cuvettes to form hydrogels of dimensions 10 x 10 x 20 mm and sealed with Parafilm.™ Samples were aged overnight prior to analysis.

3.2.3 Sample Analysis:

Absorbance measurements were made using a Cary 400 UV-visible spectrophotometer (Varian Canada, Quebec) over the range of 400-600 nm. Steady state fluorescence anisotropy measurements were performed using a SLM 8100 spectrofluorimeter (Spectronic Instruments, Rochester, NY) as described in detail elsewhere.[9] Pyranine-labeled polymers were excited at 455 nm with emission monitored at 505 nm, while fluorescein-labeled polymers were excited at 495 nm with emission monitored at 520 nm. All other parameters were adjusted as previously described.[9]

Time-resolved fluorescence intensity and anisotropy decay data were acquired in the time-domain using an IBH 5000U time-correlated single photon counting fluorimeter (Glasgow, UK), as described in detail elsewhere.[9] Pyranine-labeled samples were excited using a 455 nm NanoLED source (pulse duration at FWHM of 1.4 ns) with emission collected at 505 nm, while fluorescein-labeled samples were excited using a 495 nm NanoLED source with emission collected at 520 nm. The excitation bandpass was set to 16 nm and the emission bandpass to 32 nm. Appropriate shortpass and longpass filters were employed in the excitation and emission path to avoid scattering effects.

The experimentally obtained parallel ($I_{VV}(t)$) and perpendicular ($I_{VH}(t)$) fluorescence decays were used to generate the sum, $S(t)$, difference, $D(t)$, and time-resolved anisotropy, $r(t)$, functions as follows:[23,24,25]

$$r(t) = \frac{I_{VV}(t) - GI_{VH}(t)}{I_{VV}(t) + 2GI_{VH}(t)} = \frac{D(t)}{S(t)} \qquad (3.1)$$

where G is the polarization bias of the fluorescence detection system. The anisotropy decay was fit to a two-component hindered rotor model according to the following equation:[26]

$$r(t) = fr_0 \exp(-t/\phi_1) + (1 - f - g)r_0 \exp(-t/\phi_2) + gr_0 \qquad (3.2)$$

where ϕ_1 reflects rapid rotational motions on the picosecond timescale, ϕ_2 reflects reorientation of probes on the nanosecond timescale, f is the fraction of fluorescence originating from ϕ_1, (1-f-g) is the fraction of fluorescence owing to ϕ_2, g is the fraction of fluorescence due to probes rotating slower than can be measured with fluorescein or pyranine (ϕ > 50 ns) and r_0 is the time-zero or limiting anisotropy. In some cases, the value of gr_0 is denoted as r_∞, the residual anisotropy. Fits were considered acceptable if the reduced chi-squared (χ_R^2) was close to 1.0 and the weighted residuals were randomly distributed about zero.

3.2.4 Molecular Modeling:

The structures of pyranine and the polyamines were constructed using a semiempirical Austin method (AM1) and Gaussian 98 software in Hyperchem.[27] Energies of the polymer chains and the N-N distances were minimized using Molecular Mechanics (MM+),[28] which is fairly crude but often used to model polymeric chains.[29] Energy minimizations were terminated when the energy difference between two successive iterations was less than 0.01 kcal.mol^{-1}.

3.3 Results and Discussion

3.3.1Polyamine-probe ionic complexes

The formation of ionic complexes between fluorescent probes and polyelectrolytes has recently been described in detail[9,30] and is the basis for non-covalent labeling of proteins.[1,2] Here, we used the anionic fluorescent probes fluorescein and pyranine in complex with homogenous cationic polyamines to explore the effect of the label attachment on the dynamic information obtained by TRFA. Ionic complexes of poly-D-lysine (PL), poly-L-ornithine (PO), poly-L-arginine (PR), poly-allylamine (PAM) and poly(ethyleneimine) (PEI) (0.05 wt %, 5 mM Tris-HCl, pH 8.3) with fluorescein and pyranine were formed at a polymer:probe mole ratio greater than 10:1 to ensure that no more than one probe was attached to a single polymer chain. PO, PL and PR consist of a peptide backbone with alkyl side chains that increase in linear length by one rotatable –CH2- bond (i.e., 4, 5 and 6 bonds, respectively). In addition, PO and PL both contain a single amino group through which ionic binding can occur, while ionic binding to the PR sidechain can occur through interaction with the cationic guanidinium moiety. PAM and PEI polymers both have ethylene-based backbones that are significantly more rigid than the peptide-based polymers due to charge repulsion of the closely spaced amine groups.[32] The PAM sidechain contains two rotatable bonds and a single primary amine through which ionic labeling can occur while PEI has no side chain and its secondary amino group mediates ionic labeling directly to the backbone. All the polyamines used were homogeneous to ensure uniform motions were present in the polymer-probe systems, and

were sufficiently long (> 13 kDa) to minimize binding of the probe to the chain-ends, where main-chain mobility is often greater than in the centre of the polymer chain.[33]

The ionic nature of the complexes was demonstrated by red shifts in the absorption spectra of these complexes relative to the spectra of free fluorescein (e.g. λ_{max}, 492→ 498 nm for PAM) or pyranine (e.g. λ_{max}, 455→459 nm for PAM) Table 3.1:[9,30]

Vol 2.5 M KCl added[a]	[KCl] mM	PAM-Fl λ_{max} (nm)	PAM-Pyr λ_{max} (nm)	PL-Fl λ_{max} (nm)	PL-Pyr λ_{max} (nm)	PO-Fl λ_{max} (nm)	PO-Pyr λ_{max} (nm)	PR-Fl λ_{max} (nm)	PR-Pyr λ_{max} (nm)	PEI-Fl λ_{max} (nm)	PEI-Pyr λ_{max} (nm)
0	0.00	498	459	494	457	494	457	497	460	498	460
1	1.25	498	459	494	457	494	457	497	460	498	460
10	12.44	496	459	493	457	493	457	497	460	498	460
20	24.75	495	459	493	457	492	457	496	459	494	460
40	49.02	493	459	492	457	492	456	495	459	493	460
100	119.05	492	459	492	456	492	456	494	459	492	460
300	326.09	492	459	492	456	492	455	492	458	492	460
500	500.00	492	459	492	455	492	455	492	458	492	459
900	775.86	-[b]	458	-	455	-	455	-	456	-	458
1400	1029.41	-	457	-	455	-	455	-	455	-	457

Table 3.1. Absorption Shift Data for Polymers in the presence of increasing [KCl]. a) Concentrated KCl was titrated into a solution containing 0.05% peptide in 5mM Tris-HCl buffer, pH 8.3 containing either 1.4 μM fluorescein or 2 μM pyranine to determine the ionic strength required to reverse the red shift seen when the fluorescent dyes bind to the charged polymers. Note that λ_{max} for free fluorescein in the same buffer was 492 nm and for free pyranine in buffer was 455 nm. b) Data points for the fluorescein labeled polymers were not taken beyond 500 mM KCl as complete reversal of the red shift was seen well before 500 mM KCl in all cases, indicating that fluorescein was no longer bound (see accompanying steady-state anisotropy data, Fig 3.1, as well).

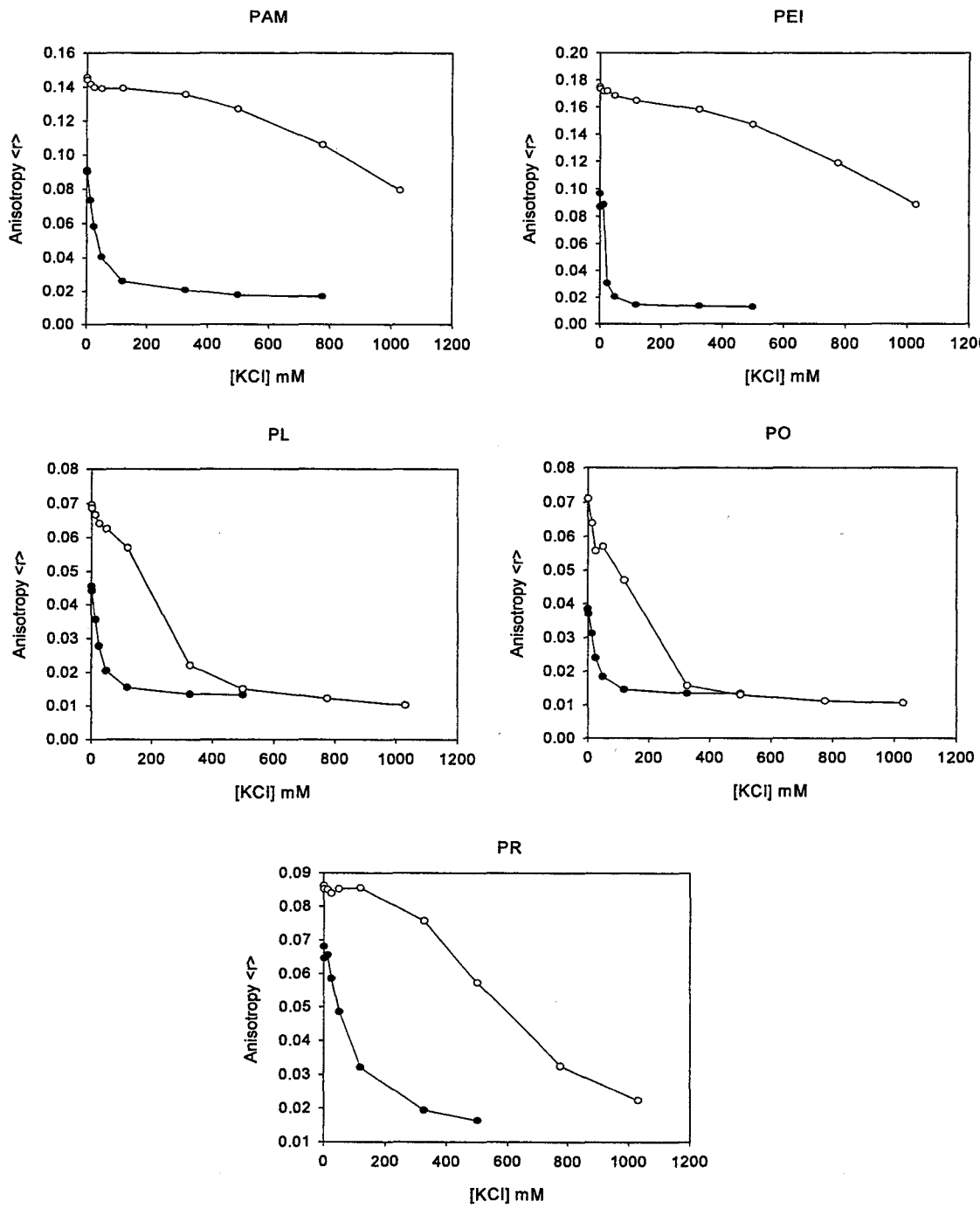

Figure 3.1: Steady state anisotropy data for the polyamine-fluorescein (closed circles) and polyamine-pyranine (open circles) complexes in the presence of increasing concentration

of KCl. A concentrated KCl solution was titrated into a solution containing 0.05 wt % of a given polyamine in 5mM Tris-HCl pH 8.3 and either 1.4 μM fluorescein or 2 μM pyranine. *The steady-state anisotropy, <r>, for free fluorescein in ~1M KCl + buffer was determined to be 0.014 ± 0.003 and for free pyranine in 1M KCl was 0.012 ± 0.002.

The red shift observed for PAM-fluorescein was completely reversed by adding ~0.1 M KCl, while the red shift for PAM-pyranine, was only partially reversed (λ_{max}, 459→457 nm), even at higher ionic strength (~1M KCl; Table 3.1), indicating stronger ionic binding of pyranine to PAM. Additionally, the two complexes showed a large difference in steady-state anisotropy values relative to each other (e.g. 0.091 ± 0.003 for PAM-fluorescein and 0.146 ± 0.004 for PAM-pyranine; see Table 3.2), indicating a more restricted mobility of the pyranine fluorophore when bound to PAM.

	Buffer	**PAM**	**PEI**	**PL**	**PR**	**PO**
Fluorescein r_{ss}	0.0094 ± 0.0011	0.090 ± 0.001	0.097 ± 0.002	0.046 ± 0.002	0.069 ± 0.002	0.040 ± 0.002
Pyranine r_{ss}	0.0074 ± 0.002	0.142 ± 0.004	0.179 ± 0.004	0.073 ± 0.002	0.086 ± 0.004	0.074 ± 0.003

Table 3.2: Steady state anisotropy (r_{ss}) data for 0.05% polymer in 5mM Tris-HCl buffer labelled with either 1.4 μM fluorescein or 2 μM pyranine

Titration with KCl led to a reduction in steady-state anisotropy for both systems, but again a much higher concentration of KCl was required to significantly reduce the steady state anisotropy value of pyranine-labeled polymers relative to fluorescein-labeled

polymers (see Fig 3.1). Also noteworthy is the scaling of the steady-state anisotropy of pyranine with the shortening of the side chain length in the host polyamine (PL ~ PO < PR < PAM < PEI), an observation which is explained in more detail below. Collectively, these differences between fluorescein-labeled and pyranine-labeled polyamines strongly suggest that pyranine forms a stronger electrostatic interaction with the polyamines than does fluorescein and that pyranine is more rigid when attached to the polyamine molecules.

3.3.2 Molecular modeling of probe-polyamine complexes

The potential for pyranine to undergo multi-point binding to the polyamines was investigated by performing molecular mechanics calculations on pyranine and the different polyamines used in this study. Optimization of the three-dimensional structure of pyranine showed that the three highly acidic sulfonate groups ($pK_a \sim 0.5$[19]) are spaced ~4.8-5.5Å apart along the short axis (i.e. sulfonate groups at positions 1 and 3) and ~6.0-7.1Å apart along the long axis (i.e. sulfonate groups at positions 3 and 6) of the molecule (Fig. 3.2). The distance between amino groups situated two positions apart (i.e. sidechains *i* and *i*+2) in a 16-member segment of the polyamines is within the same distance range according to molecular mechanics optimizations (Fig 3.2), in agreement with previous modeling of homogeneous polyamines using the Gaussian chain model.[34] The correlation in distances between the negatively charged sulfonates in the pyranine molecule and positively charged sidechain groups in the polyamines suggests that pyranine is able to form a two-point ionic interaction with residues *i* and (*i*+2) along the

polymer backbone. Since the N-N distances for the peptide based polymers match the distances between the sulfonate groups along both the long and short axis of the pyranine molecule it is possible for the pyranine:polyamine complex to form either with the sulfonate groups at positions 1 and 3 or positions 3 and 6 paired with the positive charges on the polymer.

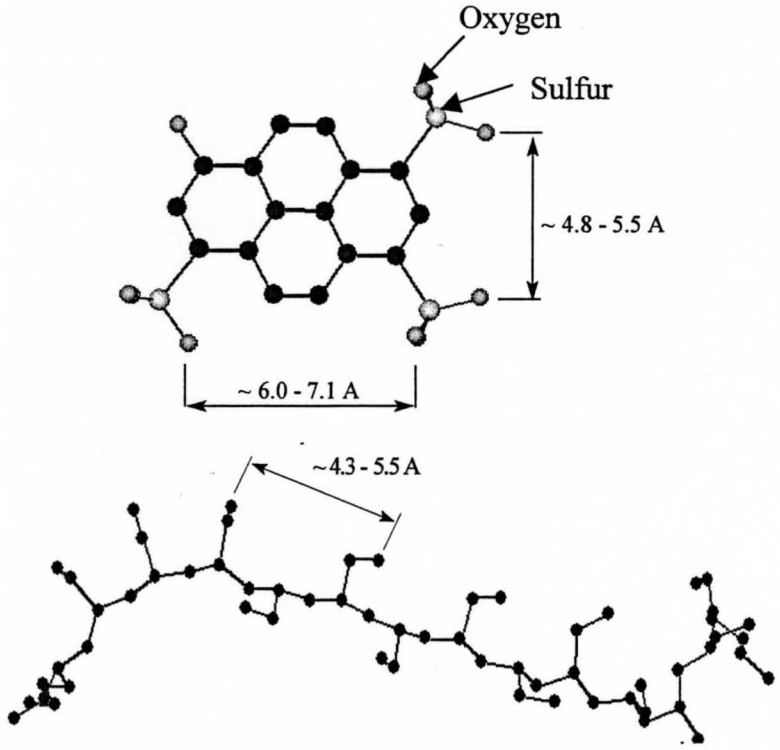

Note that the end of each side chain contains an amine group and the distance shown refers to the distance between these amine groups.

Homopolymer	N-N distance, Å	Sidechain Length
Poly-L-arginine	4.0 – 8.6	6
Poly-D-lysine	3.8 - 8.2	5
Poly-L-ornithine	4.6 – 7.8	4
PAM	4.3 – 5.5	2
PEI	4.5 – 5.0	0

Figure 3.2. Distances between adjacent sulfonate groups on pyranine and the N-N distance of two spatially close nitrogen atoms of the side chains calculated from the three dimensional structures of a 16-member segment of PAM. N-N distances for other polyamines used are listed below. Structures were optimized using the semiempirical AM1 method. Aromaticity in the benzene rings of pyranine was omitted for clarity.

Because pyranine has 3 sulfonate groups there does exist the possibility for three-site binding of the pyranine to the charged polyamines. However, the sulfonate group that is free when pyranine forms a double-point ionic bond is located on the opposite side of the pyranine molecule (Fig. 3.2) and its orientation relative to the closest ammonium group in the polymer would require considerable bending of the polymer backbone. Given the steric and geometrical requirements for this to occur and considering the limited overall flexibility of the backbone[32,35,36] three-site binding of pyranine is unlikely, an assumption that is also supported by mass spectrometry of non-covalent complexes of proteins with trisulfonated pyrene receptors.[17] Hence, double-point binding of the pyranine probe to the cationic polymers is expected to be the dominant interaction.

In contrast to pyranine, fluorescein contains a moderately acidic carboxylate group and a much less acidic phenol group ($pK_a \sim 4.34$ and 6.68, respectively[37]). Therefore, the carboxylic acid is likely to be the only possible point of attachment to the amino side chain. Since a single ionic bond allows a considerable degree of rotation of the label around that bond, the probe motion would not be significantly compromised after binding. This explains the experimental data obtained for fluorescein-labeled

polyamines. From these theoretical considerations and given the disparity in experimental data with respect to the reversibility of absorption shifts and the increased steady-state anisotropy values for pyranine relative to fluorescein, the increased rigidity of the pyranine-polyamine complexes is attributed to pyranine being rigidly bound to the polyamines through two points of attachment.

3.3.3 Time-resolved Fluorescence Anisotropy

TRFA data was collected to compare the information on rotational dynamics of polyamines labeled with different fluorophores: fluorescein vs. pyranine. Also, the effect of subtle structural variations in the side chain length of polyamine on the TRFA decay parameters was studied. The intensity decay functions used to construct the anisotropy decays, were essentially monoexponential, however each probe did show a slight contribution from a second—and in the case of PEI, a third—shorter lifetime component (~ 2 ns for fluorescein and ~ 3 ns for pyranine) that is likely due to a slight alteration of the charge on the probe as a result of ionic binding (Table 3.3).[9]

Polymer	**PL**		**PO**		**PR**		**PAM**		**PEI**	
Probe:	Fluorescein	Pyranine	Fluorescein	Pyranine	Fluorescein	Pyranine	Fluorescein	Pyranine	Fluorescein	Pyranine
τ_1 (ns)	4.28 ± 0.01	2.76 ± 0.008 (0.024[b])	2.05 ± 0.01 (0.04)	2.73 ± 0.009 (0.036)	2.17 ± 0.01 (0.08)	2.85 ± 0.005 (0.026)	2.20 ± 0.01 (0.07)	2.87 ± 0.06 (0.033)	0.172 ± 0.01 (0.32)	2.65 ± 0.007 (0.048)
τ_2 (ns)	-	5.51 ± 0.005 (0.976)	4.01 ± 0.01 (0.96)	5.52 ± 0.004 (0.964)	4.33 ± 0.01 (0.92)	5.80 ± 0.004 (0.973)	4.13 ± 0.01 (0.93)	5.77 ± 0.006 (0.967)	1.37 ± 0.01 (0.39)	5.42 ± 0.004 (0.952)
τ_3 (ns)	-	-	-	-	-	-	-	-	2.92 ± 0.01 (0.29)	-
χ^2_R	1.23	1.05	1.21	1.04	1.10	1.03	1.25	1.05	1.10	1.01
ϕ_1 (ns)	0.220 ±	0.651 ±	0.200 ±	0.636 ±	0.460 ±	0.910 ±	0.562 ±	1.25 ±	0.17 ± 0.02	1.29 ±

	0.03	0.03	0.02	0.03	0.04	0.05	0.02	0.08		0.07
ϕ_2(ns)	1.63 ± 0.05	2.91 ± 0.06	1.34 ± 0.05	3.49 ± 0.03	1.40 ± 0.04	4.03 ± 0.10	3.69 ± 0.09	6.07 ± 0.17	1.29 ± 0.05	7.91 ± 0.18
r_o	0.333	0.324	0.399	0.301	0.390	0.324	0.359	0.319	0.376	0.335
r_∞	0.002	0.00	0.004	0.001	0.006	0.018	0.004	0.014	0.012	0.003
g	0.006	0.00	<0.001	0.003	0.015	0.056	0.014	0.044	0.032	0.009
f	0.371	0.317	0.470	0.354	0.357	0.251	0.206	0.170	0.122	0.092
$1\text{-}f\text{-}g$	0.623	0.683	0.530	0.645	0.628	0.693	0.780	0.786	0.846	0.899
χ^2_R	1.03	1.04	0.99	1.02	1.02	1.02	1.04	1.02	1.04	1.00

Table 3.3. Rotational Anisotropy Decay Parameters for pyranine and fluorescein-labeled polyamines (0.05%) in 5mM Tris-HCl, pH8.3[a]. τ, fluorescence lifetime; ϕ_1, ϕ_2, rotational correlation times; f, fractional contribution to anisotropy decay owing to ϕ_1; $1\text{-}f\text{-}g$, fractional contribution to anisotropy decay owing to ϕ_2; r_0, limiting anisotropy; r_∞, residual anisotropy; g, fraction of motion > 60 ns ($g = r_\infty / r_0$); χ^2_R, reduced chi-squared. b) fractional contributions from lifetimes. All errors in intensity and anisotropy decay times represent one standard deviation.

The anisotropy decays were successfully deconvoluted into two time components, ϕ_1 and ϕ_2, for both fluorescein and pyranine complexes and showed a negligible residual anisotropy (r_∞), consistent with a high degree of polymer flexibility[38] and the absence of contributions from the overall polymer rotation in the measured decays (Fig. 3.3). Comparison of the anisotropy decays for fluorescein and pyranine-labeled PL, PR and PAM shows that when the polymer is labeled with pyranine the fluorescence anisotropy decays more slowly compared to fluorescein-labeled polymers, indicating a more rigid

complex between pyranine and the polymers (Fig. 3.3). The rigidity of the pyranine complex is dependent upon the polymer and hence the sidechain group to which the probe is bound, as indicated by the different decay profiles for pyranine labeled-PL, PAM and PR (Fig 3.3b, 3.3d, 3.3e, respectively) and the differences in the two time components derived from the slopes of the double exponential decay curves (Table 3.3).

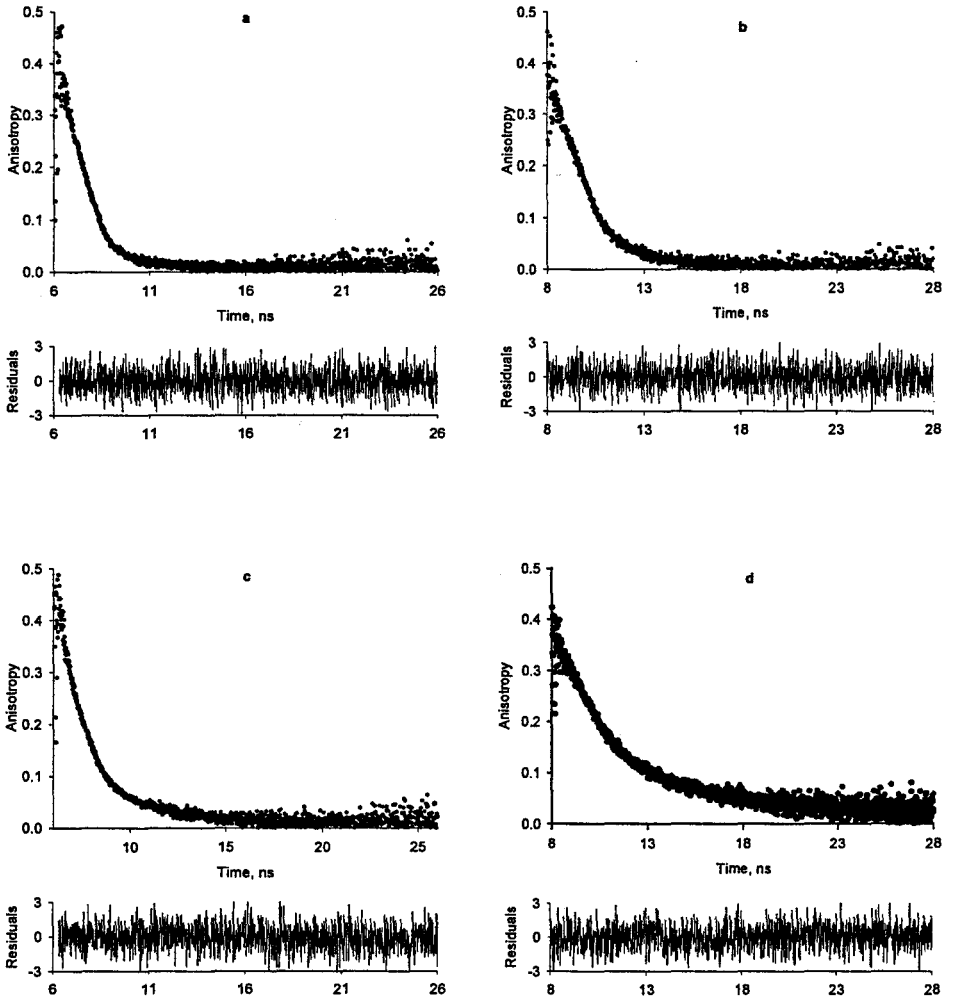

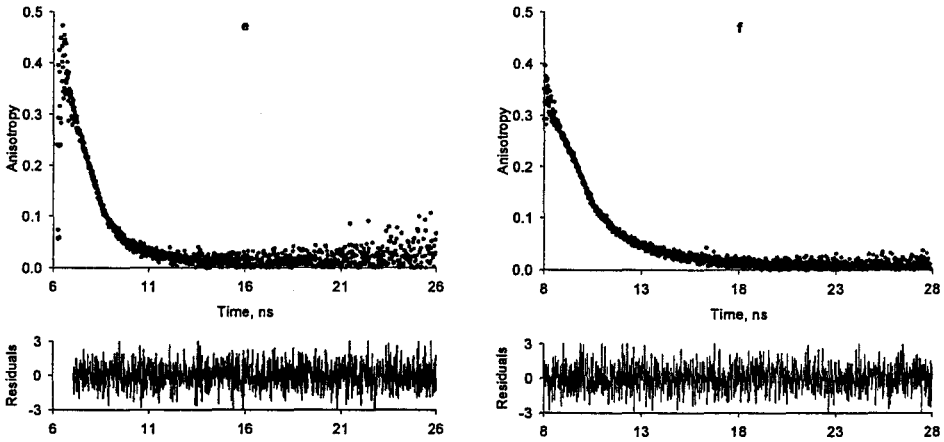

Figure 3.3. Time-resolved anisotropy decays and residual plots for difference fits of (a) PL-fluorescein; (b) PL-pyranine; (c) PAM-fluorescein; (d) PAM-pyranine; (e) PR-fluorescein and; (f) PR-pyranine. Solvent, 5 mM Tris-HCl, pH 8.3; 0.05% peptide concentration; 1.4 μM Fluorescein; 2 μM pyranine. Plots (a) and (c) have been published previously[9] and are shown for comparison.

3.3.3.1 Side-chain and Backbone Dynamics of Fluorescein-labeled Polypeptides

The two rotational correlation times, ϕ_1 and ϕ_2 ($\phi_1 < \phi_2$) obtained from the fit of TRFA decay to a biexponential function (Eq. 3.2) have been attributed to the motion of the sidechain segment to which the probe is bound and the motion of a short segment of the polymer backbone, respectively.[9] Because the probe-binding site involves the sidechain of the polymer, the freedom of the probe to undergo independent motion relative to the polymer is reflected in the shorter correlation time, ϕ_1. Hence, ϕ_1 can be used as an

indicator of the rigidity of the interaction between the probe and the polymer; that is, a larger ϕ_1 value signifies a more rigid interaction.

Both fluorescein-labeled PO and PL showed very short correlation times (~ 0.20 ns) that likely result from the long sidechain and the high flexibility due to the large number of degrees of freedom (Fig. 3.4). The ϕ_1 values are significantly increased when sidechain length and flexibility are reduced, as seen, for example, from the ϕ_1 correlation time for PAM (~0.56 ns), where the sidechain contains only two degrees of freedom and flexibility of the sidechain is hindered. Notably, PR also shows a significant reduction in ϕ_1 (~2-fold) relative to the other peptide-based polymers despite having a longer sidechain (6 atoms linearly) and more degrees of freedom. This result likely reflects the rigidity of the planar geometry of the guanidinium group at the end of the arginine sidechain, causing the probe to become more rigid and less mobile. Interestingly, the side chain correlation time for PEI shows the presence of very fast depolarization despite the absence of a sidechain. This small ϕ_1 value likely reflects the internal rotation within the fluorescein probe resulting from rotation about the C-C bond connecting the single benzene group to the xanthene ring or rotation about the C-N bond axis in the backbone itself, an effect that would not be seen in the peptide-based polymers due to the partial double-bond character of the peptide bond.

3.4 a)

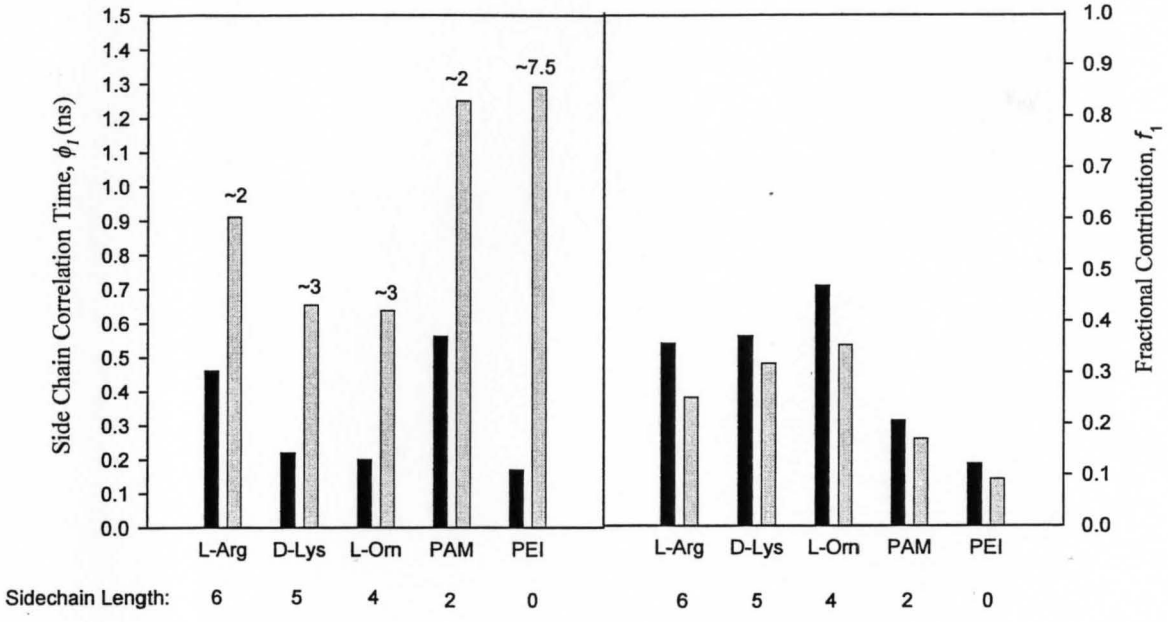
Side Chain Correlation Time, ϕ_1 (ns)
Fractional Contribution, f_1
~2
~3
~3
~2
~7.5
L-Arg
D-Lys
L-Orn
PAM
PEI
Sidechain Length: 6 5 4 2 0

3.4 b)

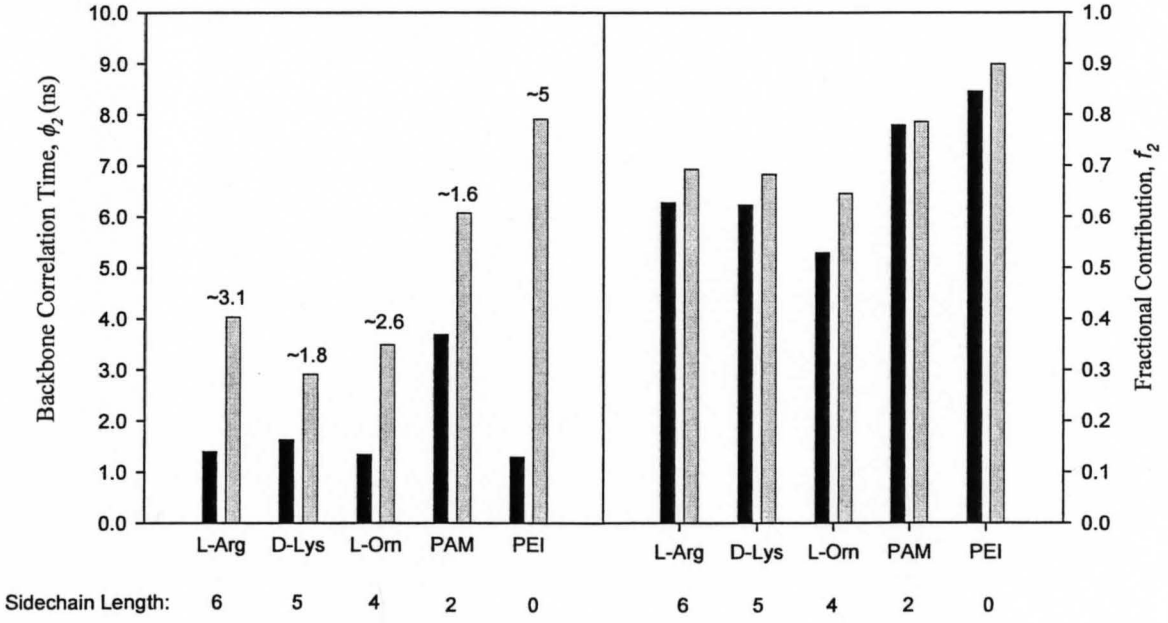
Backbone Correlation Time, ϕ_2 (ns)
Fractional Contribution, f_2
~3.1
~1.8
~2.6
~1.6
~5
L-Arg
D-Lys
L-Orn
PAM
PEI
Sidechain Length: 6 5 4 2 0

Figure 3.4: Comparison of time-resolved fluorescence anisotropy data for (a) sidechain and (b) backbone motions using single-point (■) and double-point (▒) ionic labeling with fluorescein and pyranine, respectively. Left panels show correlation times; right panels show fractional contributions. Data for fluorescein labeled PL and PAM were previously published[9] and are shown for comparison.

To determine how well the ϕ_2 component reflects the segmental dynamics of the labeled macromolecules, we have compared the measured ϕ_2 values for the peptide-based polymers to previous ^{13}C NMR relaxation measurements.[39-42] Several previous studies have shown that while both NMR and TRFA methods can yield identical rotational correlation times,[43,44] in many cases, rotational correlation times determined by TRFA are shorter than those obtained from NMR data,[45,46] likely due to the effect of independent probe motions in fluorescence experiments. The averaged rotational correlation time for C_α atoms in PL measured by ^{13}C NMR at 28 °C in water is ~4.5 ns.[36] In the present study the ϕ_2 values obtained by TRFA were in the range of ~1.5 ns for all the fluorescein-labeled polymers with the exception of PAM, which showed a ϕ_2 value of ~3.7 ns (Fig 3.4). The higher ϕ_2 value for PAM is expected, however, given the rigidity of the backbone imparted by the closely spaced amine groups on the sidechain.[32] These results indicated that the ϕ_2 obtained for the fluorescein-labeled peptides by TRFA is ~3-fold shorter than the correlation times obtained in NMR experiments, a result that highlights the significant decoupling of the probe motion from the polymer segmental motion, as expected given the short ps motion of the long sidechains. Importantly, shortening of the

sidechain for these polymers had no significant effect on the ϕ_2 values of the peptides, as the three peptides showed similar correlation times despite the differences in side chain length (Fig. 3.4). Hence, for probes bound through a single ionic bond it is not possible to accurately determine the rates of protein segmental motions, in agreement with previous studies involving covalently bound probes.[45,46]

3.3.3.2 Side-chain and Backbone Dynamics of Pyranine-labeled Polymers

With the exception of PEI, ionic labeling of the polymers with pyranine resulted in a ~2-3-fold increase in the sidechain correlation time, ϕ_1, relative to those seen with fluorescein-labeled polymers, regardless of sidechain length (Fig. 3.4). The observed slower motion of the sidechain in general is in agreement with steady-state anisotropy data, and is indicative of more rigid binding of the probe to the polymer owing to the double-point binding between pyranine and the polymers.[7,18,20] Specifically, PAM and PEI both show sidechain correlation times in the nanosecond range (ϕ_1=1.25 ns and 1.29 ns, respectively) while the peptide-based polymers show significantly longer ϕ_1 values (~0.60-0.90 ns) compared to fluorescein labeled peptides (~0.20-0.45 ns; Fig. 3.4). In all cases the fractional contribution, f_1, slightly decreases for pyranine-labeled polymers relative to fluorescein-labeled polymers, giving further indication that the local probe motions are reduced for all polymers when labeled with pyranine.

As was the case with the sidechain correlation times, Figure 3.4 shows that, with the exception of PEI, labeling of the peptide-based polymers with pyranine led to roughly a ~2-3-fold increase in the ϕ_2 correlation times relative to those obtained with fluorescein-

labeled polymers. The overall increase in both the value and fractional contribution of ϕ_2 results from the ability of pyranine to form a more rigid complex with the polymers (as indicated by the increased ϕ_1 correlation times), which in turn leads to improved coupling of the probe to the backbone motion of the polymers. More importantly, the ϕ_2 values determined from TRFA analysis of pyranine-labeled peptides more accurately reflect the backbone correlation times measured by NMR spectroscopy (ϕ = 4.5 ns), particularly in the case of PR (ϕ_2 = 4.0 ns). Poorer agreement was observed for PO (ϕ_2 = 3.5 ns) and PL (ϕ_2 = 2.9 ns), consistent with the greater degree of motion for these sidechains relative to the sidechains in PR. Taken together, these results suggest that the ability of pyranine to couple to the backbone motion of the polymer is improved as the length of the sidechain to which the probe is attached decreases. It is worth noting that double-point labeling does not lead to artificial restriction of the backbone motion, as indicated by the very low g-value obtained in solution (g<0.05 in all cases) and the fact that the backbone correlation times are lower than those seen in NMR experiments.

It is important to further consider the TRFA results obtained for pyranine labeled PR. On the basis of chain length alone, one should expect a lower ϕ_1 value and hence less rigid coupling of the probe to the backbone motion relative to PL or PO, which is opposite to the data obtained. The origin of the increased ϕ_1 value for pyranine-labeled PR could be due to the planarity of the guanidinium group at the end of the arginine sidechain, or the ability of arginine to form a bidentate "ring-structured" salt bridge with a single sulfonate group.[47,48] The latter scenario is thought to be responsible for the increased specificity between arginine sidechains and sulfonate dyes[17,18] and in the

current study, provides the opportunity for four potential points of contact between the pyranine molecule and the sidechains in PR (two per sidechain), facilitating a much stronger and more rigid interaction between the probe and polymer. This highlights the fact that both chain length and chain rigidity influence the coupling of the probe to the backbone, and suggests that optimal coupling of pyranine to proteins should be obtained for proteins containing appropriately spaced Arg residues on their surface.

TRFA data for pyranine complexes with PAM and PEI also warrant further discussion. In the case of PAM, the sidechain length is minimal and the proximity of the charged sidechains provides a rigid connection between the probe binding site and the polymer backbone. This provides optimal conditions for pyranine coupling to the backbone motion of the polymer, which is supported by the high fractional contribution of the ϕ_2 correlation time of the polymer (~78%) when labeled with pyranine. Interestingly, the fractional contribution for ϕ_2 observed for fluorescein-labeled PAM was approximately the same, indicating that both fluorescein and pyranine are well coupled to the backbone motion of PAM, likely due to the rigidity and short sidechain length. A difference in the ϕ_2 correlation times for fluorescein (ϕ_2 ~3.69 ns) and pyranine (ϕ_2 ~6.07 ns) labeled PAM highlights the effect that rapid local motions in the fluorescein-labeled polymer systems have on observing the true segmental motion of the polymers.

As shown in Figure 3.4, the difference in ϕ_1 and ϕ_2 was particularly large for fluorescein and pyranine-labeled PEI, which has no sidechain. Despite the lack of a sidechain, a significant fraction of a relatively fast motion (9% of a 1.3 ns component) remained when PEI was labeled with pyranine (Fig. 3.4). The slower correlation time

relative to fluorescein (170 ps) suggests that this is not due to a fraction of pyranine that is bound through a single site. Furthermore, the significant increase in ϕ_2 for pyranine (ϕ_2 = 7.9 ns) relative to fluorescein (ϕ_2 = 1.3 ns) supports the binding of pyranine through two sites. The small fraction of relatively rapid motion for pyranine-bound PEI is thus most likely due to "wobbling" of the dye around the long axis of the polymer, which will not be completely restricted when only two bonds form between the dye and polymer chain. Clearly, increases in chain length will result in significant increases in the degree of wobbling motion, combined with torsional motion owing to the potential for rotation of bonds in the longer sidechains. This leads to the observed increase in fractional contribution and decrease in ϕ_1 for the other pyranine-polymer systems as chain length increases.

3.3.4 Behaviour of Fluorescein and Pyranine-Polymer Systems Entrapped in Silica:

To demonstrate the utility of TRFA measurements using pyranine-labeled polymers, we reinvestigated the dynamics of two model polyamines when entrapped in sol-gel derived silica. A previous study of fluorescein-labeled PL and PAM entrapped in sodium silicate derived hydrogels showed that the entrapment of PAM-fluorescein in sodium silicate resulted in a significant increase in ϕ_2 relative to solution (e.g. 3.7 ns in solution vs. 10.7 ns in sodium silicate), while the mobility of entrapped PL appeared to be almost identical to that in solution.[9] The latter result was not expected, given that PL should show significant dampening of motion owing to electrostatic interactions with the silica

surface. Indeed, such interactions have been utilized in the templating of silica to form mesostructured materials.[49]

The above results were initially attributed to the increased flexibility of PL relative to PAM as a result of increased spatial freedom for flexion of the peptide backbone within the pores formed in PL doped silica. Evaluation of the pore size distributions in PL templated silica materials by Hawkins et al. (49), however, revealed average pore sizes in the range of 1.5 nm for silica materials synthesized using α-helical PL as a templating agent.[49] Furthermore, materials derived from PL in the random coil conformation revealed a much lower surface area and total pore volume, suggesting that the mobility of PL would be considerably restricted in these materials due to the confinement imparted by the small pores. These findings, together with the fact that PL should be electrostatically adsorbed to the anionic pore walls in silica hydrogels, strongly suggests that the PL polymer ought to demonstrate considerable restricted motion relative to that seen in solution, and has prompted us to revisit the behaviour of polyamines entrapped in sodium silicate.

In contrast to the fluorescein-labeled PAM and PL, the two polyamines labeled with pyranine both showed a significant restriction in motion upon entrapment in sodium silicate, as seen by the high residual anisotropy of the entrapped polyamines relative to solution (Fig. 3.5, top). This is in contrast to the results seen previously with encapsulated fluorescein-labeled polymers, which showed a high fraction of hindered motion for PAM but not for PL (Fig. 3.5, bottom). The significant amount of hindered motion observed for entrapped Pyr-polymer complexes is consistent with the expected binding of the

polymers to the silica surfaces, and thus the apparent mobility of fluorescein-labeled PL (and PAM) is consistent with the inability of fluorescein to effectively couple to the segmental motion of the polymer.

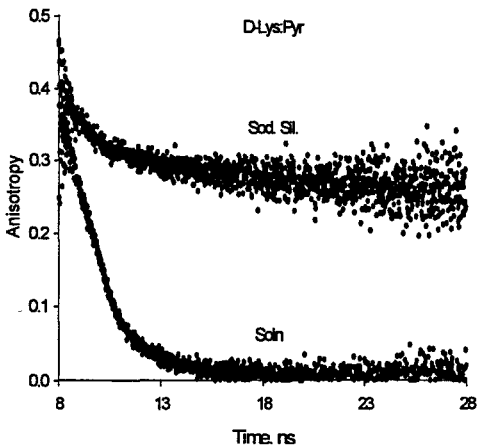

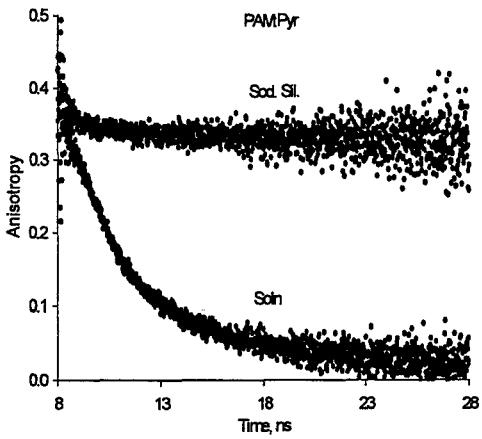

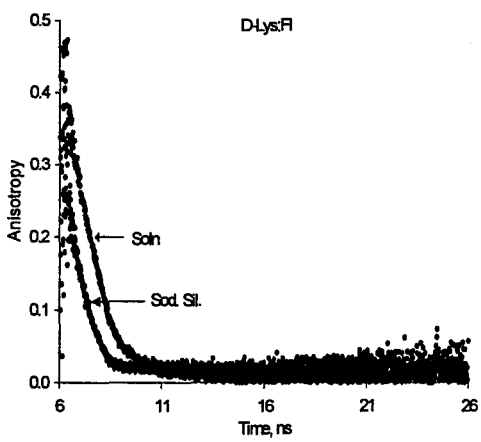

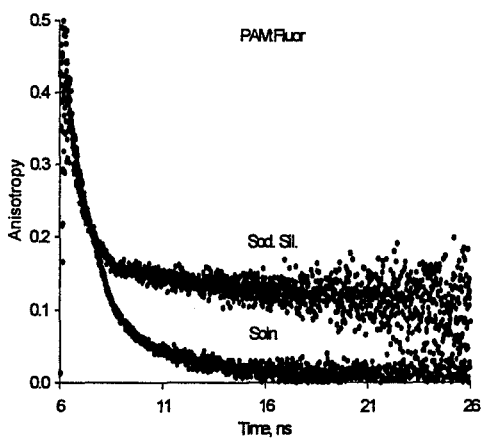

Figure 3.5: Comparison of anisotropy decays for fluorescein and pyranine-labeled PL and PAM entrapped in sodium silicate hydrogels. The pyranine labeled species (top) show a large degree of restricted motion compared to previous studies with the fluorescein labeled polymers (bottom) (from ref 9).

In accordance with the increased *g*-value, the ϕ_2 value for pyranine labeled PL showed evidence of decreased mobility upon entrapment (ϕ_2 = 10.3 ns in silica vs. 2.9 ns in solution; Table 3.4; Fig 3.6, right). The ~10 ns backbone correlation time for entrapped pyranine-labeled PL is, again, markedly different from that obtained for the entrapped fluorescein labeled species, which previously showed a ϕ_2 value of 4.0 ns.[9] Interestingly, pyranine labeled PAM also showed an increase in the backbone correlation time ($\phi_2 \sim$ 41 ns) compared to the entrapped fluorescein labeled species ($\phi_2 \sim$ 10.6 ns) further highlighting the effect that local probe motions have on the correct interpretation of anisotropy decay data (Fig. 3.6).

Polymer:	**PL**	**PAM**
τ_1 (ns)	2.62 ± 0.01 (4.56%)	2.65 ± 0.01 (6.87%)
τ_2 (ns)	5.46 ± 0.01 (95.44%)	5.52 ± 0.01 (93.13)
χ^2_R	1.08	1.11
ϕ_1 (ns)	0.37 ± 0.06	0.50 ± 0.10
ϕ_2 (ns)	10.30 ± 0.08	41.40 ± 3.52
r_o	0.409	0.371
r_∞	0.245	0.304
g	0.601	0.819

f	0.018	0.002
$1\text{-}f\text{-}g$	0.381	0.179
χ^2_R	1.05	1.03

Table 3.4: TRFA data for pyranine labeled polymers entrapped in sodium silicate derived hydrogels.[a] (a) All symbols are as defined in Table 3.3.

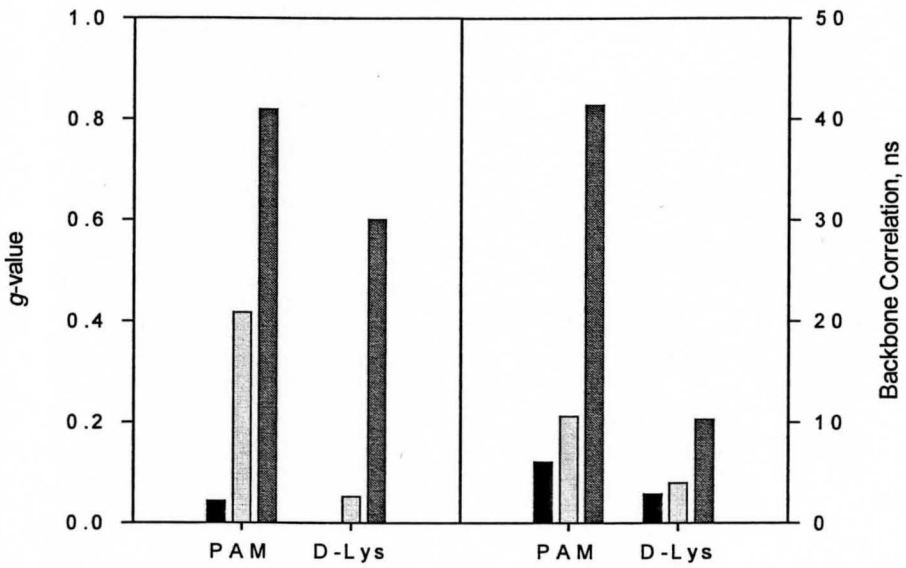

Figure 3.6: Comparison of g-values (left) and backbone correlation times, ϕ_2, (right) for Pyr-PL and Pyr-PAM complexes in solution (■), fluorescein-PL and fluorescein-PAM in sodium silicate (■, from ref 9) and Pry-PL and Pyr-PAM in sodium silicate (■).

Collectively, the increase in g-value and backbone correlation times indicates that there is indeed a significant reduction in polymer mobility for both PL and PAM resulting from the electrostatic interaction between the polymer and the silica surface. It is worth noting that entrapped PAM shows a higher degree of hindered motion ($g \sim 0.8$) relative to

entrapped PL (g = 0.6) and a higher ϕ_2 value (41 ns vs. 10.3 ns), indicating that the reduction in mobility upon entrapment is dependent on the degree of polymer flexibility, in keeping with our initial findings.[9] This is likely due to more efficient templating of the silica around the more rigid PAM polymer, a process that would be inherently less efficient for more flexible species such as PL. It is worth mentioning that the current results support our original hypothesis that more flexible polyamines retain a higher degree of flexibility compared to more rigid polymers when entrapped,[9] however, the difference is clearly not nearly as great as we originally predicted.

The ability to accurately assess the segmental motion of polymers within silica is likely to have significant ramifications in future studies of pyranine-labeled proteins within such materials. Currently, there is a large body of literature on protein dynamics in silica, a great deal of which has relied on the use fluorescence spectroscopy[50,51,52] owing to the small amount of protein contained in these materials, which precludes NMR dynamics studies.[53] These studies often provide contrasting views on the effects of encapsulation on protein mobility within silica, perhaps due in part to the fact that such studies usually employ probes that are bound through a single bond. It is possible that proteins are in fact much less mobile in silica than is currently thought, a possibility that could have implications in the overall function of these systems, given the importance of dynamic motions in protein function.[42,54] To our knowledge, no two-point labeling technique (covalent or non-covalent) has been applied to study protein dynamics in sol-gel materials. Clearly, the potential to non-covalently label proteins through a 2 point interaction will provide a new tool for probing protein dynamics within silica, and is

likely to result in new insights into the nature of protein-silica interactions and the effects of protein dynamics on activity.

3.3.5 Implications of Two-Point Ionic Labeling

The side group mobility and its relation to the backbone chain dynamics measured by TRFA is a complex problem recently addressed by Duhamel.[55] The important conclusion from those studies is that a residue located inside the polymer coil probes only a finite volume of the polymer. As a first approximation, the polymer can be described as a consistent, flexible model of interconnected rigid bonds and the probe as a fast-rotating species fixed at one terminal bond. The rotation of the probe can be completely uncoupled from the polymer movement by using a long, flexible connection separating it from the rest of the polymer.[8,9,10,55] We have shown that even in cases where the probe is attached by a short linker (e.g. PAM and PEI), the possibility of rapid probe motions skewing the interpretation of fluorescence anisotropy data still exists when the probe is attached through a single bond.

Covalent bifunctional probes have been used previously to minimize the effects of independent probe motions in both EPR[13] and fluorescence experiments.[14,15] The synthesis of improved bifunctional fluorescent probes has also provided tools for determining specific structural features of a protein, including subunit orientation,[11] and effective methods to label specific recombinant proteins to more effectively monitor intracellular activity.[56] However, despite the clear advantages of these probes for accurately determining the rotational motions of biomolecules, fluorescent probes

utilizing two points of attachment have not yet been widely used in TRFA experiments aimed at studying segmental protein motions, likely because the majority of these probes require surface-accessible cysteine residues that are appropriately spaced for labeling.

The present study represents the first successful use of fluorescent probe attached via two ionic bonds to study backbone segmental motions using TRFA. Improved coupling to the polymer movement was demonstrated based on improved correlation with NMR dynamics data, even in the presence of a long linker. Furthermore, the method was amenable to studies of both free and entrapped polymers, highlighting the versatility of the labeling method. This technique provides a specific advantage over the covalent dimaleimide probes in that the positively charged sidegroups that are required for the two-point interaction to occur are prevalent on the surface of a protein. Indeed, even though the chain lengths of Lys and Arg groups are 5 and 6 carbons, respectively, double point binding to these groups leads to significant improvements in coupling of the probe to the backbone motion. Given that several proteins, including lysozyme, cytochrome c, RNAse A, myoglobin, adenylate kinase, aldolase and HSA, have been shown to have greater than 1:1 binding stoichiometry between amino groups and sulfonated dyes,[18,19,20] it is likely that this labeling method should be widely applicable. In comparing Lys to Arg, the latter shows significantly better coupling of the probe to the biomolecule and our results indicate that the double-point ionic interaction between pyranine and PR is preserved up to 150 mM ionic strength, while that for PL is not, suggesting that selective labeling of Arg should be possible when operating under physiological conditions. Thus, proteins with R-X-R motifs are likely to be best suited to TRFA studies using ionically

bound pyranine. While such a motif is not generically present in all proteins, incorporation of such a motif should be relatively straightforward using recombinant methods. Thus, the 2-point labeling method should be applicable to a wide range of proteins.

3.4 Acknowledgements

The authors thank the Natural Sciences and Engineering Research Council of Canada, MDS-Sciex, the Ontario Ministry of Energy, Science and Technology, the Canada Foundation for Innovation and the Ontario Innovation Trust for support of this work. JDB holds the Canada Research Chair in Bioanalytical Chemistry.

3.5 References:

1. Patonay, G.; Salon, J.; Sowell, J.; Strekowski, L. *Molecules* **2004**, 9, 40-49.

2. Colyer C. *Cell Biochem. Biophys.* **2000,** *33,* 323-337.

3. Xu G.; Takamoto, K.; Chance, M. R. *Anal. Chem.* **2003**, *75*, 6995-7007.

4. Salih, B.; Zenobi, R. *Anal. Chem.* **1998**, *70*, 1536-1543.

5. Matulis, D.; Lovrien, R. *Biophys. J.* **1998**, *74*, 422-429.

6. Haugland, R. P. in *Handbook of Fluorescent Probes and Research Chemicals*; Spence, M. Z.; 6th ed; Molecular Probes Inc: Eugene, OR, 1996.

7. Gutman, M.; Nachliel, E.; Huppert, D. *Eur. J. Biochem.* **1982**, *125*, 175-181.

8. Tao, T. *FEBS Lett.* **1978,** *93*, 146-150.

9. Tleugabulova, D.; Czardybon, W.; Brennan, J. D. *J. Phys. Chem. B* **2004**, *108,* 10692-10699

10. Cohen, B. E.; Pralle, A.; Yao, X.; Swaminath, G.; Gandhi, C. S.; Jan, Y. N.; Kobilka, B. K.; Isacoff, E. Y.; Jan, L.Y. *Proc. Natl. Acad. Sci.* **2005**, *102*, 965-970.

11. Corrie, J. E.; Craik, J. S.; Munasinghe, R. N. *Bioconjugate Chem.* **1998**, *9,* 160-167.

12. Mercier, P.; Ferguson, R.E.; Irving, M.; Corrie, J.E.T; Trentham, D.R.; Sykes, B.D. *Biochemistry* **2003**, *42*, 4333-4348.

13. Wilcox, M. D.; Parce, J. W.; Thomas, M. J.; Lyles, D. S. *Biochemistry* **1990**, *29*, 5734-5743.

14. Packard, B.; Edidin, M.; Komoriya, A. *Biochemistry* **1986**, *25*, 3548-3552.

15. Timbs, M. M.; Thompson, N. L. *Biophys. J.* **1990**, *58*, 413-428.

16. Forkey, J.N.; Quinlan, M.E.; Shaw, M.A.; Corrie, J.E.T.; Goldman, Y.E. *Nature* **2003**, *422*, 399-404.

17. Friess, S. D.; Zenobi, R. *J. Am. Soc. Mass Spectrom.* **2001**, *12*, 810-818.

18. Friess, S. D.; Daniel, J. M.; Zenobi, R. *Phys. Chem. Chem. Phys.* **2004**, 6, 2664-2675.

19. Gutman, M.; Huppert, D.; Nachliel, E. *Eur. J. Biochem.* **1982**, *121*, 637-642.

20. Yam, R.; Nachliel, E.; Kiryati, S.; Gutman, M.; Huppert, D. *Biophys. J.* **1991**, *59*, 4-11.

21. Cha, J. N.; Birkedal, H.; Euliss, L. E.; Bartl, M. H.; Wong, M. S.; Deming, T. J.; Stucky, G. D. *J. Amer. Chem. Soc.* **2003**, *125*, 8285-8289.

22. Bhatia, R. B.; Brinker, C. J.; Gupta, A. K.; Singh, A.K. *Chem. Mater.* **2000**, *12*, 2434-2441.

23. Demas, J. N. *Excited-State Lifetime Measurements*; Academic Press: New York, 1983.

24. Lakowicz, J. R.; Gryczynski, I. *Topics in Fluorescence Spectroscopy*; Vol. 1 Plenum: New York, 1991.

25. a) Bright, F. V.; Betts, T. A.; Litwiler, K. S. *CRC Crit. Rev. Anal. Chem.* **1990**, *21*, 389-405, b) Bright, F. V. *Appl. Spectrosc.* **1995**, *49*, 14A-20A.

26. Geddes, C. D.; Karolin, J.; Birch, D. S. *J. Phys. Chem. B* **2002**, *106*, 3835-3841.

27. Gaussian 98, Revision A.9, M. J. Frisch, G. W. Trucks, H. B. Schlegel, G. E. Scuseria, M. A. Robb, J. R.; Cheeseman, V. G. Zakrzewski, J. A. Montgomery, Jr., R. E. Stratmann, J. C. Burant, S. Dapprich, J. M. Millam, A. D. Daniels, K. N. Kudin, M. C. Strain, O. Farkas, J. Tomasi, V. Barone, M. Cossi, R. Cammi, B.; Mennucci, C. Pomelli, C. Adamo, S. Clifford, J. Ochterski, G. A. Petersson, P. Y. Ayala, Q. Cui, K.;Morokuma, D. K. Malick, A. D. Rabuck, K. Raghavachari, J. B. Foresman, J. Cioslowski, J. V. Ortiz, A. G. Baboul, B. B. Stefanov, G. Liu, A. Liashenko, P. Piskorz, I. Komaromi, R. Gomperts, R. L. Martin, D. J. Fox, T. Keith, M. A. Al-Laham, C. Y. Peng, A. Nanayakkara, M. Challacombe, P. M. W. Gill, B. Johnson, W. Chen, M. W. Wong, J. L. Andres, C. Gonzalez, M. Head-Gordon, E. S. Replogle, and J. A. Pople, Gaussian, Inc., Pittsburgh PA, 1998.

28. Allinger, N. L. *J. Am. Chem. Soc.* **1977**, *99*, 8127-8134.

29. Weiner, S. J.; Kollman, P. A.; Nguyen, D. T.; Case, D. A. *J. Comput. Chem.* **1986**, *7*, 230-252.

30. Caruso, F.; Donath, E.; Mohwald, H.; Georgieva, R. *Macromolecules* **1998,** *31*, 7365-7377.

31. Welder, F.; Paul, B.; Nakazumi, H.; Yagi, S.; Colyer, C. L. *J Chromatogr B* **2003,** *793*, 93-105.

32. Itaya, T.; Ochiai, H. *J. Polym. Sci., Polym. Phys. Ed.* **1992,** *30,* 587-590.

33. Debnath, P; Cherayil, B. J. *J. Chem. Phys.* **2004,** *120*, 2482-2489.

34. Kundrotas, P. J.; Karshikoff, A. *Biochim. Biophys. Acta.* **2004,** *1702*, 1-8.

35. Kobayashi, S.; Suh, K. D.; Shirokura, Y. *Macromolecules* **1989**, *22*, 2363-2366.

36. Wittebort, R. J.; Szabo, A.; Gurd, F. R. N. *J. Amer. Chem. Soc.* **1980**, *102*, 5723-28.

37. Smith, S. A.; Pretorius, W. A. *Water SA* **2002**, *28*, 395-402.

38. Spyros, A.; Dais, P.; Heatley, F. *Macromolecules* **1994**, *27*, 5845-5857.

39. Ishima, R.; Torchia, D. A. *Nature Struct. Biol.* **2000**, *7*, 740-743.

40. Palmer, A. G. *Annu. Rev. Biophys. Biomol. Struct.* **2001,** *30*, 129-55.

41. Columbus, L.; Hubbell, W. L. *Trends Biochem. Sci.* **2002,** *27*, 288-295.

42. Eisenmesser, E. Z.; Millet, O.; Labeikovsky, W.; Korzhnev, D. M.; Wolf-Watz, M.; Bosco, D. A.; Skalicky, J. J.; Kay, L. E.; Kern, D. *Nature* **2005**, *438*, 117-121.

43. Moncrieffe, M. C.; Juranic, N.; Kemple, M. D.; Potter, J. D.; Macura, S.; Prendergast, F. G. *J. Mol. Biol.* **2000**, *297*, 147-163.

44. Alexiev, U.; Rimke, I.; Pöhlmann, T. *J. Mol. Biol.* **2003**, *328*, 705-719.

45. Palmer, A. G.; Hochstrasser, R. A.; Millar, D. P.; Rance, M.; Wright, P. E. *J. Am. Chem. Soc.* **1992,**

115, 6333-6345.

46. Kemple, M. D.; Buckley, P.; Yuan, P.; Prendergast, F. G. *Biochemistry* **1997**, *36*, 1678-88.

47. Ichimura, S.; Mita, K.; Zama, M. *Biopolymers* **1978**, *17*, 2769-2778.

48. Condie, C. C.; Quay, S. C. *J. Biol. Chem.* **1983**, *258*, 8231-8234.

49. Hawkins, K. M.; Wang, S. S.; Ford, D. M.; Shantz, D. F. *J. Am. Chem. Soc.* **2004**, *126*, 9112-9119.

50. Jordan, J. D.; Dunbar, R.A. Bright, F.V. *Anal. Chem.* **1995**, *67*, 2436-2443.

51. D. S. Gottfried, A. Kagan, B. M. Hoffman, J.M. Friedman, *J. Phys. Chem. B* **1999**, *103*, 2803-2807.

52. Sui, X.; Cruz-Aguado, J.A.; Chen, D.Y.; Zhang, Z.; Brook, M.A.; Brennan, J.D. *Chem. Mater.* **2005**, *17*, 1174-1182.

53. Brennan, J. D. *Appl. Spectrosc.* **1999**, *53*, 106A-121A.

54. Basner, J.E., Schwartz, S.D. *J. Amer. Chem. Soc.* **2005**, *127*, 13822-13831.

55. Duhamel, J.; Kanagalingam, S.; O'Brien, T. J.; Ingratta, M. W. *J. Am. Chem. Soc.* **2003**, *125*, 12810-12822.

56. Girouard, S; Houle, M. H.; Grandbois, A.; Keillor, J. W.; Michnick, S. W. *J. Am. Chem. Soc.* **2005**, *127*, 559-566.

Chapter 4

The Development of an Automated On-line Continuous Flow Competitive LC-MS Method for Screening Small Molecules Against Immobilized Receptors

This chapter is based on work performed by me in collaboration with Dr. Travis Besanger and Erica Forsberg. Dr. Besanger and Dr. Brennan are responsible for the concept of the competitive assay and designed the majority of the experiments. Dr. Besanger performed the initial proof of concept experiments not presented in this thesis. The data presented in this chapter is a direct result of experiments performed by me in co-operation with Erica Forsberg, an undergraduate summer student with continual input from Dr. Besanger and Dr. Brennan.

This chapter is targeted for submission to *Analytical Chemistry*.

Abstract

Although screening techniques that employ mass spectrometry detection have been widely successful, the inability of conventional techniques, such as frontal affinity chromatography-mass spectrometry (FAC-MS), to easily identify weak binding molecules (i.e. low μM) using small amounts of target protein (sub-picomole levels) represents a significant impediment to the widespread use of these methods in the routine screening of low abundance membrane receptors. Competitive displacement methods involving the displacement of an indicator ligand offer a more sensitive alternative, as the ability to generate an appreciable signal through various methods, including transient over-concentrations of indicator compounds, provides an unambiguous means for identifying weak affinity ligands. In this work we describe a novel on-line continuous flow competitive assay based on the principles of FAC-MS that can be widely used to identify and characterize weak affinity ligands using low levels of the *nicotinic* acetylcholine receptor from *Torpedo Californica* (*n*AChR). The validity of the assay is shown through the ability to identify nicotine (K_d~1 μM) with columns containing <2 pmol of active binding sites. Multiple injections of nicotine on a single column produces reproducible peaks in the signal of the indicator compound, epibatidine (K_d~ 2nM) showing minimal degradation in signal intensity between trials (~5%). The intensity of the peaks is dependent on the concentration of nicotine being injected and binding curves and dose-response curves can be generated through multiple injections on the same column. We investigate and optimize various parameters, including assay speed and injection volumes and concentrations and demonstrate an automated assay format with

the potential for use as a high-throughput screening tool. The potential to screen for weak binders of more pharmacologically relevant membrane receptors in a high-throughput screening format is considered.

4.1 Introduction

Several affinity screening formats have been coupled with MS detection in recent years and have been reviewed extensively,[1,2] most notably affinity selection[3,4] (AS-MS), pulsed-ultrafiltration[5] (PUF-MS) and frontal affinity chromatography[6] (FAC-MS). FAC-MS has become increasingly used in recent years, as it provides a simple method to identify novel target-ligand interactions and can rank ligand affinity while providing quantitative data on the kinetics of ligand binding. In the FAC-MS screening approach a mixture of compounds is continually infused into an affinity column resulting in an equilibrium being established between the target and individual test compounds. The relative affinities of compounds are ranked based on differences in their order of elution from the column, higher affinity ligands eluting first followed by lower affinity ligands, as governed by the relationship described in equation 4.1.[7,8,9]

$$V = V_o + \frac{B_t}{K_d + [L]} \qquad (4.1)$$

where V_o is the elution volume of a void marker that does not interact with the target, V_e is the elution volume of the analyte of interest, B_t is the total binding sites on the column, K_d is the dissociation constant for the ligand-target complex and [L] is the concentration of ligand being infused. The potential for FAC-MS to identify and characterize novel ligands in a mixture of compounds has been demonstrated for a wide range of protein targets, including β-galactosidase,[10] N-acetylglucosaminyltransferase V (GnT-V),[11]

erythropoietin-producing hepatocellular B2 (EphB2) kinase domain[12] and dihydrofolate reductase (DHFR).[13] More recently, both Wainer et al. and Besanger et al. have individually shown the capacity of FAC-MS to identify and characterize agonists, antagonists and non-competitive inhibitors of ligand-gated ion channels (LGICs), such as the *nicotinic* acetylcholine receptor (*n*AChR).[14,15] Several other reports exist that demonstrate the utility of FAC-based experiments in screening other membrane receptors, including the P-glycoprotein,[16] the $GABA_A$ and NMDA receptors[17] and several G-protein coupled receptors (GPCRs).[18,19]

Despite these noteworthy achievements, however, the use of FAC-MS in the routine screening of membrane receptors has been hindered by several factors related to column performance. Most notably, since identification of ligands using FAC-MS depends on the frontal separation of a ligand from a void marker, the ability to resolve weak binding ligands (K_d=1-10 μM) for low abundance (i.e., low to sub-picomole amounts on column) membrane receptors is significantly compromised (refer to equation 4.1). Indeed, columns with a higher loading capacity (i.e., increased B_t) can be used to improve frontal resolution, however, the challenge of producing large quantities of membrane receptors using over-expression systems can be complicated by factors, such as toxicity to host organisms and the improper orientation of receptors in host membranes.[20] Additionally, the use of larger columns to increase B_t can also increase the capacity for non-specific retention of compounds thereby making interpretation of results difficult. High backpressures with larger bead-packed affinity columns can also be problematic, as these

columns can require high flow rates that compromise the ability to directly interface these columns to low flow electrospray ionization (ESI) sources.

Alternatively, displacement chromatography using both zonal and frontal chromatographic separations has proven successful in characterizing both high and low affinity ligand-receptor interactions and in characterizing ligand-receptor interactions for low abundance targets. In zonal displacement experiments, shifts in the chromatographic capacity factor (k') of an analyte on a column equilibrated with varying amounts of a competitive ligand can be used to identify and determine dissociation constants for low affinity ligands, as demonstrated by Jozwiak et al. using affinity columns containing the $\alpha_3\beta_4$-*n*AChR subtype.[22] Similarly, in frontal displacement experiments, various concentrations of a competitive binding ligand can be infused into a bioaffinity column along with a higher affinity indicator ligand and displacement in the frontal elution times of an indicator ligand can be correlated to the binding constants of both the indicator and displacer ligands.[18,21,22] The indicator mode developed by Schriemer et al. using MS-based detection is a variation of the previous frontal displacement method that correlates changes in breakthrough volumes of an indicator in the presence of weak affinity ligands to the binding affinities of the ligand-target interaction (i.e. $K_{d\ indicator} < K_{d\ weak\ ligand}$).[23] A transient 'roll-up' response in the weak ligand MS signal that results from the competition between the two ligands is also used to extract information on the binding kinetics of the interaction.

While the competitive techniques described above have proven successful in characterizing low affinity ligands on columns with low loading densities of target,[22]

affinity columns with extremely low densities (<2 pmol) of membrane receptor targets require the ability to resolve small shifts in retention times (<10 s) when these competitive techniques are employed, making them impractical. However, a transient over-concentration effect, similar to that seen in the weak ligand signal in FAC-MS indicator mode experiments, may provide a more robust signal output to monitor the interaction of weak ligands with stationary phases containing extremely low levels of target. Herein, we demonstrate an improved assay format that relies on the transient over-concentration of a strong indicator ligand that results from the competition between weak affinity test ligands and a strong affinity indicator ligand pre-equilibrated on the column. The method is used to identify and characterize weak affinity ligands on a model target receptor, namely the *nicotinic* acetylcholine receptor (*n*AChR) from *Torpedo Californica.* A unique aspect of the assay is the use of direct-flow nanoLC pumps, which allow a continuous flow competitive assay format to be used in conjunction with uses of small volumes of reagent (μL per assay) and capillary-scale bioaffinity columns directly coupled to an ESI-MS detector. The method is amenable to automation using an autosampler to achieve higher throughput analysis of discrete compounds in mixtures.

4.2 Experimental

4.2.1 Materials:

Torpedo californica electroplax was purchased from Aquatic Research Consultants Inc. (San Pedro, USA). Microsomal membranes enriched with *n*AChR were purified from the electroplax tissue, as described previously by Raftery et al.[24] The receptor

containing membranes (microsomes) were resuspended in 50 mM HEPES•NaOH pH 7.4 containing 100 mM NaCl, and divided into 50 - 200 μL fractions and stored at -86 °C until needed. The enriched *n*AChR microsomes were analyzed by standard radioassay methods using ^{3}H-epibatidine as a test ligand (Sigma-Aldrich), where ligand saturation experiments yielded a stock receptor binding site concentration of 770 ± 20 nM (protein concentration of 385 nM assuming two binding sites per receptor) and a K_d for epibatidine of 10 ± 2 nM nM and 12 ± 2 nM in HEPES•NaOH and NH_4OAc•NH_4OH respectively. Diglycerylsilane (DGS) was prepared by methods described elsewhere[25] using tetramethylorthosilicate (Aldrich, Burlington, Canada) and anhydrous glycerol (Fluka, Germany). HPLC grade water was purchased from Caledon Laboratory Chemicals, (Georgetown, Canada) and was used for all experiments. 10 kDa poly(ethylene oxide) (PEG) was obtained from Sigma-Aldrich (Oakville, Canada). Fused silica tubing was purchased from Polymicro Technologies (Phoenix, USA). 96 well filter plates containing 1.0 μm glass fiber, type B filters (Multiscreen™ Assay System) were supplied by Millipore (Toronto, Canada). 96-well microtiter plates were purchased from Nalge Nunc International (Rochester, USA). ^{3}H-epibatidine (53 Ci/mmol specific activity) was purchased from GE Healthcare (Pittsburgh, USA).

4.2.2 Instrumentation and Set-up:

A two-channel, Eksigent nanoLC pump equipped with two 5 mL stainless steel sample loops was used for mobile-phase delivery to an MDS Sciex Q-trap mass spectrometer equipped with a turbospray ionization source. The Eksigent pump uses

direct pneumatic pumping of mobile phase up to a maximum rate of 20 μL/min, with no flow splitting. Mobile-phase was delivered to the column under isocratic conditions using Eksigent nanoLC software v 2.08. An Eksigent AS-1 48 vial autosampler fitted with a 250-μL withdrawal syringe and a 60-μL sample loop of 250-μm-i.d. fused silica tubing was placed in-line with the LC pump prior to the MS detector and was used to aspirate test compounds from a 48-vial autosampler and deliver small volumes of test solutions (60 μL) into the column for various experiments (Fig. 1A). Test compounds were prepared in 1mL glass vials by dissolving the compounds in the assay buffer containing both the indicator and void marker compounds. Mobile phases were run directly into the MS system, using methanol "make-up" flow (8μl per minute) to facilitate the ionization process. Mass spectrometer control and data acquisition was done using Analyst v.1.4 software. Precursor-product ion pairs were followed using MRM mode in positive ion mode under the following conditions: curtain gas 30.0; collision gas, medium; ion spray voltage, 5500 V; temperature, 150 °C; ion source gas 1, 30.0; ion source gas 2, 30.0. The total scan time was 2 s per point.

4.2.3 Calculations and Corrections:

To correct for ion suppression, the signal from a non-binding ligand (fluorescein) was used to correct the epibatidine signal in areas where the fluorescein signal clearly showed the effects of ion suppression. The following formula was applied:

Corrected Epibatidine Signal = (Epibatidine Signal) x (Correction Factor) (4.2)

The correction factor represents the degree of change in the flourescein signal resulting from injection of the test compound (e.g. nicotine):

Correction Factor = (Avg. Flourescein Signal) ÷ (Actual Flourescein Signal) (4.3)

Note that in calculating the correction factor, the average flourescein signal was calculated using a 10 minute window that showed a stable signal prior to injection of the test compound, while the actual flourescein signal represents the portion of the signal affected by ion suppression during injection of the test compound.

In calculating the area under the curve (AUC) for quantitative experiments the beginning of the epibatidine spike was taken to be the first point in a series of 50 consecutive points that were all above the calculated average and the end of the spike was determined to occur when the difference in the above two signals was less than 10 cps for ten consecutive data points. Note that calculations were applied to the raw data and not the smoothed data for better accuracy.

The following relationship was used to calculate the binding constant of the test compound from the dose-response curve:

$$K_{d(\text{test compound})}=IC_{50}/(1+[I]/K_I) \quad (4.4)$$

where IC_{50} is the mid-point of the dose-response curve, [I] is the concentration of indicator being infused and K_I is the dissociation binding constant of the indicator.

Data smoothing was performed using SigmaPlot v. 10.0 with the running average transform function at a sampling proportion of 0.01.

4.3 Results and Discussion

4.3.1 Development of CDC in MRM Mode:

The competitive displacement technique we have developed utilizes an on-line assay that monitors the amount of free native marker (i.e., an indicator ligand), providing a means to identify and screen for low affinity ligands that bind to a particular target. The signal output is also analogous to the roll-up response seen in indicator mode FAC-MS experiments, where the presence of a strong affinity ligand results in an over-concentration in the signal of weak affinity ligands pre-equilibrated on the affinity column. The assay format presented here, referred to as competitive displacement chromatography (CDC), uses MS detection in MRM mode to identify transient increases or "spikes" in a strong affinity indicator signal that result from the introduction of test ligands. The setup requires four basic components, namely, a two-channel nanoLC solvent pump, a 48-vial autosampler, a micro bore monolithic affinity column and an ESI-based MS detector equipped with an internal syringe pump (Fig 4.1A). The LC pump is set up in line with the autosampler pre-column to allow introduction of test compounds into the column via the autosampler. The eluant from the column is combined with the 100% methanol from the internal syringe pump to help stabilize signals and the combined flow is introduced directly into the ESI-based MS detector for real-time detection (see methods for instrument specifics).

4.1 A

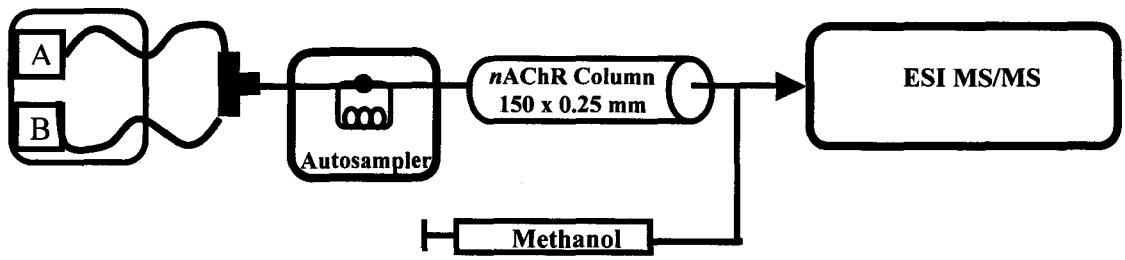
A
B
Autosampler
nAChR Column
150 x 0.25 mm
ESI MS/MS
Methanol

4.1 B

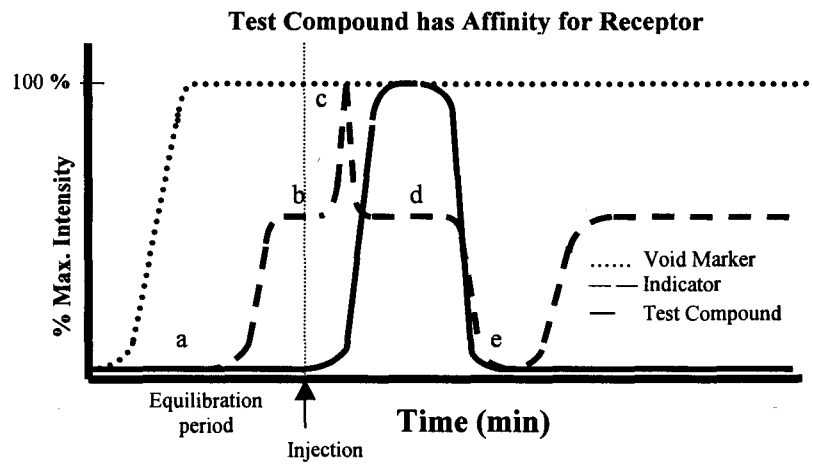
Test Compound has Affinity for Receptor
100 %
% Max. Intensity
a
b
c
d
e
..... Void Marker
— — Indicator
— Test Compound
Equilibration period
Injection
Time (min)

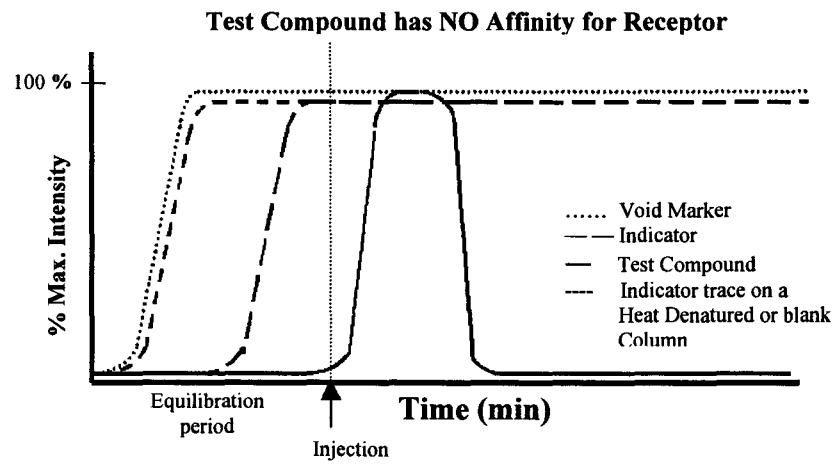
Test Compound has NO Affinity for Receptor
100 %
% Max. Intensity
..... Void Marker
— — Indicator
— Test Compound
---- Indicator trace on a Heat Denatured or blank Column
Equilibration period
Injection
Time (min)

Figure 4.1: Instrument setup (A) and expected signal output (B) for CDC (A) Assay buffer containing an indicator (I) and void marker (V) is loaded into both channels of the LC pump. Buffer is continuously infused directly into the affinity column (e.g. *n*AChR) under isocratic conditions on a flow path that initially by-passes the autosampler. The eluant is mixed with 100% methanol from an internal syringe pump on the MS detector and the combined flow enters the MS ESI source. The predetermined MRM signals for the void and indicator are monitored in real-time to determine when the column is equilibrated, as in conventional FAC experiments. After equilibration, the flow path is changed to include the sample loop of the autosampler, which contains compounds to be tested on the affinity column. (B) [top] The high affinity indicator is retained on column longer than the void markers during equilibration (a). Once equilibrated (b), injection of a low affinity test compound as a short plug causes a transient spike in the indicator signal (c) due to a transient over concentration of the indicator or column. The test compound briefly establishes a new equilibrium on column (d) until it traverses the entire column, where upon a drop in the indicator signal occurs (e) until the indicator re-equilibrates in the absence of the test compound (f). [bottom] A test compound with no affinity will show no change in indicator signal when injected. An inactive or blank column will show the same trend, with no retention of the indicator during equilibration (broken line with void marker).

Using the aforementioned arrangements, an affinity column is first equilibrated under isocratic conditions by continually infusing an MS compatible buffer containing a void

marker and a known high affinity indicator ligand in a manner similar to conventional FAC experiments (equilibration period). The equilibration buffer is loaded into both channels of the LC pump and the pump is operated with a 50% conserved flow from each channel to maximize the available mobile phase. During equilibration, the LC flow path is diverted straight to the affinity column and bypasses the autosampler to reduce solvent transit time. Once equilibrated, as determined by the plateau of the indicator front, the LC flow path is channelled through the sample loop of the autosampler, which contains the compound(s) that is to be tested on the affinity column. The sample loop injects multiple bed volumes onto the column to achieve equilibrium with test compounds.

A compound that has affinity for the receptor of interest will compete for active receptor sites on the column. The net effect would be a transient over concentration of the indicator ligand as a new equilibrium is established while the indicator and potential ligand (test compound) are both present on column (Fig 4.1B). Once the entire plug of test compound has traversed the column, a short re-equilibration period follows while the indicator ligand re-occupies receptor sites that were occupied by the test compound. Conversely, a compound with no affinity for the protein of interest will not perturb the indicator ligand, since the equilibrium between the mobile phase and the solid phase does not change. Hence, no change indicator signal above the blank will be seen. Note that for this latter point to be true, it is imperative that the test ligands are dissolved in the equilibration buffer so that the concentration of indicator ligand remains the same throughout the entire experiment.

4.3.2 Demonstrations of CDC Principles Using nAChR:

To demonstrate the principles of CDC, affinity columns were prepared using *n*AChR from *Torpedo Californica*, as previously described.[15] The *n*AChR target provides a suitable model to demonstrate CDC due to its relatively high abundance and low cost and due to previous studies showing *n*AChR activity in sol-gel derived monolithic materials.[15,26] Epibatidine was used as the indicator ligand (209→126 parent:daughter ion pair) due to its high affinity for the αγ and αδ sites on *n*AChR and flourescein (333→287 parent:daughter ion pair) was used as the void marker since it has no affinity for *n*AChR or the negatively charged silica surface of the sol-gel derived column material. Nicotine provides a suitable test compound (163→130 parent:daughter ion pair), as it weakly binds to the same receptor sites as epibatidine and does not show significant retention in a typical FAC based experiment under the given conditions (B_t~12 pmol).

Equilibration of a 150 x 0.25 mm *n*AChR affinity column with 20 nM epibatidine and 500 nM fluorescein showed 12-15 min frontal separation between the indicator and void markers at a flow rate of 5 μl/min, demonstrating the high affinity of epibatidine for the *n*AChr receptor (Fig 4.2A). Under the given equilibrium conditions the *n*AChR on column is likely in the desensitized state. Injection of 60 μl plug of 10 μM nicotine following equilibration of epibatidine resulted in a transient over-concentration of epibatidine, as seen by the brief spike in the MRM signal for epibatidine (209→126 ion pair). A drop in the epibatidine signal is then seen once the nicotine plug has traversed the column and the epibatidine re-equilibrates with free receptor sites. Finally, the

epibatidine signal plateaus again at the original concentration being infused, indicating that the column is re-equilibrated.

a) *n*AChR Column with Nicotine

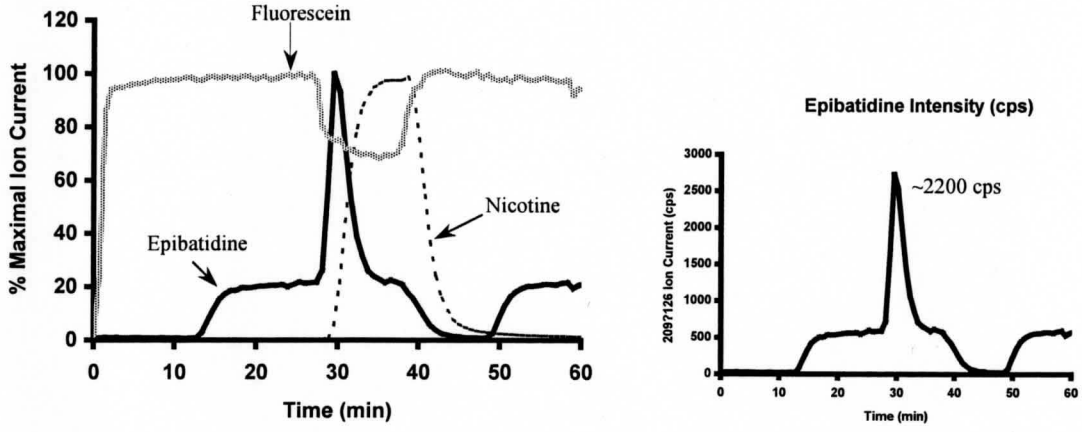

b) Blank Silica Column with Nicotine

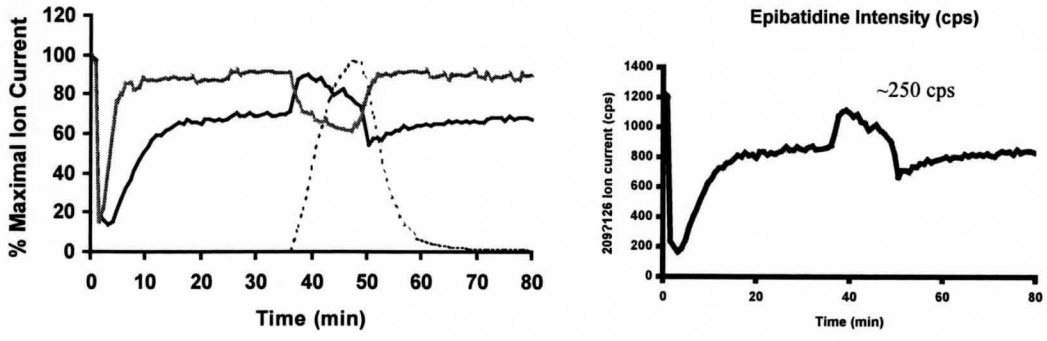

c) hd *n*AChR Column with Nicotine

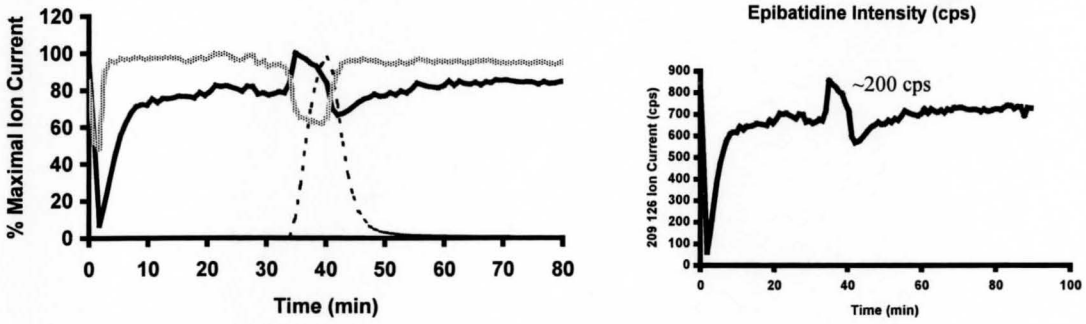

Figure 4.2: Demonstration of CDC Concept using *n*AChR Affinity Columns. Equilibration of a *n*AChR column with 20 nM epibatidine (indicator) and 500 nM flourescein (void) showed significant retention of epibatidine relative to flourescein (a). Injection of 10 μM nicotine resulted in a transient over concentration of the epibatidine signal followed by drop while the column re-equilibrates. Injection of 10 μM nicotine on a blank column (b) and a heat denatured *n*AChR column (c) under the same conditions showed a negligible change in the epibatidine signal. Note that the actual flourescein signal is shown for areas that have been corrected for ion suppression. Data was processed as described in the materials and methods section.

The profile of the epibatidine signal was compared to trials performed with nicotine on a blank silica column and a heat denatured *n*AChR column to confirm that the observed effect was indeed due to competition for the epibatidine binding sites on the *n*AChR column and not a result of competition for non-specific sites on the column

matrix or the lipid membrane. The size of the spike seen on these two control columns was negligible (~10%) compared to the active *n*AChR affinity column, demonstrating that the effect was indeed specific for the *n*AChR active sites (Fig 4.2B, 4.2C, respectively).

It should be noted here that the size of the epibatidine spike will be affected by several factors including i) the effect of ion suppression resulting from the injection of test compounds, ii) the concentrations of indicator and test compound injected into the column, iii) the amount of active receptor on the column and iv) the flow rate at which the experiment is conducted. In the current experiment, it was assumed that the effect of ion suppression was equivalent for both the void marker (fluorescein) and the indicator ligand (epibatidine). As such, the signal for the void marker was used as an internal standard to normalize the signal of the indicator ligand (see corrections and calculations), thereby correcting for the effect of ion suppression on the indicator signal and enhancing the magnitude of the transient spike by nearly 1.5-fold. In addition, the concentration of indicator used in these experiments was chosen to reduce the length of the equilibration period prior to nicotine injection and to maximize the size of the 'spike' upon injection of nicotine. A concentration of 20 nM epibatidine (~10 K_d) decreases V-Vo in the equilibration period (see equation 4.1) and ensures near complete saturation of *n*AChR on the column. Finally, 10 μM nicotine was used to minimize the length of washing steps in between consecutive injections. The effect of the amount of active receptor and the effect of flow rate are more complex issues and are dealt with below.

4.3.3 Reproducibility & Reusability:

The reproducibility and reusability of the CDC assay format was tested by repeatedly injecting a known test ligand onto a single column pre-equilibrated with the void marker and indicator compounds. Three injections of 100 μM nicotine onto a 150 x 0.25 mm *n*AChR column pre-equilibrated with 20 nM epibatidine and 500 nM flourescein predictably resulted in three reproducible spikes in the epibatidine signal (Fig 4.3a). The peaks heights for the epibatidine spike were generally of equal magnitude, showing approximately five percent degradation in signal intensity between trials and slight variation in the base width of each peak after 3 trials. The minor variations in peak height and width may be attributed to incomplete washing of nicotine off the column between subsequent injections, given that a saturating concentration of nicotine was used (100 μM). While saturating concentrations of test ligands may be more effective at producing a larger epibatidine spike, for experiments involving multiple injection of test compounds on a single column it is more practical to use lower concentrations of test ligands to minimize peak tailing, to reduce the amount of time required for washing and to reduce carry-over of the test ligand between subsequent trials. Figure 4.3b shows that trials performed using 10 μM nicotine result in epibatidine spikes with less variation in peak height, width and peak area (~5-6%) between trials.

a)

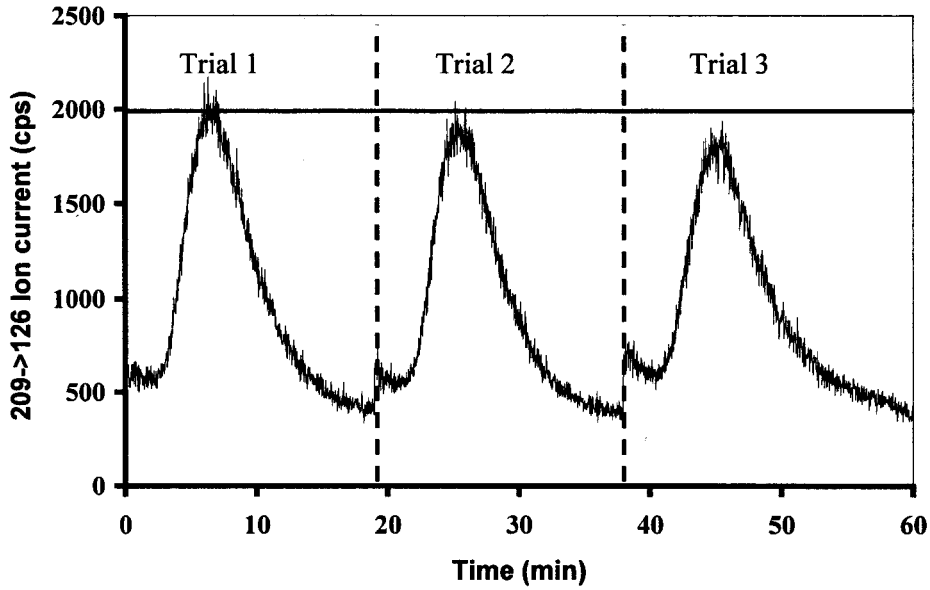
Trial 1
Trial 2
Trial 3
209->126 Ion current (cps)
2500
2000
1500
1000
500
0
0
10
20
30
40
50
60
Time (min)

b)

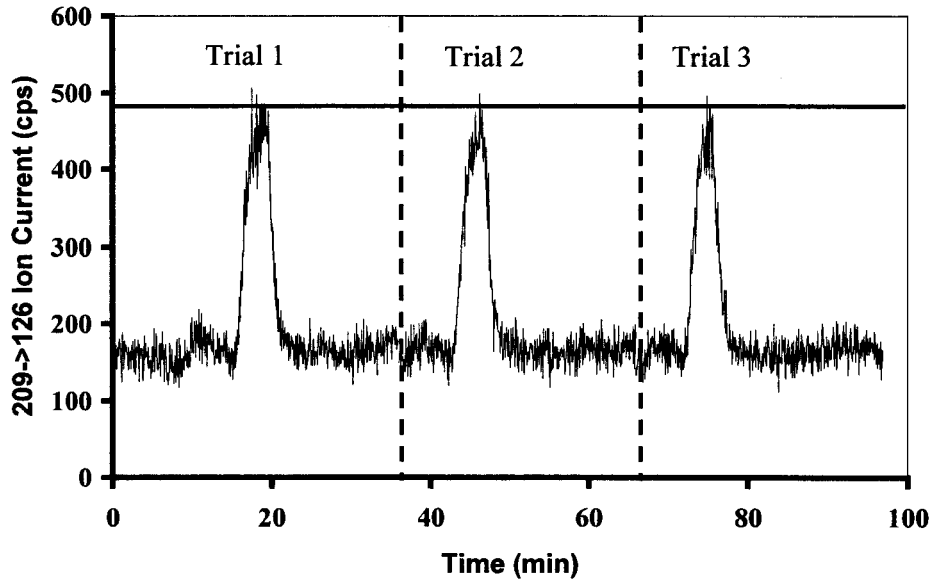
Trial 1
Trial 2
Trial 3
209->126 Ion Current (cps)
600
500
400
300
200
100
0
0
20
40
60
80
100
Time (min)

Figure 4.3: Reproducibility & Reusability. a) Multiple injections of 100 μM nicotine onto a *n*AChR column pre-equilibrated with 20 nM epibatidine shows transient spikes of equivalent size and shape. Slight degradation in peak intensity, width and area is seen between subsequent trials due to compound carryover and incomplete washing. b) Multiple injections of 10 μM under the same conditions improved reproducibility. For ease of comparison, the signals are plotted as a percentage of the maximum signal for each epibatidine and nicotine and the fluorescein signal is omitted.

It is worth mentioning that the ability to perform multiple reproducible injections is desired when considering the CDC assay as both a screening tool to identify new ligands and as a quantitative tool to determine ligand binding constants, given that both cases require multiple data points generated from a single column. Based on the data presented in figures 4.2 and 4.3, it is clear that many injections can be performed using high concentrations of weak ligands on a single column before the signal intensity of the epibatidine spike has degraded to a level near the background intensity seen on control columns. If injections are made at a low concentration of test compound (i.e. 1-10 μM) to reduce peak tailing, compound carry-over and the length of washing steps, it is reasonable to assume that a greater number of injections (>40) can be achieved on a single affinity column, provided that the receptor is not irreversibly spoiled by an unknown test compound. Multiple injections of mixtures containing non-ligands should have minimal effect on column activity; however, the presence of a strong or covalent inhibitor in test mixtures will rapidly degrade the column.

4.3.4 Assay Speed:

As mentioned above, the size of the epibatidine spike is dependent on the flow rate at which the experiment is conducted. The flow rate can affect the size and appearance of the spike in two ways: i) by altering the ionization efficiency of the indicator ligand and ii) by increasing or decreasing the time required for the complete epibatidine spike to traverse the column. The ionization efficiency of typical ESI-based ion sources has been seen to decrease with increased flow rates in certain applications.[27] Intuitively, the length of time required for the complete spike to traverse the column is expected to decrease with increasing flow rates, thereby reducing the base width of the peak.

While the experiments above used conditions that provided a well-defined, easily quantifiable output for simplicity, these conditions may not be optimal when considering the use of this technique for quantitative measurements or screening purposes, as the time required to generate a single data point in the above experiments is not ideal. Hence, the assay was also tested at flow rates of 15 and 20 μL/min (maximum flow rate of the Eksigent pump) to determine the maximum speed of the assay and to determine the robustness of the assay at higher flow rates (Fig. 4.4). At flow rates as high as 15 μl/min a discernable spike can be seen when 100 μM nicotine was injected into an affinity column pre-equilibrated with 20 nM epibatidine. The peak intensity is significantly lower than seen when injections were performed at 5μL/min, likely owing to reduced ionization at higher flow rates. This effect is also seen with injections at an even higher flow rate of 20 μL/min, which shows further suppression of peak intensity (2-fold decrease from 5 to

15 μL/min) and peak area. While the increased flow rates reduce the signal intensity, it is worth mentioning that the time required for full re-equilibration of the *n*AChR column following a single injection is reduced from ~50 minutes at a flow rate of 5 μL/min to ~20 minutes at 15 μL/min and less than 15 minutes at 20 μL/min. This result suggests that if the assay was employed for small molecule screening using multiple test compounds per injection (e.g. 100 compounds per injection as in other FAC-based screens), a rate of up to 5 compounds per minute per column could theoretically be achieved using CDC. The ability to perform the assay at higher flow rates also allows for the determination of quantitative data related to binding affinities in a reasonable time period. It should be noted that although the ability to run the assay at 20 μL/min does provide for more rapid screening of compounds, operating at this flow rate may compromise the integrity of sol-gel based affinity columns due to the high backpressures reached at these flow rates. The results suggest that assays should be run at low flowrates, highlighting the advantages of the direct flow nanoLC set-up.

a) 5μl/min

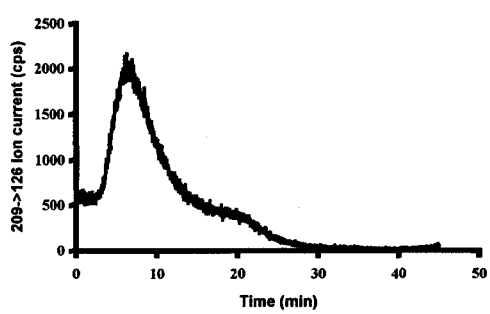

b) 15 μl/min

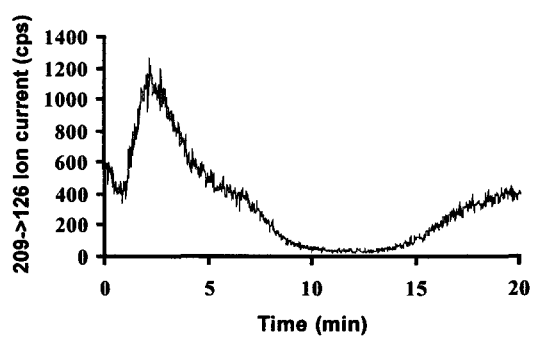

c) 20 µl/ min

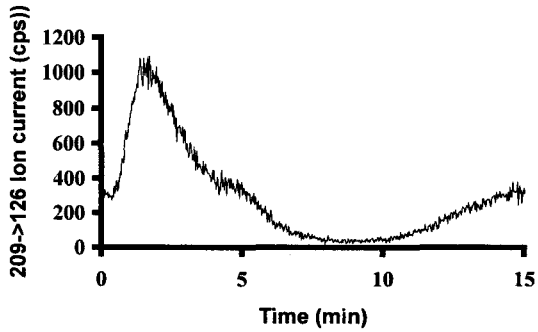

Figure 4.4: Assay Speed. A comparison of the signal output generated by CDC method using flow rates of 5, 15 and 20 µl/min is shown. Peak intensity is slightly compromised at higher flow rates, but a discernable signal is achievable at flow rates as high as 20 µl/min. Note that the length of the re-equilibration period also decreases with increasing flow rate. At a flow rate of 15 µl/min, complete re-equilibration occurs within ~15 minutes.

4.3.5 Quantification & Validation:

As further validation of the CDC assay we examined the utility of CDC as a quantitative tool for determining the binding constant of a low affinity ligand. The area under the curve (AUC) for the epibatidine signal was taken to represent the number of moles of epibatidine displaced by a given concentration of test ligand injected. For the AUC to be easily calculated, it is imperative that the tailing edge of the epibatidine spike

returns to the level observed prior to injection of the test compound. To ensure this occurs, the volume of the test compound injected must be sufficiently large to allow complete equilibration of both the indicator and the test compound while both are present on column. A 60 μl sample loop (~10 bed volumes) was determined to sufficient to achieve this goal under the given assay conditions.

Initial experiments were performed on a 150 x 0.25 mm *n*AChR column pre-equilibrated with 20 nM epibatidine and 500 nM fluorescein at a flow rate of 10 μL/min. Ten injections of nicotine ranging in concentration from 0.01 to 20 μM nicotine were performed on a single column, resulting in epibatidine spikes that increased in intensity and base width with increasing concentration of nicotine (Fig 4.5a). The resultant competitive binding curve (Fig. 4.5b) yielded an apparent K_d of ~0.34 μM for nicotine. When corrected for the conditions used in the current experiment, the actual K_d for nicotine was determined to be ~0.031 μM. The dose-response curve (Fig 4.5c) yielded an IC_{50} of ~0.9 μM, giving a K_d for nicotine of ~0.08 μM using the Cheng-Prusoff relationship (equation 4.4). These values are approximately a factor of 10 lower than expected, as previous studies have shown the K_d of nicotine to be in the 1 μM range for *n*AChR entrapped in sol-gel based materials.[26] The values obtained in this study are in closer agreement with competitive-based fluorescence experiments (~5-fold difference) that report an apparent K_d of 1.36 μM (actual K_d ~0.48 μM when corrected for experimental conditions) for nicotine when probing the high affinity binding site of *n*AChR.[28]

a)

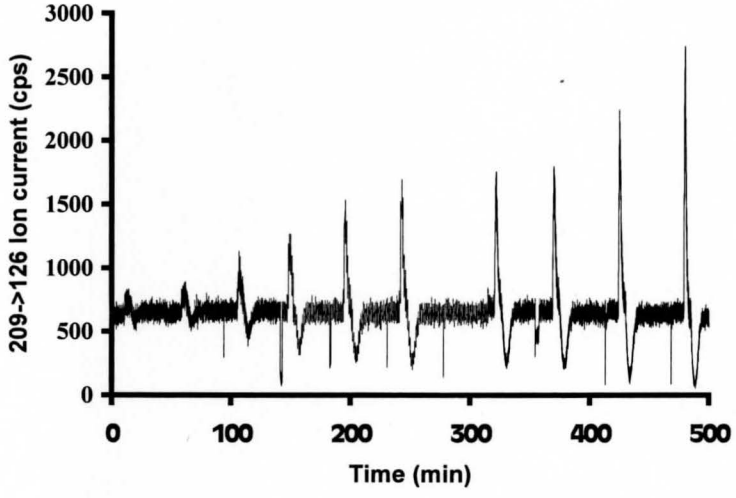
209->126 Ion current (cps)
3000
2500
2000
1500
1000
500
0
0
100
200
300
400
500
Time (min)

b)

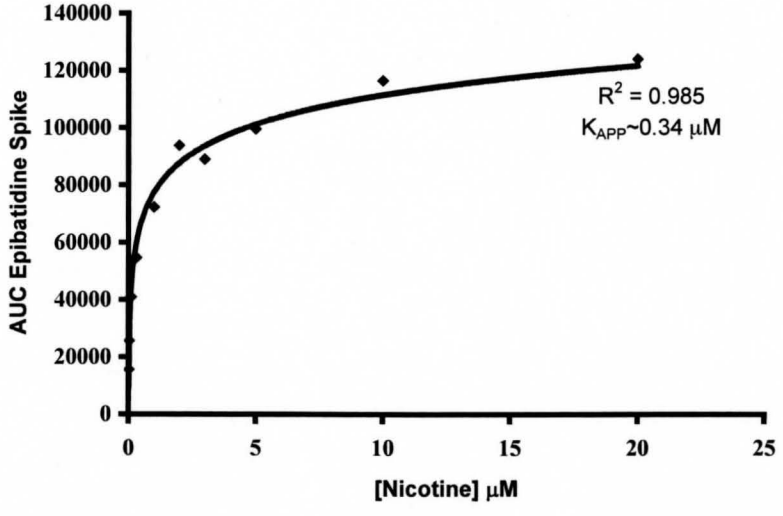
AUC Epibatidine Spike
140000
120000
100000
80000
60000
40000
20000
0
0
5
10
15
20
25
[Nicotine] μM
R² = 0.985
K_APP~0.34 μM

c)

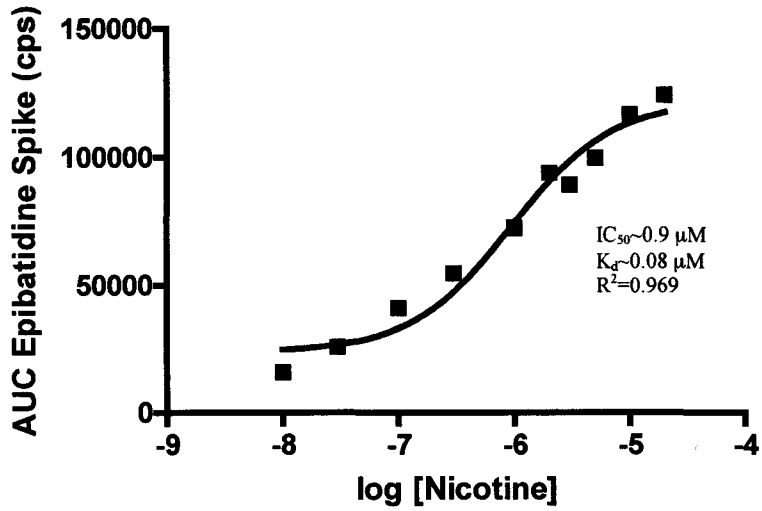

Figure 4.5: Signal Intensity and Competitive Binding Curves for Nicotine using 20 nM Epibatidine. The intensity of the epibatidine signal increases with increasing concentrations of nicotine (a). A discernable signal can be seen with nicotine injections as low as 1-2 μM. Competitive binding curves (b) and dose-response curves (c), yielded a K_{APP} of ~0.34 μM and an IC_{50} of ~0.9 μM and a K_d~0.08 μM.

Examination of figures 4.5b and 4.5c shows that both the competitive binding curve and dose-response curve fail to completely plateau at the higher concentrations of nicotine, hence the discrepancy between expected results and the results obtained in this study may be a result of to fitting to an incomplete binding curve. With an additional data point at ~50-100 μM nicotine, the complete binding curve and dose-response curve would likely yield complete set of binding data; however, the need to inject large concentrations

of test ligand for such quantitative studies significantly increases washing times and increases the possibility of compound carry-over between subsequent trials, as discussed above. This latter point has been seen to significantly compromise the shape of the epibatidine spike and has comprised the ability to accurately calculate the AUC for the epibatidine spike when multiple injections were performed on a single column (data not shown). Therefore, rather than injecting large concentrations of the test compound to obtain a complete binding curve under the previous conditions (i.e. 20 nM epibatidine), the concentration of the indicator compound was decreased (i.e. 2 nM epibatidine) to reduce the amount of test ligand needed to completely compete off the indicator compound. Preliminary results suggest that reducing the epibatidine concentration indeed results in a plateau in the binding curves at lower concentrations of nicotine, thereby allowing for easier analysis of competitive binding data (Fig. 4.6). The resultant binding data generated from these curves is again 20-fold lower than previous studies preformed in sol-gel based materials and ~6-fold lower than previous fluorescence-based competitive experiments, suggesting that the discrepancy between observed data and expected data is not a result of fitting to an incomplete curve. Rather, the K_d value for nicotine determined in the current study likely reflects the binding constant for the high binding site on *n*AChR and differences between data obtained in this study and fluorescence-based studies is likely a result of differences in the heterogeneous assay set-up used here and the homogeneous assay set-up used in the latter experiments.

a)

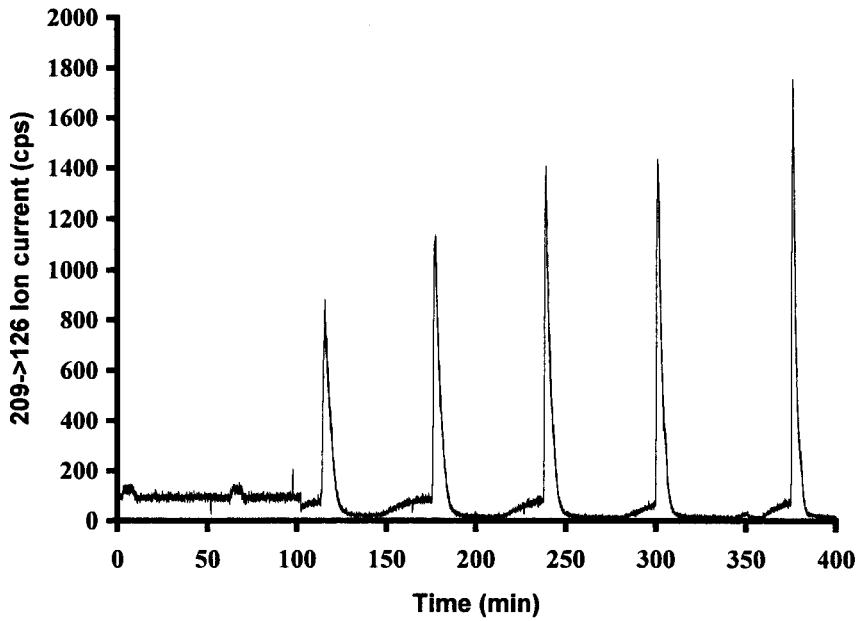
209->126 Ion current (cps)
2000
1800
1600
1400
1200
1000
800
600
400
200
0
0
50
100
150
200
250
300
350
400
Time (min)

b)

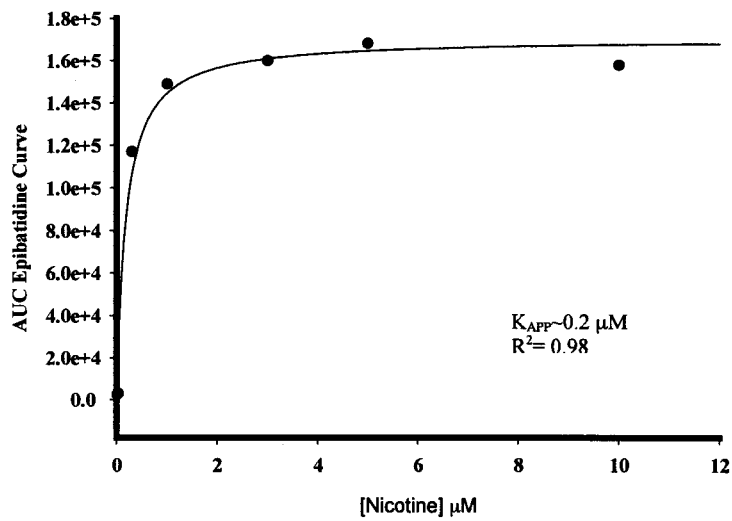
AUC Epibatidine Curve
1.8e+5
1.6e+5
1.4e+5
1.2e+5
1.0e+5
8.0e+4
6.0e+4
4.0e+4
2.0e+4
0.0
0
2
4
6
8
10
12
[Nicotine] μM
K_{APP}~0.2 μM
R^2= 0.98

c)

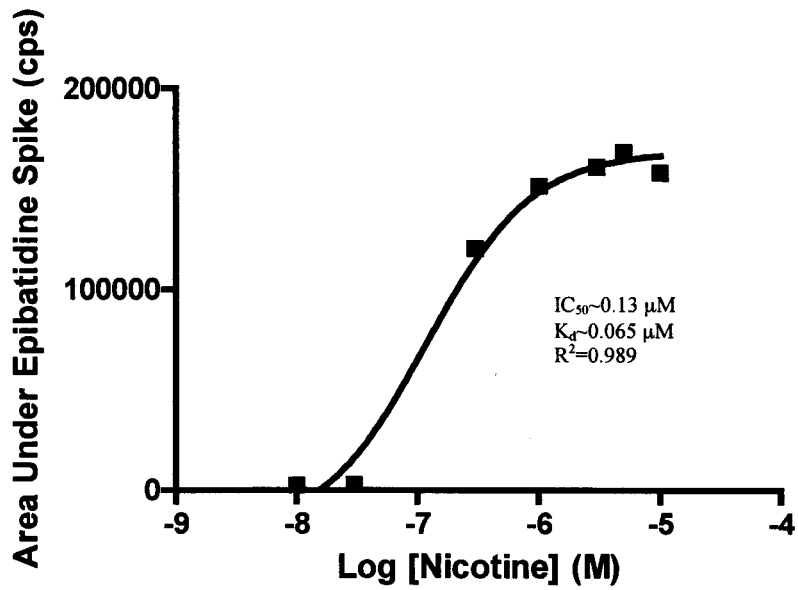

Figure 4.6: Competitive Binding Curve for Nicotine using 2 nM Epibatidine. Preliminary data shows that binding curves generated using lower concentrations of indicator compound plateau at lower concentrations of test ligand. This result suggest that complete binding curves can be generated using lower concentrations of test ligand, thereby avoiding problems with ion suppression and compound carry-over that complicate data interpretation.

It should be noted that while the present study uses columns containing ~12 pmol of active receptor on column, the signal generated under certain conditions can be significantly higher than baseline level of the indicator. Previous plate-based assays performed on the dopamine 2 receptor (D2R) entrapped in sol-gel derived materials showed that the amount of active receptor was approximately 12 times less than the amount of active receptor contained in similar preparations using *n*AChR (i.e. 16 fmol of active D2R per volume of silica to 210 fmol nAChR).[26] Given the present data, it is envisioned that under the appropriate conditions, the current assay format may well be useful for identifying and characterizing target-ligand interactions on columns prepared using D2R, despite having fewer active binding sites present on column. More specifically, the signal generated on *n*AChR columns (net signal without background ~2000cps) can be as much as ~10-fold greater than the signal resulting from non-specific binding on control columns (net signal 225±25 cps) (Fig. 4.2). Given, the current signal (S) to background (B) ratio (i.e. 3σ~75cps; hence, S/B=2000cps/75cps or ~27), the competitive assay can in principle be used to detect target-ligand interactions using a factor of 27 less target protein or as little as ~44 fmol of active target on column. With the current bed volume of ~7.5 μL, the ability to identify ligands using sol-gel derived columns containing D2R can be attained. This assumption is reasonable, given that similar frontal displacement studies have been conducted on columns containing as little as 5 fmol of active receptor.[29]

4.3.6 Implications for Compound Screening of Low Abundance Receptors Using CDC:

The results presented above indicate that the CDC assay format may provide a dynamic method for screening small molecule compounds against low abundance receptor targets with the potential to effectively identify low affinity ligands in mixtures of unknown composition. Specifically, at flow rates of up to 15 μL/min the potential to screen a large number of compounds exists, as compound mixtures containing >100 compounds may be injected onto an affinity column in a single assay. The need to only monitor the signal of the indicator compound alleviates the need to individually monitor 100 compounds per vial as is required in conventional FAC-MS approaches; such a task is not easily accomplished, especially for compounds with poor ionization efficiency. Both figures 4.5a and 4.6a also demonstrate the ability to generate a discernable signal output at a test ligand concentration below 2 μM on columns equilibrated with saturating concentrations of indicator (~10K_d). The use of lower concentrations of indicator or perhaps a less potent indicator may well provide the opportunity for identifying test ligands at even lower concentrations and may allow for screening compound mixtures of up to 1000 compounds per vial, as a lower concentration of test ligands can avoid problems with precipitation of components in the test mixture.

The ability to generate a discernible signal output at both high (e.g. 10 μM) and low (e.g. 1 μM) test compound concentrations also allows for specific tuning of the screening stringency through adjustment of the compound library concentration. For example, if a low hit rate is desired (e.g., 0.1%) vials containing 1000 compounds per vial at low concentrations (e.g., 0.5-1 μM) can be used for screening. Alternatively, if a high hit rate

is desired (e.g., 2% hit rate), vials containing 100 compounds per vial at a higher concentration (~10-20 μM) can be prepared for screening. Although the present studies were specifically designed to identify a known low affinity ligand for *n*AChR, the former scenario would present an opportunity for identifying higher affinity ligands for a given receptor target while the latter scenario would be ideal for identifying lower affinity ligands, as well.

Based on a flow rate 15 μL/min and using a minimum of 100 compounds per vial, a rate of 5 compounds per minute per column can be achieved using the current automated set-up. This gives rise to a screening rate of ~7200 compounds per day which is comparable to the current standard of 10,000 compounds per day for compound screening using the FAC-MS approach. By screening compound mixtures of up to 1000 compounds, this standard can be easily surpassed, though deconvolution of the mixture will require additional time. Further automation of the current system using column actuators that allows for handling of multiple columns such that washing steps are performed off-line between trials can further reduce the time required for a single injection to from ~20 minute to ~7 minutes per injection and can potentially double screening throughput, thereby allowing for the current standard of 10,000 compounds per day to be easily surpassed on a single instrument. The use of multiple instruments with multiplex ESI MS systems can further increase the potential of this technique as a viable HTS screening tool.[30]

While the potential to increase throughput using the aforementioned methods provides great opportunity for small molecule screening, the need to perform appropriate controls

to ensure the receptor is not irreversibly damaged should not be over looked. In addition, although the technique presented here avoids the need to monitor multiple compounds as in conventional FAC-MS screening, deconvolution steps are still required once a hit is identified in a given mixture. However, isolating the hit in a mixture can be done using straightforward fractionation or solid-phase extraction methods. We also note that the technique presented here requires a known high affinity ligand to be used as the indicator. Several high affinity ligands are known for common membrane receptor targets and may be used to perform the competitive assay described here. In cases where no high affinity ligand is known, as is the case for orphan receptors, it is envisioned conventional FAC approaches may be used to a identify high affinity ligand for low abundance targets and the current technique can be used to identify other bioactive compounds acting on the given target once a high affinity ligand is found.

4.3.7 Conclusions:

The competitive displacement assay presented here has been shown to be an effective method for identifying low affinity ligands for membrane receptor targets using affinity columns containing low to sub-picomolar amounts of active receptors. The transient spikes generated in the indicator signal allows for the facile identification of compounds having affinity for a given receptor without the need to monitor retention of multiple compounds in test mixtures, thereby avoiding the need for multiple separation steps to identify specific components of a test mixture. The ability to generate multiple reproducible signal outputs allows the user to acquire quantitative data related to binding

affinities of compounds from a single column in a reasonable period of time. In addition, the above method provides the opportunity for screening low abundance membrane receptors against large compound libraries with the potential to surpass the current standard of 10,000 compounds per day in a large scale screening campaign. The above method provides an opportunity for screening pharmacologically relevant orphan receptors, such as GPCRs, to identify new chemical probes that can be used to elucidate function of these targets.

4.4 Acknowledgements

The authors thank MDS-Sciex, NSERC, the Ontario Ministry of Energy, Science and Technology, the Canada Foundation for Innovation and the Ontario Innovation Trust for support of this work. JDB holds the Canada Research Chair in Bioanalytical Chemistry.

4.5 References:

1. Comess, K.M.; Schurdak, M.E. *Curr. Opin Drug Discov. Devel.* **2004**, *7*, 411-416.

2. Shin, Y.G.; van Breemen, R.B.; *Biopharm Drug Dispos.* **2001,** *22*, 353-72.

3. Kaur, S.; McGuire, L.; Tang, D.; Dollinger, G.; Huebner, V.; *J. Protein Chem.* **1997** *16*, 505-11.

4. Kelly, M.A.; McLellan, T.J.;Rosner, P.J. *Anal Chem.* **2002**, *74*,1-9.

5. Johnson, B.M., Nikolic, D. and van Breemen, R.B. Mass Spectrom Rev. 2002 Mar-Apr;21(2):76-86.

6. Ng, E.S., Yang, F., Kameyama, A., Palcic, M.M., Hindsgaul, O. and Schriemer, D.C. Anal Chem. 2005 Oct 1;77(19):6125-33.

7. Kasai, K; Ishii, S. *J. Biochem.* **1975**, *14*, 261-264

8. Kasai, K; Oda, Y.; Nishikata, M.; Ishii, S. *J. Chromatogr.* **1986**, *376*, 33-47.

9. Slon-Usakiewicz, J.J.; Ng, W.; Dai, J.R.; Pasternak, A.; Redden, P.R. *Drug Discov. Today* **2005**, *10*, 409-16.

10. Chan, N.W.; Lewis, D.F.; Hewko, S.; Hindsgaul, O.; Schriemer, D.C. *Comb Chem High Throughput Screen* **2002**, *5*, 395-406.

11. Zhang, B.; Palcic, M.M.; Schriemer, D.C.; Alvarez-Manilla, G.; Pierce, M.; Hindsgaul, O. *Anal. Biochem.* **2001**, *299*, 173-82.

12. Toledo-Sherman, L.; Deretey, E.; Slon-Usakiewicz, J.J.; Ng, W.; Dai, J.R.; Foster, J.E.; Redden, P.R.; Uger, M.D.; Liao, L.C.; Pasternak, A.; Reid, N. *J Med Chem.* **2005,** *48*, 3221-30.

13. Hodgson, R.J.; Chen, Y.; Zhang, Z.; Tleugabulova, D.; Long, H.; Zhao, X.; Organ, M.; Brook, M.A.; Brennan, J.D. *Anal Chem.* **2004,** *76*, 2780-90.

14. Baynham, M.T.; Patel, S.; Moaddel, R.; Wainer, I.W. *J Chromatogr B Analyt Technol Biomed Life Sci.* **2002**, *772*, 155-61.

15. Besanger, T.R.; Hodgson, R.J.; Guillon, D.; Brennan, J.D. *Analytica Chimica Acta.* **2006**, *561*, 107-118.

16. Moaddel, R.; Bullock, P. L.; Wainer, I. W. *J. Chromatogr. B. Analyt. Technol. Biomed. Life Sci.* **2004**, *799*, 255-263.

17. Moaddel, R.; Cloix, J. F.; Ertem, G.; Wainer, I. W. *Pharm. Res.* **2002**, *19*, 104-107.

18. Beigi, F.; Chakir, K.; Xiao, R. P.;Wainer, I. W. *Anal. Chem.* **2004**, *76*, 7187-7193.

19. Beigi, F.; Wainer, I. W. *Anal. Chem.* **2003**, *75*, 4480-4485.

20. Dobrovetsky, E.; Menendez, J.; Edwards, A. M.; Koth, C. M. *Methods* **2007**, *41*, 381-387.

21. Slon-Usakiewicz, J.J.; Dai, J.; Ng, W.; Foster, J.E.; Deretey, E.; Toledo-Sherman, L.; Redden, P.R.; Pasternak, A.; Reid, N. *Anal Chem.* **2005** *77*, 1268-74.

22. Jozwiak, K.; Haginaka, J.; Moaddel, R.; Wainer, I.W. *Anal. Chem.* **2002**, *74*, 4618-24.

23. Chan, N. W. C.; Lewis, D. F.; Rosner, P. J.; Kelly, M. A.; Schriemer, D. C. *Anal. Biochem.* **2003**, *319*, 1-12.

24. Wu, W.C.; Raftery, M.A. *Biochemistry* **1981**, *20*, 694-701.

25. Brook, M. A.; Chen, Y.; Guo; K.; Zhang, Z.; Brennan, J.D. *J. Ma.t Chem.*, **2004**, *14*, 1469-1479.

26. Besanger, T.R.; Easwaramoorthy, B.; Brennan, J.D. *Anal. Chem.* **2004**, *76*, 6470 - 6475

27. El-Faramawy, A.; Siu, K.W.; Thomson, B.A. *J. Am. Soc. Mass Spectrom.* **2005**, *16*, 1702-7.

28. Krauss, M.; Korr, D.; Herrmann, A. Hucho, F. *J. Biol. Chem.* **2000**. *275*, 30196-30201.

29. Moaddel, R.; Jozwiak, K.; Whittington, K.; Wainer, I. W. *Anal. Chem.* **2005**, *77*, 895-901.

30. Want, E.; Greig, M; Compton, B.; Bolanos, B.; Siuzdak, G. *Spectroscopy* **2003**, *17*, 663-680.

Chapter 5

Conclusions and Future Outlook

5.1 Summary and Conclusions

The research in the preceding chapters attempted to achieve specific goals related to the use of sol-gel technology in affinity-based bioassays and approached the problem from both fundamental and applied perspectives. The specific goals of fundamental studies included: (i) to develop a new fluorescence-based tool using a novel two-point interaction between pyranine and the polycationic polymers to monitor non-specific interactions resulting from electrostatic forces between cationic species, such as poly-D-lysine, poly-L-ornithine, poly-L-arginine and polyallylamine and sol-gel derived silica materials and (ii) to assess the affect of non-specific electrostatic interactions on the dynamics of polycationic polymer entrapped in materials prepared using sodium silicate. The specific goals of applied studies included: (iii) to develop a suitable affinity-based assay format based on the principles of FAC-MS that allows for the screening of weak binding ligands for low abundance membrane receptors using affinity columns prepared via the sol-gel processing method (iv) to use the affinity-based assay format identify and characterize target-ligand interactions in a high throughput manner using an automated set-up.

The first project addressed the goals of fundamental studies by exploring the TRFA parameters of pyranine labeled poly-D-lysine, poly-L-ornithine, poly-L-arginine and polyallylamine. This study showed that the new two-point labeling method provides data

for the segmental motion, ϕ_2, of polyamine species that is in good agreement with NMR dynamics studies. The two-point labeling method was seen to more accurately report on segmental motions compared to previous studies that used single-point labeling methods with fluorescein. It was found that the accuracy of the TRFA parameters describing segmental motion increased as the length of the sidechain on the polymer decreased, as a result of a more rigid complex being formed between the probe and the polymer. The increased rigidity served to reduce local motions of the probe, such as rotation around the probes bond axis and local motion of the sidechain of the polymers, thereby allowing the motion of the probe to be more closely coupled to the backbone motion of the polymer. The two-point labeling method ultimately used to reveal the significance of electrostatic interactions between polycationic species and sol-gel derived materials. Specifically, pyranine labeled poly-D-lysine entrapped in silica monoliths made from sodium silicate precursors showed significant restriction in segmental motion, as indicated by the large ϕ_2 motion and the high g-value compared to solution. This indicated that electrostatic adsorption of polycationic species to the exposed negative silica surface of sol-gel derived materials significantly restricts the dynamics of these species, contrary to the finding of our previous study with single-point labeled species.

The second project addressed the goals of applied studies by exploring target-ligand interactions on affinity columns prepared with *n*AChR using a new competitive-based affinity assay format with MS detection. The assay format was based on the principles of FAC-MS and involved monitoring a strong affinity ligand, epibatidine, pre-equilibrated on column in MRM mode to identify spikes in the epibatidine signal that results from the

injection of test compounds. Injection of compounds having affinity for the target (e.g. nicotine) produced a transient over-concentration of epibatidine resulting in a measurable transient spike in the epibatidine MRM signal. Injection of compounds known not to have affinity for the target did not produce a transient spike in the epibatidine MRM signal and provided results similar to that produced using a blank silica column and a heat denatured *n*AChR column. The method was seen to be specific for ligands of *n*AChR and was not complicated by interfering non-specific interactions with the column materials when non-ligands, such as caffeine, were injected on column, as seen in more conventional FAC-based experiments using low abundance membrane receptors. The size of the spike in the epibatidine signal was also seen to be directly related to the amount of test ligand being injected, providing the opportunity for collecting quantitative data on the binding affinities of newly identified ligands. The size of the spike was also sufficiently large enough to provide the opportunity for screening membrane targets available in sub-picomolar quantities without needing over-expression systems to obtain large quantities of a given receptor target. The method was amenable to automation and was robust at high flow-rate allowing for the potential high-throughput screening of large synthetic or natural compound libraries.

Overall the research outlined in this thesis provides new methods for assessing the non-specific interactions between cationic species and a convenient method for screening for novel target ligand interactions using low abundance membrane receptors. The novel two-point labeling method developed in the first study allows for more accurate monitoring of biomolecule dynamics in sol-gel derived silica materials and provides a

more clear understanding on how electrostatic interactions affect the dynamics, and hence activity, of entrapped biomolecules. The competitive assay developed in the second study is an easy method that can be used to screen and characterize novel target ligand interactions when low abundance receptors are used and can potentially improve the efficiency, accuracy and throughput of MS-based affinity assays. Together, the tools developed in this study can be used in tandem to further improve sol-gel based affinity assays to help identify novel chemical probes that regulate key biological processes.

5.2 Future Outlook

Mass Spectrometry affinity assays using affinity chromatography are beginning to gain recognition as a viable screening format for identifying novel ligand-target interactions. Several advantages have been outlined in this thesis and include the ability to screen targets for bioactive compound mixtures in a label-free manner, the ability to identify structural features of unknown compounds using MS-MS experiments and more recently the ability to screen membrane receptor targets involved in important biological pathways. The technique demonstrated in Chapter 4 of this thesis has provided further merit to column-based affinity screening methods with MS detection by i) reducing the complications in data interpretation that result from non-specific interactions, ii) allowing for the identification of weak affinity ligands with low abundance membrane receptors and iii) potentially improving the throughput of MS-based affinity assays through automation. Immediate future work will assess the utility of the competitive assay as a screening tool, as the work presented here only offers insight into the use of this

technique as a screening tool. This work should include experiments designed to test the upper limit to the number of compounds that can be screened in a single mixture using this technique. Definition of an appropriate hit zone for the assay is also necessary to ascertain the quality of data generated using this technique in a screening format.

Longer term studies should address several remaining obstacles that can hinder the widespread use of these techniques in the routine screening of several different membrane receptors. As discussed briefly in chapter 1, the task of fabricating columns with enough active protein to achieve efficient compound separation is difficult. The competitive assay format describe in Chapter 4 can be used to alleviate many of the complications associated with the low abundance of receptors, however, the model target used in these studies is still available in relatively large amounts compared to other pharmacologically relevant membrane targets, such as GPCRs. While GPCRs can indeed be entrapped in sol-gel based monolithic columns in an active state, the number of active binding sites available in silica materials made with these targets can be more than a factor of 10 lower than the number of active sites seen in with *n*AChR. Future studies that apply the competitive technique described in chapter 4 to a GPCR membrane receptor, such as D2R, are necessary to prove the worth of the technique as viable screening to for many membrane receptor targets.

The fluorescence technique in Chapter 3 provides a means for ascertaining non-specific interactions between cationic polymers and silica material and may well prove to be useful in column studies involving the screening of GPCR targets, as many native ligands of these targets are indeed cationic polypeptides. While the work provided in this

thesis describes the application of the two-point binding to study non-specific interactions in sol-gel derived materials made from sodium silicate, the extension of this technique to other silica materials made from biocompatible precursors, such as glycerylsilanes, are necessary to provide a clear picture on how non-specific interactions between test ligands and the column matrix may affect the quality of a screening campaign. In addition, future studies that extend the two-point binding method to study the dynamics of membrane bound receptors in sugar modified silica materials may provide insight on how to better preserve the function of entrapped membrane receptors. These studies may provide useful information on how to increase the amount of active receptor on a sol-gel based affinity column thereby allowing for more efficient separations on these columns.

The ultimate extension of the techniques presented in this thesis to study orphan membrane proteins using column-based affinity assays with MS detection is desired, as important information on cellular events associated with disease may well result. From a chemical genetics perspective, affinity screening of orphan receptors may yield chemical probes capable of providing insight into previously uncharacterized cellular pathways.